SOUND AND ULTRASOUND SOURCE DIRECTION OF ARRIVAL ESTIMATION

AND LOCALIZATION

BY

VITALIY KUNIN

DEPARTMENT OF ELECTRICAL AND COMPUTER ENGINEERING

Submitted in partial fulfillment of the
requirements for the degree of
Master of Science in Electrical Engineering
in the Graduate College of the
Illinois Institute of Technology

Approved _____
Adviser

Chicago, Illinois
December 2010

ACKNOWLEDGEMENT

I would like to express my gratitude to my thesis advisor Dr. Jafar Saniie for encouraging and challenging me and for providing a great learning experience over the course of my undergraduate and graduate education. I would also like to thank my research lab colleagues and friends, Marcos, Alireza, Richard, and Vijay, for all the technical advice they have given me throughout my graduate work.

I would like to express my gratitude to my family for all the support they provided over the many years of education. I would like to thank my father, Vladimir, whose technical expertise and assistance was a great help in many parts of this work. I would like to thank my mother, Svetlana for her support and encouragement during all of my education. I would also like to thank my sister, Alina, and brother in-law, Dmitriy, for their support and encouragement.

TABLE OF CONTENTS

LIST OF TABLES

LIST OF FIGURES

ix

ABSTRACT

Localization of sources and the detection of objects using ultrasound has been the topic of a great deal of research as there are numerous applications for these techniques. Some of the prominent applications of sound source localization are the enhancement of human speech recognition for hands free man machine interface, the separation of multiple sound sources for teleconferencing and the detection and localization of mechanical or structural failures in vehicles and building or bridges. Ultrasound source detection can also be used for the above described applications as well as for a wide variety of security systems and for robotic vision.

This work explores the fundamentals of sound and ultrasound source localization as well as ultrasound object imaging and matched filtering. The main parts of this work are the design of an acoustic chamber, measurement mound, and sensor arrays, the exploration of various sound and ultrasound acquisition systems, and the analysis of how the acquired data could be used for sound source and object detection. The acoustic chamber is used to create a clean environment which isolates the experiment from external noises and reduces reverberation. The measurement mount is used to accurately position the source. The sensor arrays are used to experiment with different geometries and with different numbers of sensors. The acquisition systems explored include a novel standalone field-programmable gate array (FPGA) micro-electro mechanical microphones (MEMS) array system and various acquisition systems consisting of independent circuits, components, and test equipment. The circuits considered are the microphone and ultrasound transducer amplification and filtering circuit. Pertinent modern test equipment, such as digital oscilloscopes and arbitrary waveform generators,

and their features which are related to acquisition and generation of data are also explained. This work concludes by discussing how several sound and ultrasound localization, matched filtering, and ultrasound imaging experiments were conducted and what the results of those experiments were.

CHAPTER 1

INTRODUCTION

1.1   Motivation

There is currently an enormous amount of research and applications which use sound and ultrasound detection and analysis. Some of the research topics of sound detection and analysis are sound source localization, sound source tracking, identification of multiply sound sources, separation of multiple sound sources, acoustic scene analysis and sensor network technology [Ben08, Bra01, Hyv00, Hyv01 Ran03, Tur10]. These techniques have a wide variety of applications such as teleconferencing, multi-party telecommunications, hands-free acoustic human-machine interfaces, computer games, dictation systems, hearing-aids, and many more [Alg08, Ben08, Bra01, Tur10, Wan96]. Similarly there is myriad of research concerning the use of ultrasound detection and analysis. Some of the prominent topics which use ultrasound are material analysis both organic and non organic, air and water security and surveillance systems, and air and water robotic vision systems. The applications of ultrasound material analysis include medical diagnostics, structural failure analysis of buildings or bridges, and mechanical failure analysis of machines such as vehicles or aircrafts. Robotic vision has applications in robotic automation, these could be for home use systems such as an automated appliances, industrial use such as assembly lines, and military use such as automated aiming and guidance systems [Har08, Li06, Lla01, Nel08, Wel06].

While all of the above topics and applications may seem straightforward from a theoretical and mathematical perspective in practice there are a large number of issues encountered in a real environment which make realistic application of the theory

significantly more difficult [Ben08, Bra01, Gri02]. The most obvious problem when working with sound and ultrasound is noise. Noise can either be ambient sound e.g. computer fans, background discussions, ambient ultrasound noise e.g. lights, or electrical noise of the sound/ultrasound acquisition system. Another difficulty when working with a variety of sources like human speech is that speech is a wideband non-stationary signal, i.e. it contains a broad range of frequencies and that range changes with time. Yet another difficulty with both sound and ultrasound is reverberation or echoes. This is a significant issue since echoes have the same spectral content as the original signal of interest. When using highly directional ultrasound this issue is somewhat less significant since the type signal does not scatter as much as sound, however this issues is still present when using omni-directional ultrasound transmitters. Another issue encounter when using ultrasound is its high frequency which requires higher speed systems and prevents the use of some algorithms which could be used for sound this happens because the error due to sound propagation becomes significant when compared to the frequency and phase of ultrasound.

1.2 **Objectives and Contributions**

The objectives and contributions of this work are the following:

- The exploration of the basic geometry and mathematics behind source direction of arrival estimation and localization.

- The exploration of ultrasound based matched filtering.

- The exploration of ultrasound based object imaging.

- The exploration of different sound and ultrasound acquisition methods including a novel self-sufficient FPGA, MEMS based system and a general oscilloscope based acquisition system with its associated circuitry.

- The design of an anechoic chamber and measurement mount which would allow for a controlled experimental setup for the exploration of the various sound and ultrasound topics while accurately varying parameters such as noise reverberation, distance, and angles.

- Design of adjustable sensor arrays which would allow source localization to be explored with a variety of sensor geometries and a variety of sound and ultrasound sensors.

- The exploration of source localization and object detection techniques which could be applied to the acquired sound and ultrasound data.

CHAPTER 2

THEORETICAL BACKGROUND

Sound and ultrasound source localization is the process of determining the position of an acoustic source, such as a human speaker, a stereo system speaker, or an ultrasound transducer using two or more receivers or microphones. A similar but separate topic is direction of arrival estimation (DOAE) which only determines the direction of the sound source but not the distance to it [Ben08, Tel07]. Both localization and DOAE can be broken down into several types. One distinction that can be made is whether 2 dimensional (2D) source localization and DOAE or 3 dimensional (3D) localization and DOA is being performed. This simply refers to only looking for a sound source in a plane, i.e. only horizontally or vertically, or in full 3D space. Yet another consideration of source localization is whether near-field or far-field modeling is being used [Ben08, McC01, Zio00]. Additionally source localization can be categorized by the type of information used to perform the localization namely delays between the source's transmit time and receivers' pickup times, delays between only the receivers' pickup times called time difference of arrival (TDOA), or power based localization. In this work the first two sets of information are used as the power based methods are not sensitive enough for accurate estimations when using a passive system.

Localization and DOAE approaches can also be separated by the type of source signal being used, which could be continuous or pulse based, single amplitude or multiple amplitude, and single frequency or multiple frequency (in this work only single amplitude and single frequency source signals are used). Lastly localization and DOAE can be separated by the type of TDOA and power based algorithms being used. For pulse

based signals the TDOA algorithm could be a threshold value detector which determines at which point a signal was transmitted or received. For continuous signals where phase is used the TDOA algorithm could be standard cross correlation, phase transform general cross correlation, or other algorithms [Ben08, Bra01, Gri02. Mun03, Tel07].

Independent of the type of approached used both localization and DOAE can be divided into three general steps: collecting data across multiple receivers and/or transmitters, finding the phase difference and/or time difference of arrival, and calculating the direction and possibly distance to the sound source. The two more complex steps are finding the phase difference/TDOA and determining the angle/distance. As stated earlier finding the difference/TDOA depends on the type of algorithm used leading to a large number of approaches. Determining the angle and distance from the phase information depends on the interpretation of the collected data and depends on a large number of factors, discussed in detail later in the chapter, such as source signal type, the model being used, the number of receivers that are used, whether 2D or 3D estimation is being performed, and whether DOAE or localization is being performed.

All of the above considerations also apply to ultrasound source DOA estimation and localization. However due to the high frequency of the source signal phase based estimations cannot be directly used due to aliasing and pulse based ranging techniques have to be used instead. Nonetheless methods have been developed to use a combination of pulse based ranging techniques with phased based techniques for highly accurate ultrasonic measurements [Que06].

2.1 2D DOAE

2D DOAE is the simplest case. Figure 2.1 below illustrates the geometry of the problem:
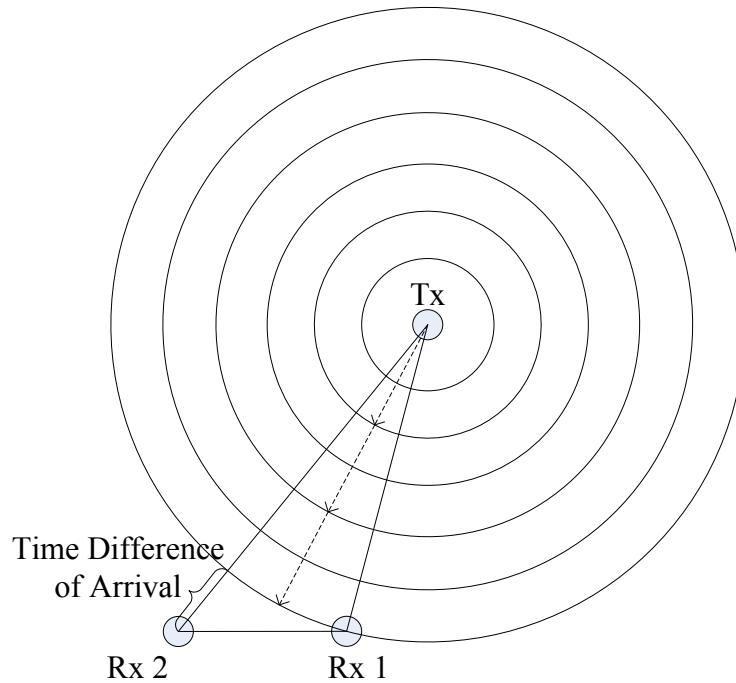
Figure 2.1. DOA Geometry Top View

In this figure a source transmitter (Tx) is emitting a signal. This signal will then propagate through the air to the two receivers (Rx1 and 2). As can be seen from the figure since the two receivers are at different distances from the source the signal will reach them at different times, this is referred to as the TDOA. Based on this TDOA the direction of the source with respect to the receivers can be estimated. From this it can be observed that the estimation will be affected by the speed of sound in the air. The speed of sound in the air is in turn affected by the pressure and temperature. However changes in pressure and temperature in a regular room environment are quite small, producing a change in the speed of sound of less than 2% and can thus be neglected for purposes of this work.

The estimation of the direction can then be obtained through two models. The first is the simplified far-field model [Ben08]. The far-field model assumes that the receivers are far enough away from the source as to allow the spherical wave propagation shown in figure 2.1 to be approximated by planes. This is similar to seeing the Earth as flat, thus if the distance between the receivers is small compared to the distance between the receivers and the transmitter the sound wave can be approximated to be a propagating plane. This model is shown below in figure 2.2:
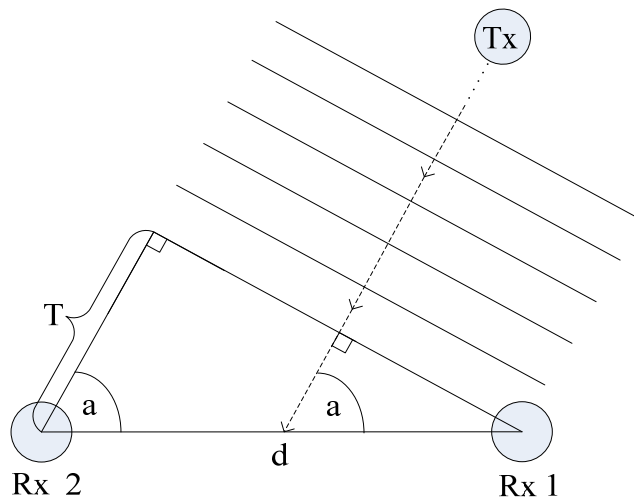
Figure 2.2. DOA Far-Field Model

In this model the angle that the source makes to the plane connecting the two receivers is given by a, the distance between the receivers is d, and the distance corresponding to the TDOA is T. At this point it should be noted that the TDOA is the information that is directly obtained from the receivers and T is given by equation (2.1) below:

$$T = TDOA * c \qquad\qquad (2.1)$$

Where c is the speed of sound, approximately 344m/s, and the TDOA is the delay in seconds between the two received the signal. The inter-receiver distance is typically

known since it can be set or measured by the designer or user. From this model it can be

seen that the angle of the direction of the source to the receivers can be related to T and d

by equation 2.2 given below:

$$T = \cos(a) * d \tag{2.2}$$

Thus equation 2.3 below is the final equation which gives the direction of the

source:

$$\text{angle} = \text{acos}(T/d) = \text{acos}(TDOA * c/d) \tag{2.3}$$

A general model without approximations is called the near-field model, even

though it is correct for both sources that are close and far away from the receivers. This

model corresponds to using the real spherical wave propagation as shown in figure 2.1.

DOA estimation with this model however cannot be obtained from only the TDOA of

two receivers, instead this model requires the distances (or equivalently the time delays

between when the signal was transmitted and when it was received) from the source to

each of the receivers. If the distance to each receiver cannot be obtained the alternative is

to use three receivers which would allow DOA estimation using the near-field model and

only the TDOA information. This model is not very useful for DOAE since the

information or number of receivers used for this model allows localization to be

performed which is superior to DOA estimation as will be discuss later in section 2.3.

The mathematics behind DOA estimation using two receivers and the near-field model is

shown in figure 2.3 below:
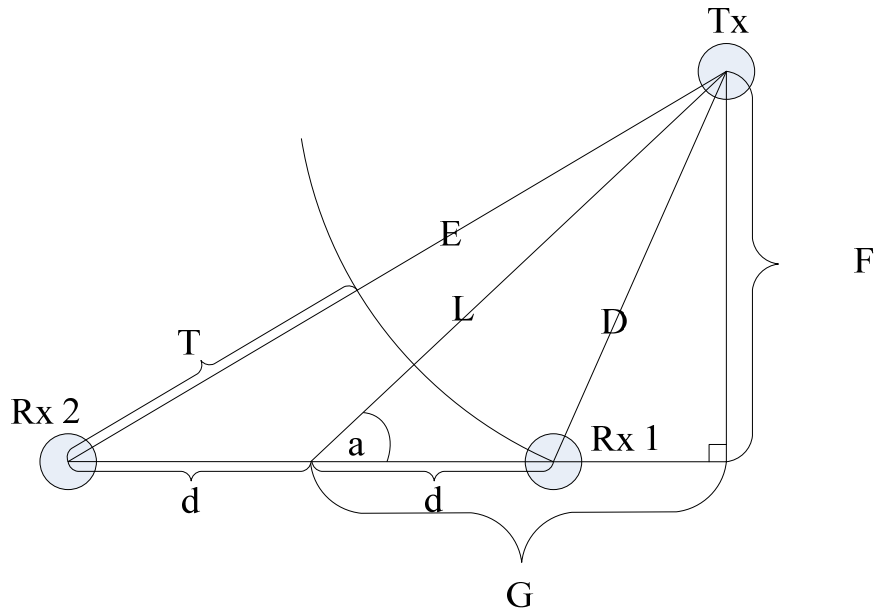
Figure 2.3. DOA Near-Field Model

In figure 2.3 above, d is half the distance between the receivers, L is the distance

from the center of the line connecting the two receivers to the source, D and E are the

distances from receivers 1 and 2 to the source, respectively, T is the distance

corresponding to the TDOA and a is the angle giving the direction of the source with

respect to the center of the plane connecting the two receivers. As last time the

conversion between the measured TDOA and T is performed using equation 2.1. As can

be seen from the figure 2.3, T can be expressed as shown by equation 2.4:

$$T = E - D \tag{2.4}$$

L can be expressed as shown by equation 2.5 below:

$$L = (E + D)/2 \tag{2.5}$$

Distances F and G can then be expressed as given by the below equations:

$$\sin(a) = F/L \tag{2.6}$$

So

$$F = \sin(a) * L \tag{2.7}$$

And

$$\cos(a) = G/L \tag{2.8}$$

So

$$G = \cos(a) * L \tag{2.9}$$

Now using the Pythagorean Theorem distance D can be expressed by equation 2.10 shown below:

$$D = \sqrt{(L * \cos(a) - d)^2 + (L * \sin(a))^2} \tag{2.10}$$

Similarly distance E can be expressed by equation 2.11 shown below:

$$E = \sqrt{(L * \cos(a) + d)^2 + (L * \sin(a))^2} \tag{2.11}$$

Plugging equations 2.1, 2.10 and 2.11 into equation 2.4 leads equation 2.12 which is the final result, giving the relationship between the TDOA and the source angle:

$$TDOA * c = T = E - D =$$

$$= \sqrt{(L * \cos(a) + d)^2 + \left(L * \sin(a)\right)^2} - \sqrt{(L * \cos(a) - d)^2 + \left(L * \sin(a)\right)^2} \tag{2.12}$$

2.2   3D DOAE

The TDOA DOA estimation in 3D is similar to that in 2D. When the far-field model is used the TDOA from three receivers is sufficient to find the direction to the source. Three receivers are necessary instead of two because two receivers actually give an arc of directions or in other words a cone of possible location of the source. This can be seen by viewing figure 2.1using an isometric view as shown in figure 2.4 below:
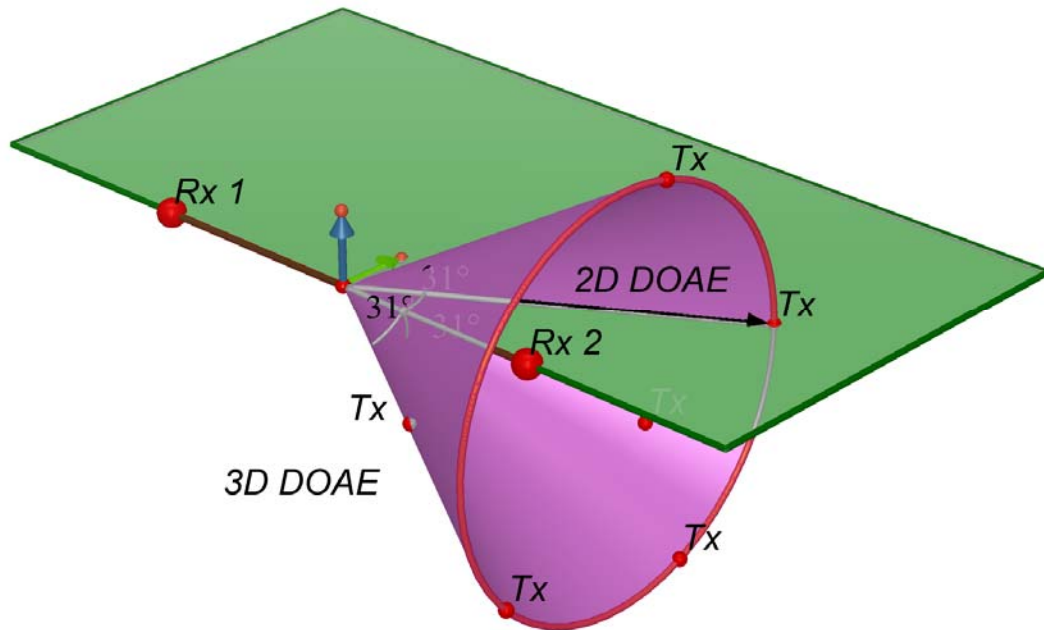
Figure 2.4. DOA Geometry Isometric View

When performing 2D DOA estimation one of the planes is assumed to be fixed thus the possible locations of the source is reduced to one which is in the plane of interest.

In 3D DOA estimation any two pairs of the three receivers could be used to determine two cones of possible points where the source could be. The location of where these two cones intersect forms a line which gives the direction of the source. Geometrically the three receivers being used have to be positioned in a plane i.e. not on a line. This is because any two pairs of receivers on a line will give the same arc of possible transmitter directions. One possible geometric arrangement of a three receiver system for 3D DOA estimation is shown in figure 2.5 below:
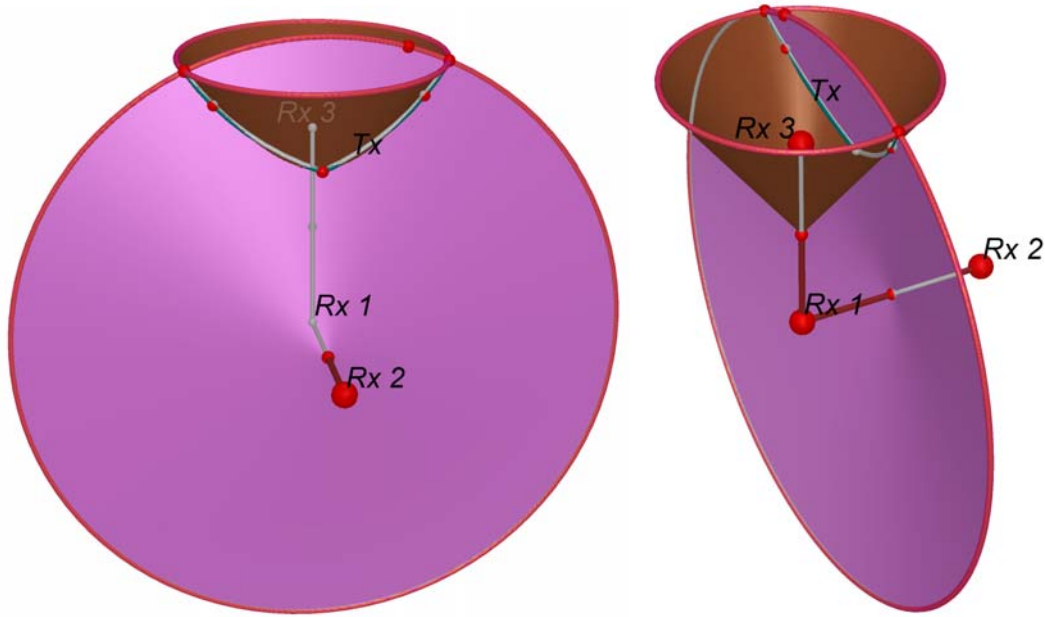
Figure 2.5. 3D DOA Using 3 Receivers

In this figure the four angles shown in each diagram are equal and represent one of the angles to the source in one of the three planes. Thus the mathematics used to determine the 3D DOA is the same as that for 2D DOA estimation, only here the operation needs to be performed twice for the two pairs of receivers and the results are interpreted as giving the two angles of spherical coordinate system. As can be seen from figure 2.5 when three receivers are used the two angles are centered on different points. This however is negligible when the distance between the receivers is significantly smaller then the distance to the source. Mathematically the result of using two different center points is that the intersection of the two cones will form a parabola instead of a line, however recalculating to compensate for the two different center points will again give a line (i.e. direction) instead of a parabola. To avoid the issues associated with having different center points a four receiver arrangement, with each pair being centered on the same point as shown in figure 2.6 below, can be used:
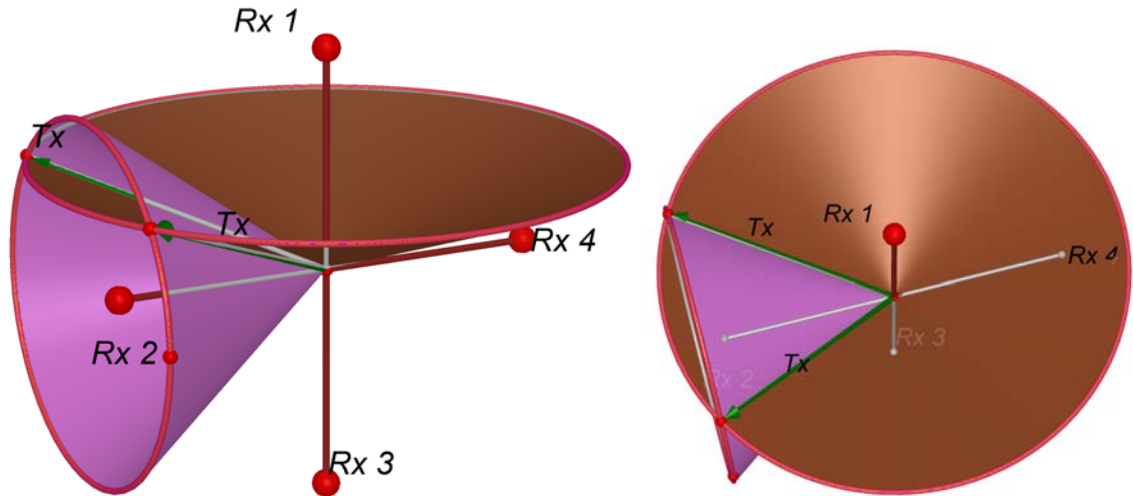
Figure 2.6. 3D DOA Using 4 Receivers

When this type of arrangement is used the cones will always intersect along their boundary making their intersection a line which gives the direction of the sound source.

If the near-field model is to be used then for a three receiver arrangement the distance between the receivers and the source needs to be known. Alternatively DOAE can be performed with the TDOA of four non collinear receivers. However as for the 2D DOAE case the near-field model is not useful since the same amount of information or the same amount of receivers could be used for localization.

2.3   2D Localization

2D localization can be performed with 2 receivers when the distances between the source and the receivers are known and with 3 receivers when only the TDOA information is known. The geometries for 2D localization using three receivers can be divided into two groups: one where the receivers are arranged in a line and the other where the receivers are arranged in a plane. The basic geometry and math with the receivers arranged in a line is shown in figures 2.7 below [Ben08]:
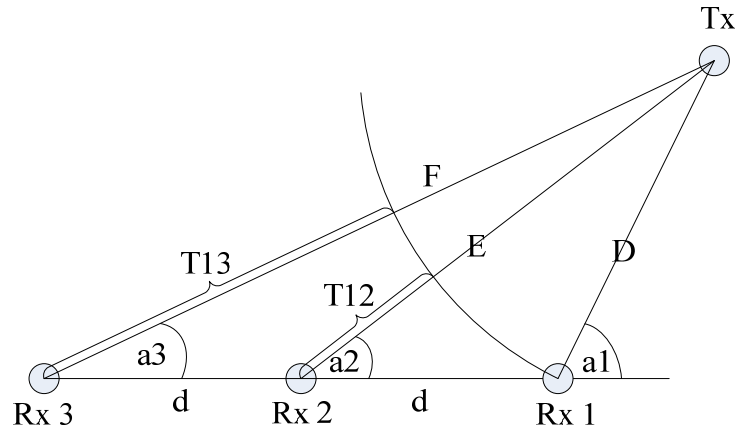
Figure 2.7. 2D Localization Geometry Type 1

In this model a1, a2, and a3 are the angles from receivers 1, 2, and 3 to the source, respectively. D, E and F are the distances from the source to receivers 1, 2, and 3, respectively. The distance between the receivers is d, in this example the two distances are made to be equal for simplicity but if they were different the calculation would still work. The distances T12 and T13 are those corresponding to the TDOA between receivers 1 and 2, and between receivers 1 and 3, respectively and are given by equations 2.13 and 2.14 below:

$$T12 = TDOA12 * c = E - D \qquad (2.13)$$

$$T13 = TDOA13 * c = F - D \qquad (2.14)$$

Using the law of cosines equations 2.15 and 2.16 can obtained to relate distances D, F, E, d and angle a1.

$$E^2 = D^2 + d^2 + 2 * D * d * \cos(a1) \qquad (2.15)$$

$$F^2 = D^2 + (2 * d)^2 + 2 * D * 2 * d * \cos(a1) \qquad (2.16)$$

From these equations it can be seen that if the distances (E or F) between the source and the receivers are known then only two receivers are necessary to localize the

source directly from one of the above equations. However if only the TDOA information is given equations 2.13 and 1.14 need to be substituted into equations 2.15 and 2.16 leading to equation 2.17 and 2.18 below:

$$(\text{TDOA12} * c + D)^2 = D^2 + d^2 + 2 * D * d * \cos(a1) \qquad (2.17)$$

$$(\text{TDOA13} * c + D)^2 = D^2 + (2 * d)^2 + 2 * D * 2 * d * \cos(a1) \qquad (2.18)$$

Equations 2.17 and 2.18 are two equations in two unknowns since the TDOA12 and the TDOA13 will be the collected data and d as well as c are known quantities. Using equations 2.17 and 2.18 the variables D and a1 can be solved for. Next equations 2.13 and 2.14 can be used to solve for E and F. Now applying the cosine rule to triangle D, d, E gives angle a2 and applying the cosine rule to triangle E, d, F gives angles a3. Thus as can be seen the distance and angle from each receiver can be obtained. Solving equations 2.17 and 2.18 can be done through the use of a computer program but from this derivation it can be observed that finding the distance and angle is computationally more complex then only finding the direction. Alternatively to the above derivation, which uses the law of cosines, two and three circle equations can be used for localization for the two and three receivers on a line geometry similarly to how they are used in the next section for receivers on a plane geometry.

The basic geometry and math with receivers arranged on a plane is shown in figures 2.8 below, here the receivers are arranged in an equilateral triangle however this is only to simplify the math and any triangle geometry would work. In this geometry it is assumed that the source is located in-between the receivers.
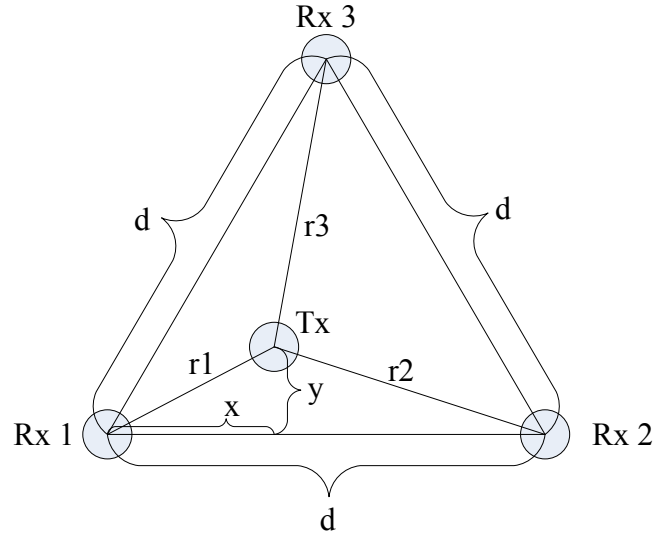
Figure 2.8. 2D Localization Geometry Type 2

In this model d is the distance between the receivers, r1, r2, and r3 are the distances between the receivers and the source, x and y are the coordinates of the source, 0 and 0 are the coordinates of receiver 1, d and 0 are coordinates of receiver 2, and d/2 and $d*\sqrt{3}/2$ are the coordinates of receiver 3. If the distances (any two such as r1 and r2) are known then only two receivers are needed, assuming the source is known to be in the front or in the back of the two receiver. In such a case r1 and r2 can be expressed as given by equation 2.19 and 2.20 below:

$$r1 = x^2 + y^2 \qquad\qquad (2.19)$$

$$r2 = (d - x)^2 + y^2 \qquad\qquad (2.20)$$

Since these are two equations in two unknowns they can be directly solved for x and y. If the distances are not known but instead only the TDOA information is known the then all three receivers are needed and the following equations also need to be used in addition to equations 2.19 and 2.20.

$$r3 = (d/2 - x)^2 + \left(d*\sqrt{3}/2 - y\right)^2 \qquad\qquad (2.21)$$

$$r3 - r1 = a \tag{2.22}$$

$$r3 - r2 = b \tag{2.23}$$

Here a and b the distances which correspond to the collected TDOA between the three receivers. These are then five equations in five unknowns which could be solved to obtain the x and y coordinates of the source as well as the distances between the receivers and the transmitter.

2.4   3D Localization

3D localization is similar to two the 2D version, however in this case three, four, or five receivers in a plane can be used. When the distances between the source and the receivers are known three non-collinear receivers are sufficient for localization, assuming the front and back of the receivers can be distinguished. The geometry is the same as that shown in figure 2.8 however now there is a z dimension. In this model d is the distance between the receivers, r1, r2, and r3 are the distances between the receivers and the source, x, y, and z are the coordinates of the source, 0, 0, 0 are the coordinates of receiver 1, d, 0, 0 are coordinates of receiver 2, and d/2, d $* \sqrt{3}/2$, 0 are the coordinates of receiver 3. Here all three receivers are placed at a 0 z coordinate for simplicity and any combination of z coordinates would also work. Additionally as for the 2D case the receivers being arranged in an equilateral triangle is a simplification and any triangle would work. The basic geometry of this problem is shown in figure 2.9 below.
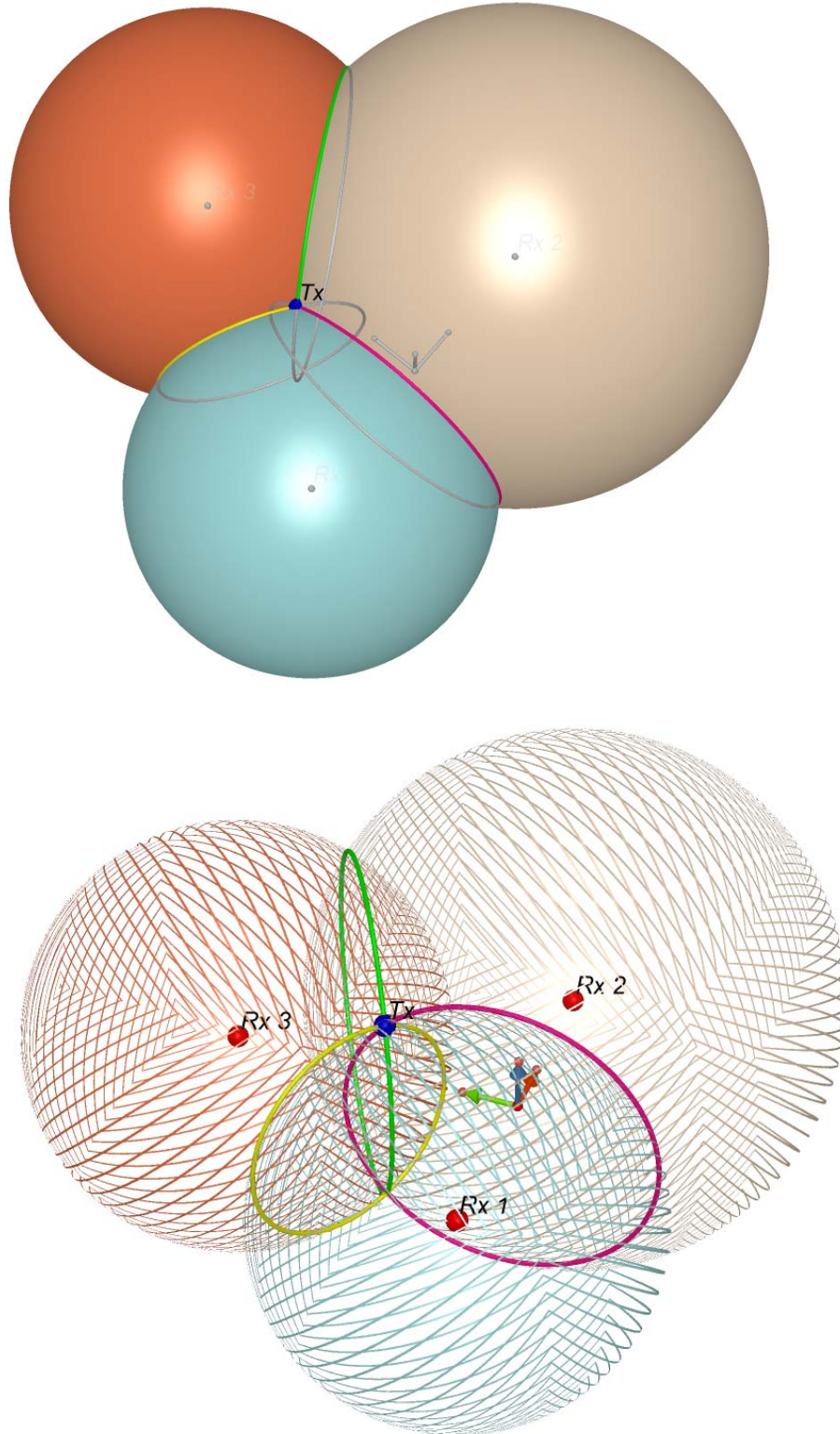
Figure 2.9. 3D Localization Using Three Receivers Type 1

The equations used for localization are three sphere equations where each sphere is centered at the location of a receiver and has a radius equal to the distance between the receiver and transmitter. These equations are given below:

$$r1 = x^2 + y^2 + z^2 \qquad (2.24)$$

$$r2 = (d - x)^2 + y^2 + z^2 \qquad (2.25)$$

$$r3 = (d/2 - x)^2 + \left(d * \sqrt{3}/2 - y\right)^2 + z^2 \qquad (2.26)$$

These are three equations in three unknowns thus allowing the x, y, and z coordinates of the source to be determined. The reason that the three receivers must be non-collinear is because three collinear spheres intersect in one circle instead of a point. When the three receivers are non-collinear the three spheres intersect in two circles and the two circles intersect at a point.

Alternatively if only the TDOA information is known and the distances between the source and receivers are not known localization can be performed using the far-field model estimation with three non-collinear receivers. This approach has the advantage of using a small number of receivers however it is the most computationally and conceptually complex, and is also a rougher estimation. In this case when three receivers are used each pair of the receivers creates a cone giving the possible direction of the source, the location of where these three cones intersect is then the location of source. Since each pair of receivers does not center on the same point some recalculation is required to get the distance and direction from a common center point. The three receiver geometry is illustrated by figure 2.10 below:
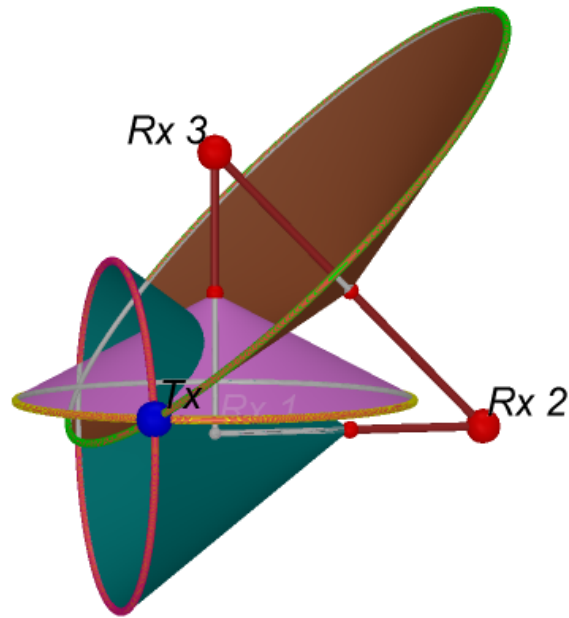
Figure 2.10. 3D Localization Using Three Receivers Type 2

When only the TDOA information is known and the near-field model is to be used four receivers are necessary. Here at least one of the four receivers must be non-collinear with the others. A sample geometry of this four receiver arrangement is shown in figure 2.11 below:
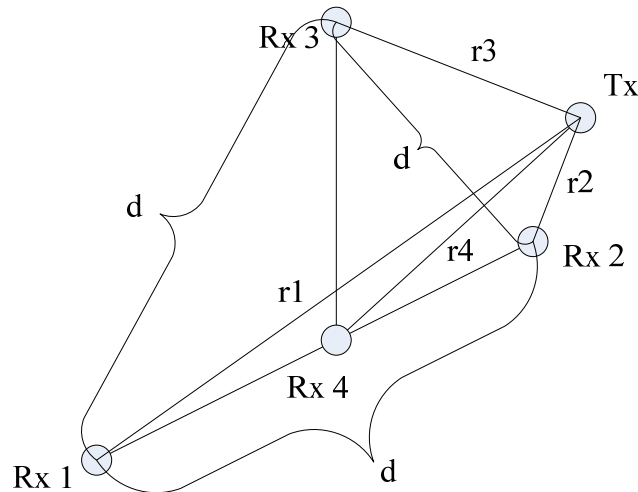
Figure 2.11. 3D Localization Using Four Receivers

In this model d is the distance between receivers 1, 2, and 3, the distance between receivers 1, 2, and 4 is d/2, the distance between receivers 3 and 4 is d $*$ $\sqrt{3}/2$, r1, r2, r3, and r4 are the distances between the receivers and the source, x, y, and z are the coordinates of the source, 0, 0, 0 are the coordinates of receiver 1, d, 0, 0 are coordinates of receiver 2, d/2, d $*$ $\sqrt{3}/2$, 0 are the coordinates of receiver 1, and d/2, 0, 0 are the coordinates of receiver 4. Here again the specific distance and geometry was used to simplify the math but and four non-collinear receiver geometry will work. The equations for this geometry are given below:

$$r1 = x^2 + y^2 + z^2 \qquad\qquad (2.27)$$

$$r2 = (d - x)^2 + y^2 + z^2 \qquad\qquad (2.28)$$

$$r3 = (d/2 - x)^2 + \left(d * \sqrt{3}/2 - y\right)^2 + z^2 \qquad\qquad (2.29)$$

$$r4 = (d/2 - x)^2 + y^2 + z^2 \qquad\qquad (2.30)$$

$$r1 - r2 = a \qquad\qquad (2.31)$$

$$r1 - r3 = b \qquad\qquad (2.32)$$

$$r1 - r4 = c \qquad\qquad (2.33)$$

Here a, b, and c are the measured TDOA. As can be seen these are seven equations in seven unknowns which could be solved to obtain the x, y, and z coordinates of the source as well as the distances between the receivers and the transmitter.

As can be seen localizing the source with four and three receivers geometries can be quite involved mathematically especially when only the TDOA information is available, for this reason the five receiver geometry may be used to simplify the mathematics. Either the distances to the receivers or the TDOA between the receivers can be used for this geometry. This five receiver geometry is shown in figure 2.12 below:
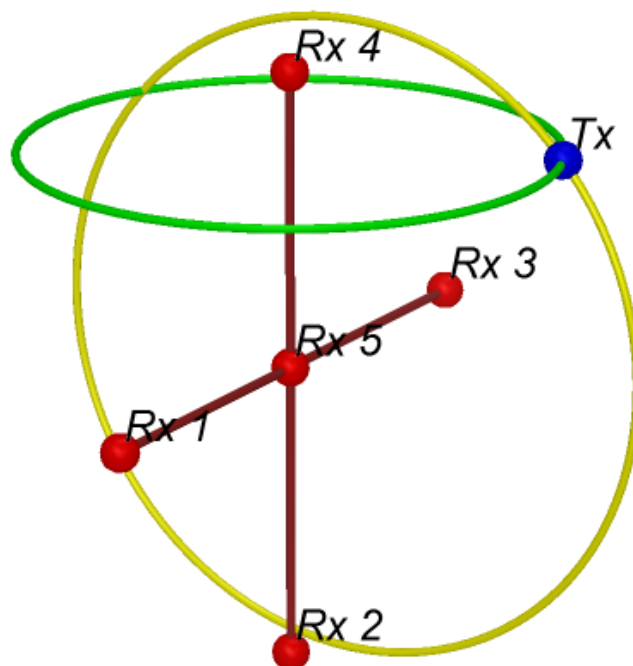
Figure 2.12. 3D Localization Using Five Receivers

The way in which this five receiver geometry helps is by reducing one three dimensional problem into several two dimensional problems. For the case in which only the TDOA information is available, three receivers in each plane are used in the same way that they were used for 2D localization type 1 shown in figure 2.7, with both results using the same coordinate system centered at receiver 5. Since two planes are used all information about the source is obtained. Geometrically this is the same as finding two circles, or semi-circles, the intersection of which is the location of the sound source.

When the distances between the receivers and transmitter are known this geometry again allows the three dimensional problem to be broken down into several two dimensional problems. It should be noted however that the basis for this simplification in this case is that the microphones form an L shape, the five receiver plus shape simply has

four L shapes providing redundancy and reducing error. Here again equations 2.15 and 2.16 are used to obtain the simplified solution.

2.5   Ultrasound DOAE and Localization

The main difference between sound and ultrasound source localization and DOA estimation is that the frequency of ultrasound is too high to get the TDOA from the phase information of the signals received by the ultrasound microphones. This occurs because as frequency of the source signal gets higher its wavelength becomes smaller and the required spatial distance between the microphones becomes shorter, as explained in section 2.6. For example a 40 kHz ultrasound signal has a wavelength of 0.0086 meters requiring a distance between the ultrasound microphones to be less than 4.3 millimeters. This is physically challenging as most microphones will be too large to be placed this close together and clearly any ultrasound frequency above 40 kHz will make the problem worse. Additionally even if the ultrasound microphones could be placed this close together the total maximum TDOA between them would be very small making the system very prone to noise errors.

To avoid the above described issues ultrasound DOA estimation and localization is based on using a train of pulses and then simply measuring the time difference between when this train of pulses begins or ends at each microphone. This removes the requirement of a maximum inter-microphone distance allowing more accurate measurements to be made. Furthermore in this type of arrangement the further the microphones are from each other the more accurate the localization and DOA estimation will be.

2.6   DOAE and Localization Restrictions and Considerations

There are several restrictions present when dealing with the above described DOA and distance estimation. When dealing with phase based experiments the most well known is the temporal sampling theorem which states that the sampling rate of the acquisition system must be at least double that of the highest frequency component of the sound source signal [Pro07]. It should also be noted that while this is the minimum requirement a sampling frequency of several times that of the maximum frequency component of the source signal is desirable so that the collected data could be understood from a visual inspection.

Another similar requirement for phase based experiments is the minimum spatial sampling theorem [Ben08, McC01]. This is basically the same issue as the temporal sampling theorem. This theorem states that for a given maximum temporal frequency in the source signal there is a minimum spatial sampling, i.e. there is a maximum distance between the receivers used in the acquisition system. Specifically this maximum distance is given by equations 2.34 below:

$$d \leq c/(2 * f_{max}) = \lambda_{min}/2 \qquad (2.34)$$

Where d is the maximum distance between the receivers, c is the speed of sound, f_{max} is the maximum frequency of the source signal, and λ_{min} is minimum wavelength of the source signal. This maximum distance requirement exists to avoid spatial aliasing. This can be seen by thinking of a situation where the distance between receivers is longer than the wavelength of the signal. In this situation it would be impossible to determine if the phase difference is equivalent to a fraction of the wavelength or one plus the fraction of a wavelength. This is illustrated in figure 2.13 below:
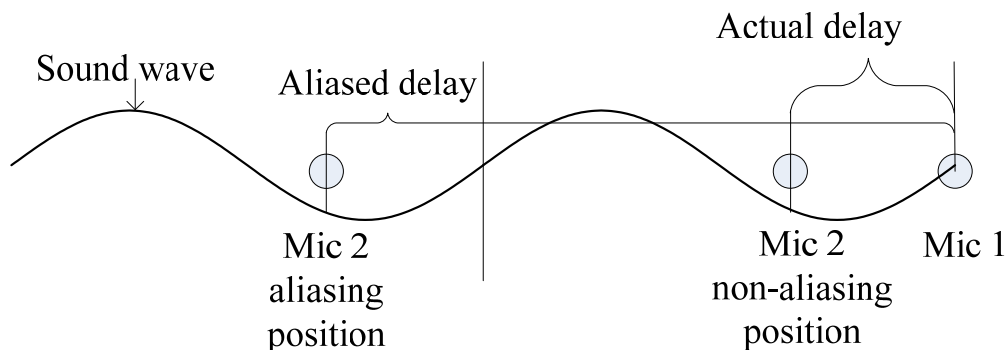
Figure 2.13. Spatial Aliasing Illustration

Yet another issue with all of the above described estimations is that they actually give two possible results one for the front of the systems of receivers and one for the back. This is not a serious concern as we typically know which way our system is looking and which general direction the source is. If these assumptions cannot be made another receiver is needed for all of the above described configurations to determine whether the source is in the back or the front of the system.

A key consideration is when localization can be performed and when the general near-field model can be used [Ben08, McC01, Zio00]. While in a theoretically perfect environment direction and distance estimation can be performed at any distance this does not work in reality. In practice the source has to be sufficiently close to the receivers, i.e. in the near-field. This occurs because the above described calculation depends on the sound wave emanating from the source having a spherical nature when it reaches the receivers. If the source is very far away the received sound wave will look like a plane, shown in figure 2.2. When this occurs the angles from each receiver to the source will be almost the same and the electronic noise error of the acquisition system, the error due to

acoustic noise, air temperature, and pressure variations will become large compared to the actual difference between the angles, leading to incorrect estimations.

Another important matter that must be considered is that when DOAE and localization are performed based on the receivers to transmitter distances the measured distances will not be the same as the theoretically expected values. This is obvious, however this results not only in measurement error but also in the lack of analytical (closed form) solutions to the systems of equations described for the ideal cases. The reason that this occurs is because the distances correspond to radii of circles or spheres centered at the receivers and thus the circles or spheres will intersect in several points (when the radii are larger than the theoretical values) or not intersect at all (when the radii are smaller than the theoretical values). Thus each pair of equations will have multiple solutions when the distances are larger than expected or no solutions when the distances are smaller than expected as opposed to one solution for the ideal case. For these reason interpolation algorithms such as nonlinear least squares and circle intersections with clustering (NLLS, CIC) [Kam07, Nis06] have to be used. It should also be noted that this issue does not arise when TDOA is used for DOAE or localization. The 2D version of this issue is shown in figures 2.14 and 2.15 below, where 2.14 shows the ideal case in which a closed form solution exists and 2.15 shows two cases in which a closed form solution does not exist.

One common point of intersection =
closed form solution exists

Rx 3

Rx 1   Rx 2
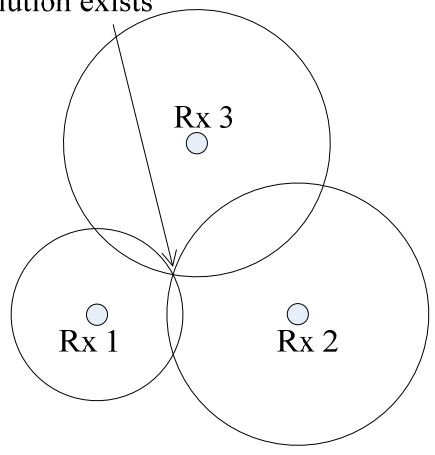
Figure 2.14. Closed Form Solution Example

Multiple points of
intersection = no
closed form
solution exists
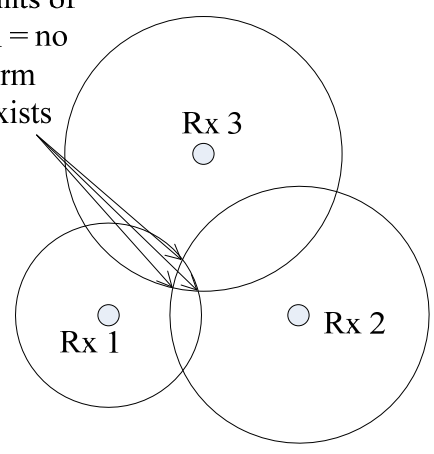
No point of
intersection = no
closed form
solution exists

Rx 3

Rx 1   Rx 2

Rx 3

Rx 1   Rx 2
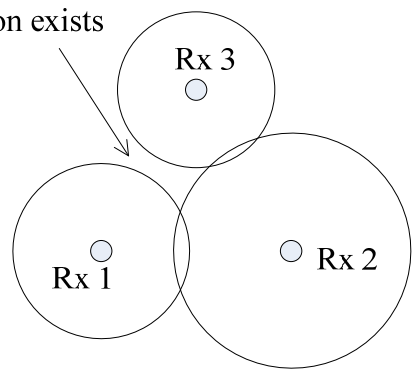
Figure 2.15. No Closed Form Solution Examples

2.7   Matched Filters

Matched filtering is considered in this work as it is a technique which has two

main advantages for DOAE, localization, and ranging. The first advantage that matched

filtering provides is an improved accuracy of DOAE, localization, and ranging

estimations [Que06B]. Specifically matched filtering is used to increase the signal to

noise ratio (SNR) and thus increase reliability for transmitting and receiving information in the presence of additive white Gaussian noise (AWGN). The second advantage that matched filtering provides is the ability to transmit and receive several signals at the same time over the same medium thus allowing the localization of multiple source at the same time.

The technique works by using a known signal template for transmission and then looking for this template at the receiving side of the communications. A key advantage of the matched filter technique is that even if the original templates are mixed with noise or with each other they can still be recovered and their position determined. Typically for matched filtering a range of parameters such as frequency, individual segment duration, overall duration for the template, amplitude, individual segment shape, and overall pattern of segments may be varied. An example of this is shown below in figure 2.15. Figure 2.16 shows how the overall signal can still be seen in the presence of noise.
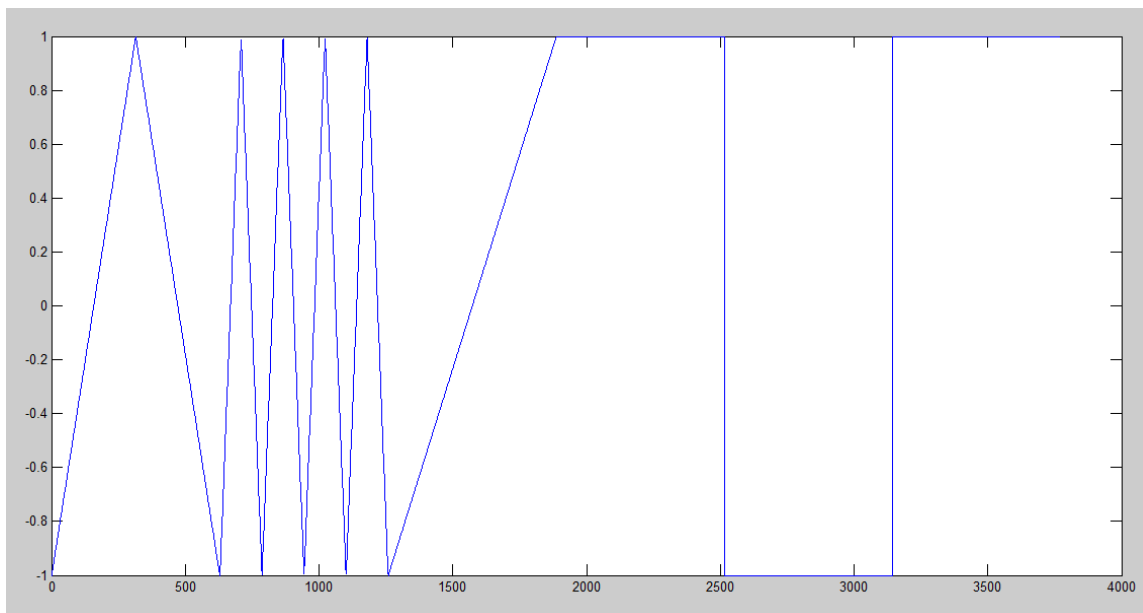
Figure 2.15. Matched Filter Template Sample
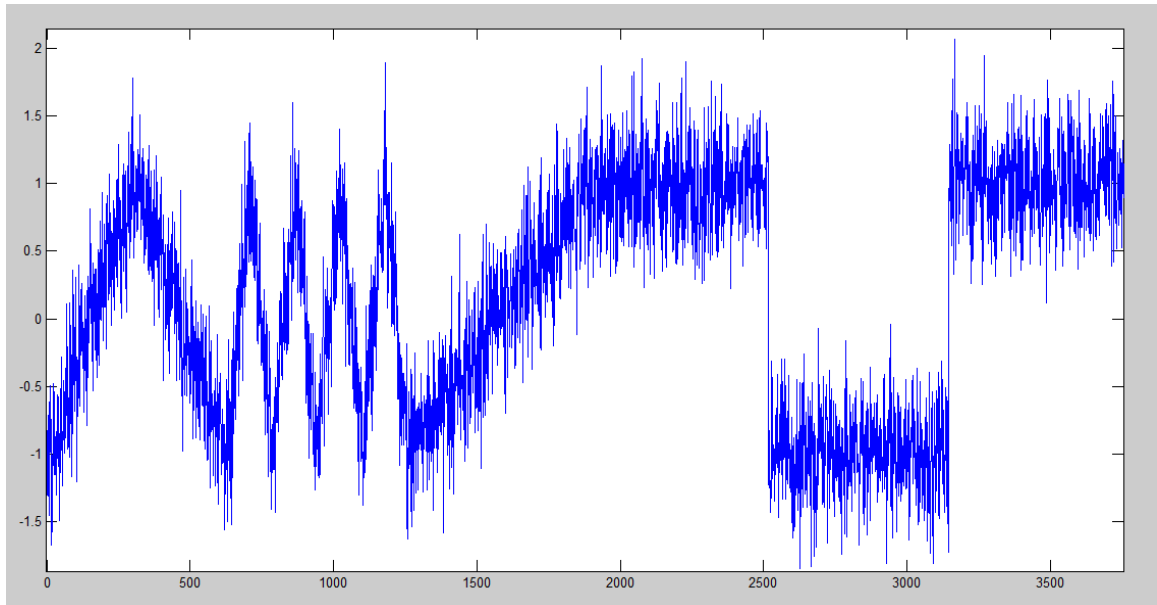
Figure 2.16. Matched Filter Template Sample with AWGN

CHAPTER 3

MICROPHONE ARRAY DATA ACQUISITION SYSTEM

3.1 Introduction

The microphone array data acquisition system (MADAS) used in this work is a

novel PC/FPGA based data acquisition system with an embedded MEMS based

microphone array. The data acquisition system is flexible, expandable, scalable, and has

both logging and real-time signal processing capability. More specifically the system can

collect data from 52 microphones simultaneously at sampling rates up to 300 Ksps

[Nat10, Tur10]. This data can be processed in real-time using the FPGA and then sent to

a PC or alternatively the raw unprocessed data can be sent to a PC. The system to PC

communications is performed through a gigabit Ethernet connection allowing high rates

of transfer for the massive amount of data. Multiply systems can be interconnected and

work in tandem through the use of standard hardware such as routers, making the system

highly expandable. Each system in a network of systems can be connected to a different

PC and different pieces of software of the system can run on different cores of a

processor making the system highly scalable [Tur10].

The system's flexibility comes from the use of a central architecture called the

Compact And Programmable daTa Acquisition Node (CAPTAN). This architecture was

designed to be generally applicable to a variety of data acquisition problems and thus

uses standardized and modular hardware, configware, and software [Tur08].

Physically the system can be separated into three parts namely the Node

Processing and Control Board (NPCB), the Gigabit Ethernet Board (GEL), and the

Acoustic MEMS Array (AMA). The NPCB is the backbone board that contains the

FPGA which contains the system's configware. The GEL board controls Ethernet communications. The MEMS board is the hardware which contains the microphones, amplifiers and analog to digital converters (ADC). Figure 3.1 below illustrates the three hardware components that make up the system [Tur10].
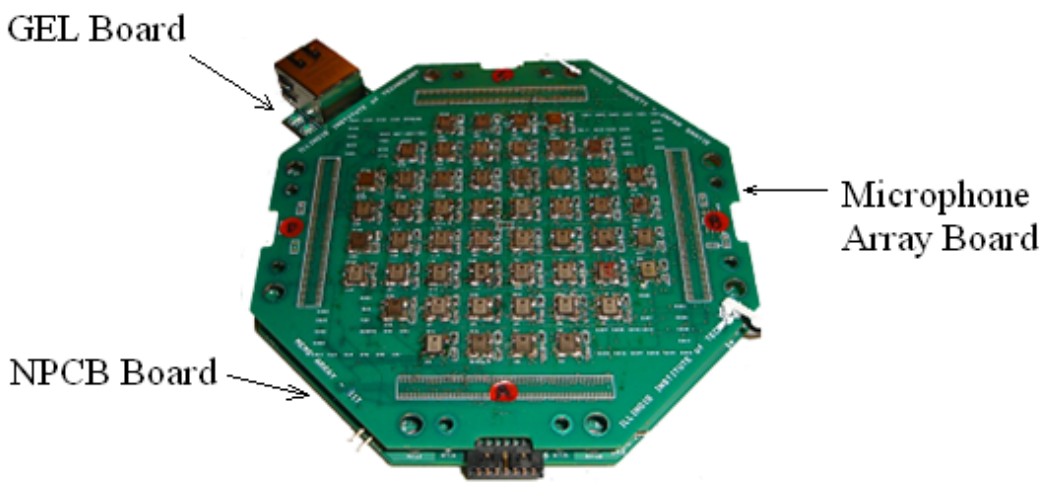
Figure 3.1. Picture of the Microphone Array Data Acquisition System
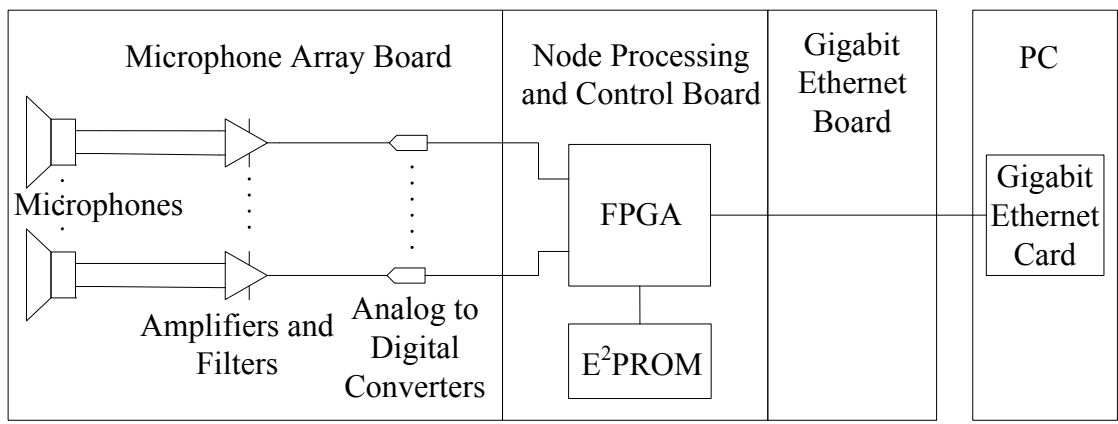
Figure 3.2. Functional Block Diagram of the Microphone Array Data Acquisition System

3.2   CAPTAN Architecture

The CAPTAN architecture is designed to support a distributed system which is based on standalone pieces called nodes. Each node is made up of several interconnected boards which have the capability of communicating with each other. An overall system can in turn be made up of a single or multiple nodes which can also communicate with each other. The CAPTAN architecture can be conceptually separated into three parts or layers: the node layer, the network layer, and the application interface layer [Tur10].

The Node Layer. This layer can be subdivided into three main parts the vertical bus, the horizontal bus, and the hardware boards. The vertical bus is a high speed, large bit width bus responsible for the intra-node communications, i.e. board to board communication within the same node. The vertical bus itself can also be subdivided into three parts: the electrical vertical data transfer bus, electrical vertical system bus, and the optical vertical data bus. The electrical vertical data bus is responsible for transferring data between the node boards. The optical vertical data bus is also responsible for data transfer between the boards in a node but allows even higher speeds. The electrical vertical system bus is responsible for transferring control data between the boards in a node.

Physically the electrical vertical data and system bus share four connectors on the top and bottom of each board. Using these connectors each board in a node is then connected in a stack format. Alternately individual pins of the connectors could be used for interfacing external circuits to the node. Each of the four connectors of the electrical vertical bus consists of 64 pin data bus, a 16 pin data bus, and a 10 pin data bus for a total of 12 data buses. Each of the vertical bus connectors also contains a 48 pin system

control bus and a 16 pin Serial Peripheral Interface (SPI) system control bus for a total of

8 system buses. Lastly the system power is also distributed through these vertical bus

connectors, providing unregulated voltages of 3.3V, 5.0V, 12V and -12V.

The layout of each of the four electrical vertical bus connectors is shown below in

figure 3.3 below:
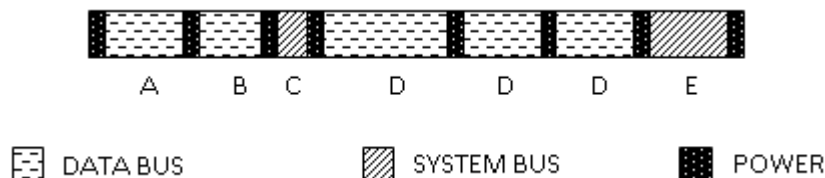
Figure 3.3. CAPTAN Electrical Vertical Bus Connector [Tur10]

In this figure the buses marked A, B, and D are the electrical vertical data buses of 16,

10, and 64 bits, respectively. The buses marked C and E are electrical vertical system

buses of 16 and 48 pins, respectively.

The vertical electrical bus supports two basic types of communication styles

namely single-ended and differential. Single-ended communications are the standard

logic scheme of using a low and high voltage to represent a logic low and logic high. The

single-ended scheme is implemented due to its ease of use. For the single-ended

communications the Low Voltage Complementary Metal Oxide Semiconductor

(LVCMOS) and the Low Voltage Transistor-Transistor Logic (LVTTL) standards are

supported. When operating in a single-ended mode functionally each pin in a bus is used

to transmit a single bit thus the bit width of the data buses are 64, 16 and 10.

Even though single-ended communications are more straight-forwarded,

differential style communications is the standard mode of communications for the

vertical bus. Differential communications are preferred because they reduce errors due to

noise and electromagnetic coupling effects and allow a faster rate of transmission. The standard used for differential communications is Low-Voltage Differential Signaling (LVDS). It should also be noted that when operating in differential mode functionally the bit width of each bus reduces to 32, 8, and 5 bits.

The optical vertical bus is another method of board to board data transfer in a node. The optical interface uses lasers to serially transfer data at rates of up to 1 Gbps. This transfer can be between any two boards in a node stack using the interface independent of the distance between the boards and number of boards being used.

The physical location of the optical transmitters is in the corner of the board in between the electrical vertical bus connectors. For this bus to be used each board in the node stack must either have an optical transceiver in this position or a window. Of course if a certain board uses a window this is only to allow other boards in the stack to use the optical bus as the board with the window will not be able to use it.

The system bus can be divided into two parts the system control bus and the system SPI bus. The system control bus is used by the system arbitration configware of each node to make sure that critical control information, such as the status of the data buses, gets transmitted without being blocked by lower priority signals. The system SPI bus is used to transfer the configware to various programmable components on a CAPTAN node. The system control bus also contains a 33MHz reference clock, the node hardware reset signal, and spare pins for future expansion of CAPTAN system.

Together the system bus arbitration configware and the SPI configware are called the system bus controller which is located on an NPCB board. For this reason each node must have at least one NPCB board. If a node has several NPCBs any one of them could

be used for the system bus controller however only one system bus controller may be used at a time.

The horizontal bus has two main responsibilities which are the inter-node communications, i.e. node to node communications, and the support for communications with secondary boards. The horizontal bus is not directly connected to the vertical bus and thus cannot transfer data between the boards in one node unless additional interfacing is added. The secondary boards connected to the horizontal bus can be systems like the GEL board, which provides an Ethernet interface to PCs and in-between nodes, or other systems that collect and process data. Similarly to the vertically bus the horizontal bus is divided into a data and control segment. The data portion of the horizontal bus uses 32 pins and the control segment, which includes clock and power pins, uses 12 pins. Again similarly to the vertical bus the horizontal bus can operate in single-ended or differential modes.

Figure 3.4 below illustrates the top down view of the standard CAPTAN board. On this figure the four large buses are the four electrical vertical connectors, the optical, mounting, cooling holes, the horizontal (lateral) bus and electronics can be seen.
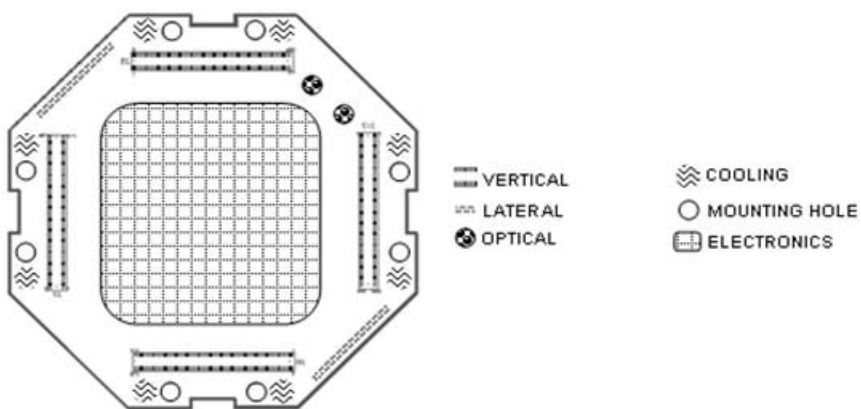
Figure 3.4. CAPTAN System Board Top Layout View [Tur08]

As can be seen from figure 3.4 the four vertical bus connecters are symmetrical around the center of the board. This was done so that the boards could be stacked in four different orientations with respect to each other. This allows for more physical flexibility of connecting external systems to the horizontal buses, since if they all lined up there would be significant size restrictions on the external systems.

The hardware boards which in this work included the NPCB, GEL, and AMA boards are also part of the node layer. The types of boards support by the CAPTAN architecture can be divided into two categories: the primary boards and secondary. The primary boards have three main features. They have direct access and are able to support communications on the vertical bus, they cannot consume more than 12W of power, and they must have the same physical characteristics such as size, shape, location of main buses and location of mounting and cooling holes. Existing types of CAPTAN primary boards are the Node Processing and Control Board (NPCB), the Data Conversion Board (DCB), the Power Electronics Board (PEB), the Mass Memory Board (MMB), and the Acoustic MEMS Array board (AMA).

The secondary boards connect with a CAPTAN node through the horizontal bus and thus must support the horizontal bus interface. They may not have direct access to the vertical bus. They don't have any physical constrains besides having the ability to be connected to the horizontal bus. The other constraints for the secondary boards are that they must not use more than 3W of power. An existing secondary board is the Gigabit Ethernet Link (GEL) board. As the CAPTAN architecture is designed to be expandable either primary or secondary boards with specific functions can be designed as necessary as long as they follow the requirements [Tur08, Tur10].

The Network Layer. This layer of the CAPTAN architecture supports node to node and node to PC communications. On the node side the GEL board is responsible for this communication. On the PC side a standard Gigabit Ethernet card is used. Routers and switches for communication distribution are also supported. To increase speed for real time applications the network layer uses the Universal Datagram Protocol (UDP). For the transport layer the Internet Protocol (IP) is used. The number of nodes in a system is only limited by the maximum transfer rate of the GEL router, and network card of the system. A single node can support up to ten GEL boards allowing for a maximum of 10 simultaneous gigabit rate transfers to one node.

The Application Layer. This layer consists of the various PC software used for user interface and PC to node interface. It was designed to be as modular, scalable and expandable as possible. These features are needed since each CAPTAN node can be made up of different types and number of boards. It is also likely that new types of boards will be used in the future. The expendability is necessary since the number of nodes needed is unknown. Lastly modularity is key since each system requires significant PC processing power thus distributing the processing demand among multiple PCs or multiple cores of a single PC is also desirable.

The application layer can be divided into the CAPTAN Global Master (GM), the CAPTAN Controller (CC), and the CAPTAN Data Acquisition User Interface (DAUC).

The GM is the top most module of the application layer and must be lunched before all others. Only one GM is required for a CAPTAN network and only one may be present at a time. The function of the GM is to manage the other applications in the

network. This consists of adding and removing devices and applications to and from the network, determining the master/slave relationship of various applications, prioritizing controls, and maintaining information about the entire network.

The addition of devices and modules is performed by listening to a specific socket for a TCP/IP connection requests. When a device such as CAPTAN node or module such as DAUC requests a connection the GM performs handshaking to verify that the request is correct and to determine who is requesting the connection. After this a new socket is opened for future communications with the requesting device.

Maintaining the information about the network such as socket numbers, types of devices, and types of applications allows the GM to control the communication between all parties. Additionally the information about the network can be sent to a user if requested.

The CC is the module that is responsible for managing and interfacing a CAPTAN node with the rest of the system. Each CAPTAN node must have one and only one CC module associated with it. The functions performed by the CC are the transmission of commands from the GM to its CAPTAN node and the transmission of data from its CAPTAN node to the GM and to a PC hard disk. Due to the high throughput of the gigabit Ethernet connection the CAPTAN architecture requires some PC memory and uses three threads. One thread is used to receive the gigabit rate data from a CAPTAN node and store it into memory, another is used to receive commands from the GM, and the last one is used to transmit the data stored in the memory to the hard disk. This three thread configuration allows the software to take advantage of multi-

core PC which can run each thread separately thus preventing higher priority command communications from being delayed by data transfers.

The DAUC is the main user interface through which a PC user communicates with the CAPTAN nodes in the network. There can be multiple DAUC running on multiple PC but only one of these may have control. This interface can be used to start and stop data transmission to a PC from the various CAPTAN nodes in the network, to view the data, and to configure any CC. Those DUACs that do not have control can only view the data recorded by the nodes [Riv08, Tur10].

3.3 Node Processing and Control Board (NPCB)

The NPCB is the central board in the CAPTAN architecture with a large number of functions. The two main functions of the board are the control and arbitration of the buses and devices on all boards in a node through the use of the system control bus and the programming of the various devices in a node through the use of the system SPI bus. The board also performs the buffering and processing of information collected by the various boards in a node. Lastly this board serves as the gateway for all information collected in its node which is to be sent to other nodes in the network or a PC. As this board is the central controller of a node at least one of these boards must be present in every node, however more than one can also be used in which case only one of them has master control of the system bus.

The central part of the NPCB is the VIRTEX-4 XC4CFX12 FPGA [Xil08]. This is the unit that performs the processing for the functions provided by the NPCB. Another important component of the NPCB is the 32MB E^2PROM. This E^2PROM is connected to

the FPGA and is used to store permanent configware which is required to run on the FPGA when the node powers on. The configware stored in the E^2PROM include the System Bus Controller, and for the microphone array data acquisition system the configware also includes the Acquisition Control Module, the Signal Processing Module, and the Ethernet Communications Module.

As its name suggests the acquisition control configware is responsible for getting data from the microphone array. This involves setting up the analog to digital converters with parameters such as sampling rate and bit resolution, receiving data from the analog to digital converters and formatting the data to be used by the signal processing configware.

The signal processing block is the next part in the configware chain and receives its data from the data acquisition module. The function of this module is to process the data collected by the microphones. The simplest and default processing performed by this configware is buffering and transmission of the microphone data in a binary format to the Ethernet communication configware. This configware is the one that would typically be modified by the user of the microphone acquisition system to perform some other processing such as filtering, averaging or other more advance processing algorithms. It should also be noted that since this processing is performed on the FPGA it significantly improves performance possibly allowing real-time functionality.

The Ethernet communications configware is the last in the chain and receives its data from the signal processing module. This module is responsible for formatting the data received from the signal processing module to a UDP format and transmitting it to the GEL board at a gigabit rate. This configware is also responsible for receiving data

through from the GEL board at a gigabit rate and converting it from a UDP format to the format necessary by the other parts of the system.

Physically the NPCB follows the guidelines of a standard CAPTAN board. It has four connecters for the electrical vertical bus, two horizontal buses, and an optical vertical bus for laser communications. In the microphone array data acquisition system the GEL board is connected the NPCB through one of the two horizontal buses. There is also one JTAG connecter on the NPCB board for programming the FPGA and EPROM.

Another important issue with the NPCB boards is that the vertical bus clock speed and in turn the maximum bus transfer rate is related to the number of boards present in a node. The maximum vertical bus clock speed is achieved when only two boards are used. This speed for a single-ended and differential mode of operation of the vertical bus is 200 MHz and 340 MHz, respectively. The largest number of boards that can be used without introducing errors to the vertical bus on both modes of operations is seven. For seven boards the maximum the speed for a single-ended and differential mode of operation of the vertical bus is 33 MHz and 125MHz, respectively.

Figure 3.5 below shows a picture of the NPCB board. The VIRTEX-4 FPGA can be seen in the center of the board. The four large connecters are the four vertical buses. One horizontal bus can be seen on the left side of the board and the second one can be seen on the opposite side of the board. The optical interface can be seen on the bottom of the board. The JTAG connecter can be seen on the top of the board [Tur08, Tur10].
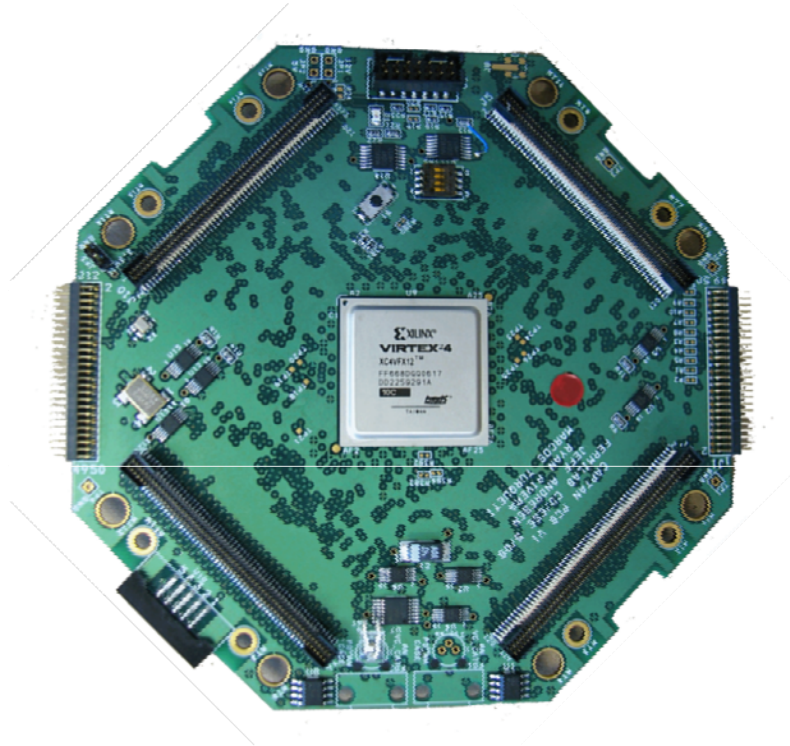
Figure 3.5. Top View Picture of the NPCB

3.4   Gigabit Ethernet Link (GEL) Board

The GEL board is the main network interface device for the CAPTAN nodes. It can be used for node to node and node to PC communications. The main function of this board is to format the information leaving a CAPTAN node into an Ethernet physical and data link layer format and to convert received data from an Ethernet physical and data link layer format. For the network layer the board uses the IP protocol and for the transport layer the board uses the UDP protocol. The physical layer of the GEL board uses the optic fiber 1000BASE-X standard [Tur08, Tur10].

The GEL board also supports the 10, 100, and 1000 Mbps speeds however the default setting and the one used for the microphone array data acquisition system is 1000 Mbps. Due to the various layer framings being used the user data transfer rate is lower

than the overall transfer rate, this relationship and the overall maximum reliable transfer rate are shown in the figure 3.6 below.
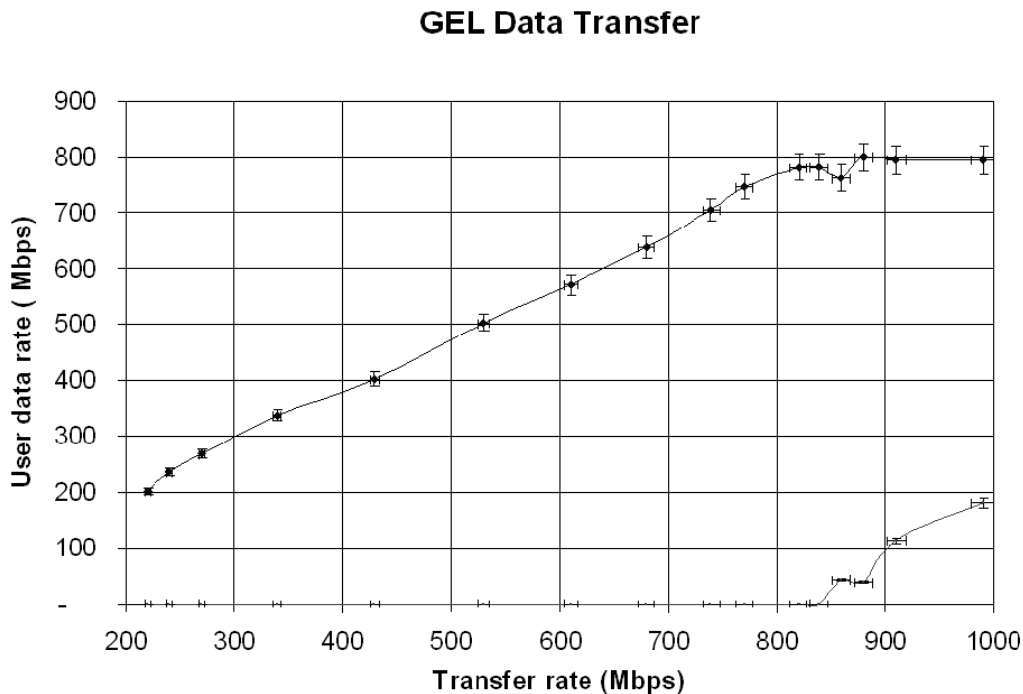
GEL Data Transfer

Figure 3.6. GEL Board Transfer Rate Graph [Tur08]

In this graph the top curve shows the data transferred and the bottom shows the data lost. The vertical axis shows the rate at which useful user data is being transferred and the horizontal axis shows the overall transfer rate which includes the framing information. From this graph it can be seen that the maximum useful transfer rate is just under 800 Mbps.

The GEL board is not a primary CAPTAN board and so it does not have to conform to the same standard CAPTAN board physical requirements. As such this board does not connect to a node through the vertical bus but only through the horizontal bus of NPCB board. Additionally for the GEL board to work the NPCB board which it is connected to must contain the Ethernet communications configware for the IP/UDP

portion of the communications. As each GEL board has its own IP and MAC address there can be as many GEL boards in a node as there are NPCB boards. However due to the high communication speeds of the gigabit Ethernet each GEL board consumes 1.25W of power [Tur08, Tur10].

The GEL board can be seen in figure 3.7 below:
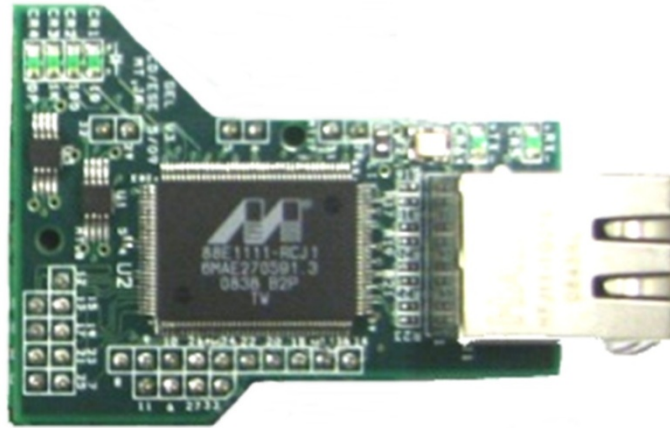
Figure 3.7. Top View Picture of the GEL Board

3.5   Acoustic MEMS Array (AMA)

The AMA board is a custom primary type CAPTAN board for acoustic and ultrasound acquisition. This board uses 52 MEMS microphones for its sound and ultrasound acquisition. In support of the 52 microphones the board also contains 52 amplifiers, 52 highpass filters, 52 analog to digital converters, and 52 of the circuits connecting and regulating the microphone, amplifier, filter, and ADC configuration [Tur10].

The 52 microphones are arranged in eight horizontal and eight vertical rows in an octagonal shape matching the shape of the board. The inter microphone spacing is 10mm center to center horizontally and vertically. The spacing of 10mm allows for spatial

sampling of sound of up to 17.2 kHz with no aliasing in the phase information. This maximum frequency value can be obtained as described in chapter 2. Figure 3.8 below shows a top down view of the AMA board.
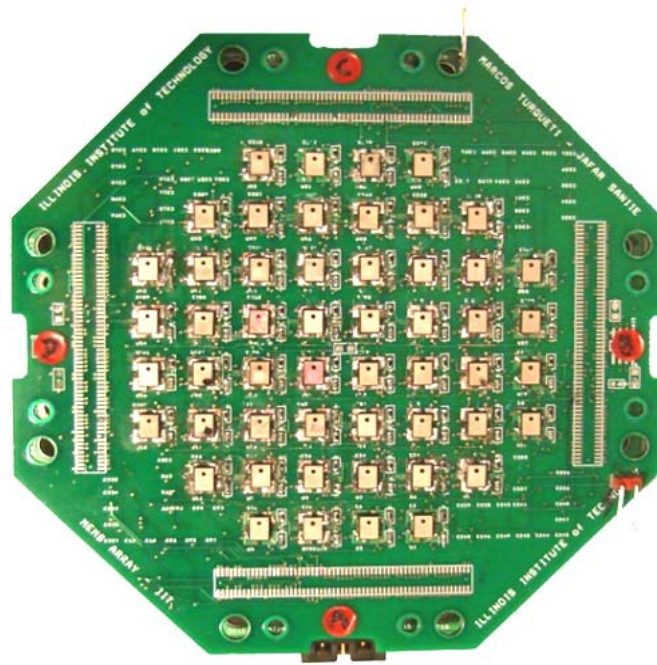
Figure 3.8. Top View Picture of the AMA Board

In this figure the MEMS can be seen as little silver rectangles with a black dot on top. From this figure it can also be seen that the AMA board has the same physical arrangement as the NPCB board having the same four vertical electrical buses, cooling connecter and mounting holes.

In order to be able to collect both sound and ultrasound data the AMA board supports the SPM0208HE5 [Kno06A] MEMS sound range microphones and the SPM0204UD5 [Kno06B] MEMS ultrasound range microphone. A key feature of the SPM0208HE5 and SPM0204UD5 microphones are that they are only 3.76mm by 4.72mm allowing for the high microphone density required by this design. These microphones are omni-direction and provide a signal to noise ratio of 59 dB nominal. The

SPM0208HE5 provide a high nominal sensitivity of -22 dB or 79 mV/Pa and the

SPM0204UD5 has a nominal sensitivity of -42 dB or 7.9 mV/Pa. The frequency response

of the SPM0208HE5 is almost flat from 0.1 kHz to 8 kHz as shown by figure 3.9 below.
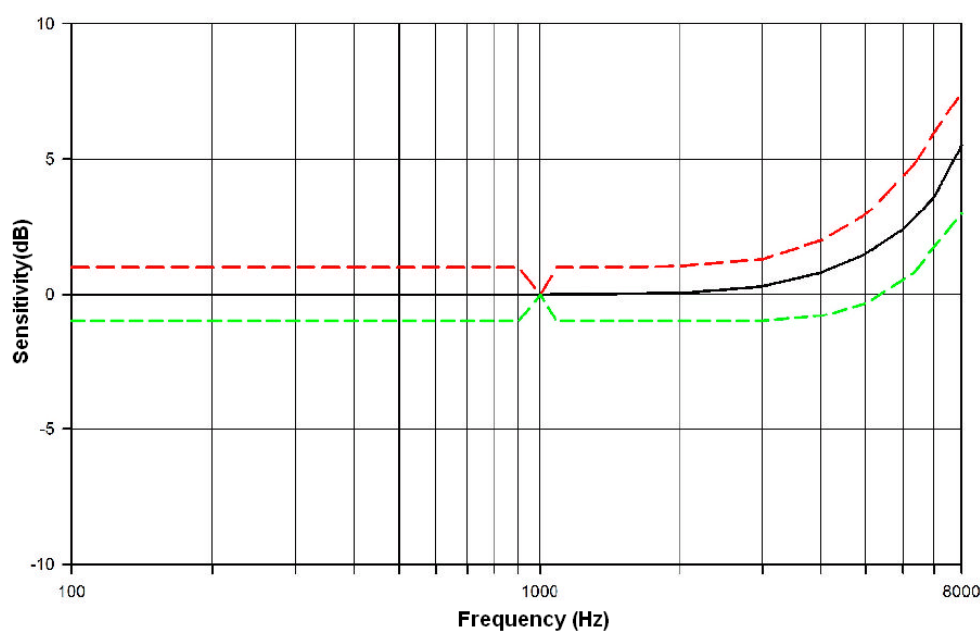
Figure 3.9. SPM0208HE5 Frequency Response [Kno06A]

The frequency response of the SPM0204UD5 varies somewhat but is acceptably

flat from 1 kHz to 100 kHz as shown by figure 3.10 below.
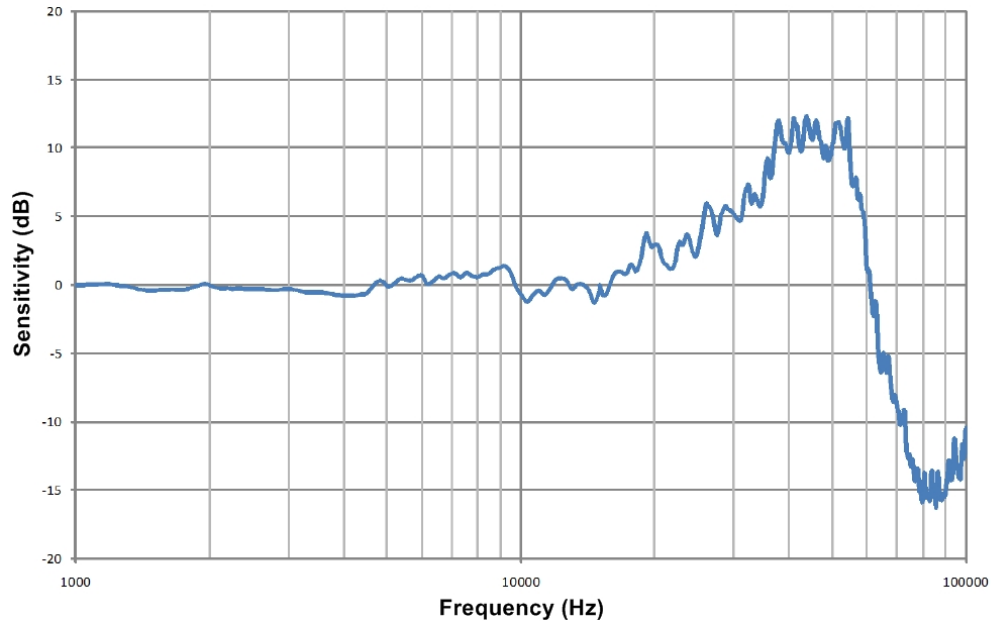
Figure 3.10. SPM0204UD5 Frequency Response [Kno06B]

The AMA board used in this work was made up of the sound range SPM0208HE5 microphones. An important feature of these microphones is that they provide an internal amplifier. The gain of this internal amplifier could be easily adjusted up to 20 dB by an external circuit. In addition to controlling the amplifier gain an external circuit could also be designed to introduce a high pass filter with a selectable corner frequency [Kno06A, Kno06B].

Even though a 20 dB internal amplifier is present in these microphones their output was further amplified by another 20 dB by the TSV991 [STMV06] external amplifier circuit. This was done to put the output voltage of the microphones in the range of the ADC used. The microphone circuit also used two high pass filters one using the internal microphone amplifier and one using the external amplifier.

The overall amplification and filtering circuit for each microphone on the AMA board is shown in figure 3.11 below:
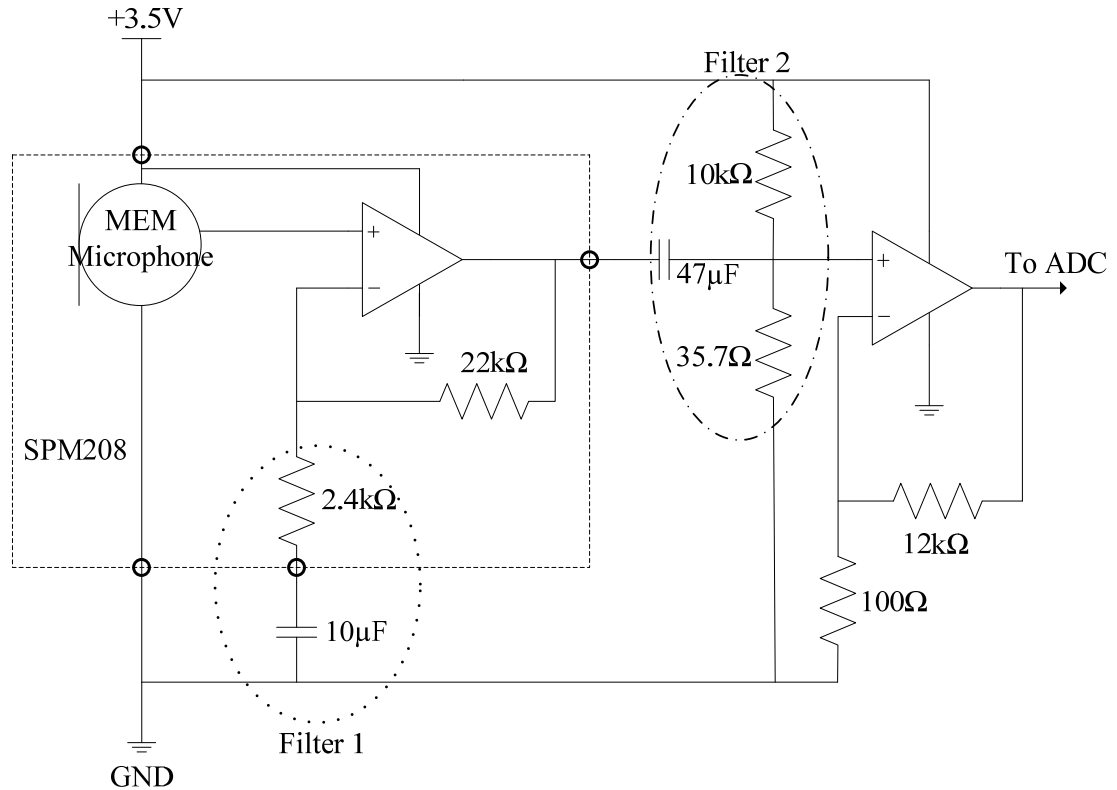
Figure 3.11. MEMS Amplification and Filtering Circuit

In this figure the components enclosed in the dashed box are those that are internal to the SPM0208HE5 microphone. The components enclosed in the dotted circle are those that make up the first high pass filter with a corner frequency of 6.6 Hz. The components enclosed in the dotted and dashed circle are those that make up the second high pass filter with a corner frequency of 130 Hz.

As can be seen from the diagram the output of the amplification and filtering circuit is then handed to the ADC. The ADC used by this system is the ADC121S101 from National Semiconductors [Nat10]. As this is a single channel ADC there is one ADC for each microphone. This is a 12 bit ADC and when used with a supply voltage of 3.3V as is done in this system has a voltage resolution of 0.806 mV. The maximum sampling rate of this ADC is 1 Msps however in this system a sampling rate between 36

Ksps and 300 Ksps is used. When used at the higher sampling rate of 300 Ksps the output of each ADC is 3.6 Mbps. The 52 microphones together generate 187 Mbps which is then transferred through the four vertical bus connecters to the FPGA on the NPCB board. From this it can be seen that the high speed of the four vertical buses and the gigabit Ethernet rate connections are necessary for real-time applications of this system.

It is also important to mention that the AMA board used in this work is the AMA II board which is the second generation of the CAPTAN acoustic array acquisition boards. The AMA I board was used for testing and exploration purposes. The AMA II board was then designed based on the observations obtained from the AMA I board. The main differences between the two boards are that the AMA I board had 48 microphones, the spacing between the microphones was 12 mm center to center, and the first board also contained a central ultrasound transmitter for calibration and range testing [Tur08, Tur10].

3.6   Restrictions and Requirements

This section summarizes the restrictions of the microphone array data acquisition system. The main restriction of this system is that it must be connected to a computer to work. Thus the system does not have its own interface and multiple nodes cannot connect to one another without at least one central PC. However since the system has a central FPGA it is possible to modify the system to have its own display, interface and node to node networking capability.

An important point to mentions is that the PC software for this system uses high speed transmission and requires a high speed processor and a significant amount of

RAM. Specifically the processor should have at least 2 cores at 2 GHz each and there should be at least 2 Gigabytes of fast RAM. The hard-drive storage requirements for this system are also high since as was shown earlier the system transmits approximately 187 Mbps to the PC. From this it can also be seen that even if a large hard drive is used either the recorded data has to be used in real time and the earlier records must be erased to make space for new ones or only a few seconds of data may be recorded.

Another restriction on the system is that the microphones are in fixed positions allowing only one geometrical arrangement. One way to bypassed this limitation is to use multiple systems in a network, however when only several microphones are required this would be an inefficient use of resources. Another way to bypass this problem is to disconnect the microphones from the board place them in required remote locations and then run wiring to the array board.

As stated earlier due to the inter microphone distance the limitation on the frequency of which the phase information can be used without aliasing is 17.2 kHz. The overall limit on the maximum frequency of a signal this system can sampling is 150 kHz since the maximum sampling of the ADC is 300 Ksps and by the Nyquist–Shannon theorem the maximum frequency is half of the maximum sampling rate. Since this system works with sound and ultrasound this is not a large problem as the sound range is significantly lower and most ultrasound applications can also be done at significantly lower frequencies.

3.7   Advantages

The microphone array data acquisition system and the CAPTAN architecture are very versatile, computationally powerful, possess high speed communications, and are designed with a broad range of applications in mind [Tur08, Tur10]. Due to these features this system has a large number of advantages over other data acquisition systems.

One significant advantage of this system is its utility for prototyping. Specifically various algorithms can be tested using a computer with high level programming, such as MATLAB, as opposed to immediately working with a hardware description language. Further due to the gigabit rate of communications algorithm testing can be extend to real-time as the transfer of the data to the PC does not form a bottleneck.

Another important feature of the system is the large processing power provided by the embedded Virtex-4 FPGA. This power can be seen from the system's ability to simultaneously process the data coming in from the 52 ADC of which each is generating 3.6Mbps. In addition to the basic processing being performed on this data the system also has the capability of running more advanced algorithms as required. As the Virtex-4 FPGA is used there is also an option to use the hardcore power PC processer for algorithm implementation [Xil08]. Thus this system allows several approaches for algorithm implementation ranging from the easy to implement but slow performing computer based implementation to the more difficult to implement but faster performing hardware description language implementation.

The large number of input channels of the array is also a key feature. Standard data acquisition systems such as oscilloscopes only use two and less frequently four channels [Agi10B]. Having access to only two or four channels poses several problems.

One is that some applications may simply need more channels of information to function. An example of this is triangulation which requires at least three channels for three sensor inputs, other applications may be distributed sensing or security which may have to collect data from dozens of places and then combine or compare it for an overall picture.

An additional issue with using a smaller number of sensors is that it may increase the computational complexity of the algorithms used to get a certain result from the collected data, that is, it may be easier to extract certain information when a larger number of sensors are used. An example of this is 3D source localization, where it is possible to get the position of a sound source using three microphones, however this would involve solving three 3D conic equations, however if five sensors are used only four 2D triangle equations have to be solved.

Another advantage of using a large number of sensors is that it allows for an increase in the confidence of your results and for a reduction of errors due to various interferences. For example suppose that the same data is being collected by twelve sensors and one or two are giving different readings than the other ten sensors. Since twelve sensors are being used it is possible to discard the data from the two mismatching sensors and still be confident of the result obtained from the other ten sensors.

An advantage of the CAPTAN architecture as a whole is that it was designed to be expandable and scalable. As stated earlier each node can have any mixture of boards as required by the application. Physically the octagonal shape of the primary boards allows for tiling with a corner slot for running cables or wires. Lastly the networking capabilities of the architecture allow a large number of systems to work together in either a distributed or tiled configuration.

CHAPTER 4

GENERAL DATA ACQUISITION AND GENERATION

4.1   Oscilloscope Based Data Acquisition

As a comparison to the custom designed microphone array data acquisition

system, the capabilities of the Agilent MSO6032A standard mixed signal oscilloscope are

explored. Specifically the various techniques of capturing and transmitting data to a PC

are presented. Several different styles of programmatic control and data acquisition are

also investigated. Lastly various interfaces and networking capabilities of the

oscilloscope are examined.

The simplest and quickest way to obtain data from the MSO6032A oscilloscope is

through the use of a USB external storage device. This simply involves connecting the

USB storage device to the scope and using the front panel to configure the scope to save

to the device under a specific name and in a specific format. The possible formats in

which the data can be saved are a graphical image of the display and an XY coordinate

data set file. Each one of the formats can be of several types such as BMP, PNG, ASCII-

XY, BIN-XY, and others. The ASCI-XY and BIN-XY formats can then be loaded to a

PC from the USB storage device. Programs such as Excel and Matlab can then use these

files for algorithm application and graphical display.

In addition to saving the waveform data the overall configuration, such as

triggering, time scale, and voltage scale of the oscilloscope could also be saved and later

recalled to avoid readjusting the settings of the oscilloscope every time it is turned on and

off. The trace of a waveform can also be saved and recalled. This somewhat mitigates the

limitation of having only two or four channels since many traces can be saved and then

recalled for comparison. Another set of information that can be saved is the measurement information of the waveform on the oscilloscope. These measurements can be things like voltage, frequency, duty cycle and many others. The limitation on this type of acquisition is that it involves several transfers one from the oscilloscope to a USB storage device, one from the storage device to a PC, and one from a file on the PC to a program like Matlab. [Agi10B].

The second option for transferring data from the oscilloscope to a PC is to use the Agilent IntuiLink Data Capture software. This is a Graphic User Interface (GUI) software which features all the capabilities described for the USB external storage device but with several advantages. First it directly connects the PC to the scope removing the need for an intermediate storage. This connection can be made using either a USB port and LAN interface, or GPIB interface. The second advantage is that it allows for a convenient PC interface to be used, otherwise the two techniques are the same [Agi09A].

The oscilloscope can also be accessed remotely through the internet using the oscilloscope's built in web server. The functions of this interface can be divided into four groups. First this interface allows you to view, and in some cases modify, information about the oscilloscope like its model number, serial number, host name, IP address, VISA (address), installed options, firmware versions, calibration status, network configuration and status information. Second this interface allows you to get screen images of the oscilloscope's display. This remote interface also allows the oscilloscope to be programmatically controlled using the oscilloscope's Standard Commands for Programmable Instruments (SCPI). The details of how SCPI programming works will be discussed next. Lastly the web server interface allows the users to see and control the

oscilloscope through a GUI of the front panel and screen of the oscilloscope. This is a Java based GUI which is a virtual equivalent of the physical oscilloscope, i.e. the virtual GUI has a screen display which looks like the real physical oscilloscope display and it also has the functionality of all the physical front panel buttons and knobs [Agi10B]. The limitation on this interface is that only the image can be transferred to a remote user and not the actual XY data points. This may be modified later as, in general, it is possible to read the data points using the SCPI commands however there needs to be a way to save this information into a file on the remote PC [Agi10A].

The most complex method but also the one that gives the most control for interfacing with the oscilloscope is through the use of its programming capabilities. This method allows the user to both control the oscilloscope and acquire data from the oscilloscope. In general programming of the oscilloscope can be divided into two groups, direct programming and driver based programming. Each of these approaches can be performed through the use of several different high level programming languages such as C, C++, Visual Basic, LabVIEW, Matlab and many others, the high level programming language used in this work was Matlab.

Direct programming of the oscilloscope is performed by using the instrument specific SCPI instructions or commands. All the functionality of the instrument, in this case an oscilloscope, can be accessed through the use of these commands. However even though these commands are somewhat standardized they still differ from oscilloscope to oscilloscope as each one has different capabilities and accordingly has a different design and different functionality [IVI09]. The commands for this approach are at a low level thus several commands might be required to perform one conceptual operation such as

getting the time scale or reading in a waveform. Additionally programming at this level requires basic knowledge of the oscilloscope's architecture as reading and writing to various status registers is involved at this level of programming. These issues make directly programming the oscilloscope somewhat difficult.

It is however not extremely difficult to program the oscilloscope at this level as the commands are somewhat standardized and are organized in to conceptually easily manageable groups. Also most of the commands correspond to oscilloscope settings and features and thus can be intuitively understood by anyone who uses the standard front panel interface of the oscilloscope. As stated earlier this approach is the most powerful as it gives access to all the features of the oscilloscope. In addition to this using the SCPI commands and a high level programming language, a variety of scripts and programs can be written for the oscilloscope to perform more complex and more controlled data acquisition. These programs can then be run as necessary by people that are not familiar with SCPI command programming.

To send the SCPI commands to the oscilloscope Matlab or another high level programming language needs to be used. This consists of establishing an interface with the oscilloscope and then sending commends or queries and receiving responses. Some of the types of interfaces that can be used are VISA, USB, Serial, GPIB, TCP/IP and UDP. This allows both local and remote control and data acquisition using the oscilloscope. The need to use a high level language on top of the SCPI commands also adds some complexity as both the high level language commands and syntax and the SCPI command and syntax need to be learned. However there are relatively few high level commands used for this purpose [Mat10].

The second programming based approach is to use drivers. Drivers are basically a mapping of SCPI commands to higher level functions and oscilloscope properties. The types of driver can be broadly divided into two groups: instrument specific and instrument type drivers. Instrument specific drivers are designed for a particular instrument such as a specific oscilloscope and thus offer access to all of the instrument's functionality. The advantage of using an instrument specific driver as compared to using SCPI command programming is that instrument specific drivers have easy to understand high level functions or methods instead of a combination of low level commands. For example functions may be as simple as run() to run the oscilloscope or channel1.range(2) to set the voltage range on channel 1 to 2 volts.

However the high level functions used by one instrument specific driver may not be the same as that of another. For example two different instrument specific drivers for two different oscilloscopes may use the following two function to read the voltage scale: agilent.channel1.range() versus teck.chn1.rng(). Additionally different high level functions must exist for different instrument specific drivers since each instrument may have different features such as one being able to calculate cross correlation between two channels and another being able to calculate the Fast Fourier Transform of a channel [IVI09].

The second category of drivers is the instrument type driver. Instrument type drivers address the limitation of the non-interchangeability of the instrument specific drivers. These drivers also have the advantage of using easy to understand high level functions or methods instead of a combination of low level SCPI commands. However the high level functions for instrument type drivers are always the same for a specific

instrument type like an oscilloscope. This is done by having high level functions only for the functionality that is common to all instruments of a specific type. Some drivers like IVI drivers further divide this into base functionality functions and extension functionality functions. Here the base functionality is the absolute least common denominator functionality for an instrument type and has to be supported for all its instrument type drivers using the same functions. The extension functionality is pretty common for an instrument type so it does not have to be supported but if it is, it also uses the same high level functions [IVI09].

Using instrument type drivers for ease of interchangeability of course comes at the price of giving up a certain level of control over the instrument and losing the ability to use all the instrument functionality and features. However the main advantage of using interchangeable drivers is that when a program is written using the functions of an interchangeable driver it can be run for any instrument of that type. The only thing that needs to be changed is the instrument driver that will perform the mapping from the instrument specific SCPI commands to the common high level functions.

Using driver is similar to using SCPI commands in that both use a high level programming language such as Matlab or others as an interface. For drivers this consists of loading the driver and establishing an interface with the oscilloscope. There is a number of ways in which this can be done depending on the driver type and on the high level language used. For example in Matlab this can be done through the command line or through a GUI and for IVI drivers either an instance of the driver or a configuration store and a session factory can be used [IVI09, Mat10]. The same type of interfaces are available for both SCPI command programming and driver programming, specifically the

types of interfaces that can be used are VISA, USB, Serial, GPIB, TCP/IP and UDP.

Thus drivers based programming control and data acquisition can also be done remotely

or locally [Mat10].

4.2   Arbitrary Waveform Based Data Generation

For the sound and ultrasound experiments performed in this work a variety of

different waveforms were needed. Generation of these waveforms was accomplished

through the use of the Agilent 33220A function/arbitrary waveform generator [Agi07]. A

typical function generator can easily generate common waveforms such as a sin, square,

and ramp however sometimes these basic waveforms are not sufficient. For example for

basic ultrasound experiments a pulse or a train of pulses waveform is necessary.

Although this is not a basic waveform some function generators, such as the Agilent

33220A, have a build in interface to allow these types of signals to be generated.

However sometimes even more complex waveforms such as several different length

pulse trains, random shape waves, combinational waves, prerecorded real signals or

prerecorded and modified real signals are needed. These types of signals can only be

obtained by using an arbitrary waveform generator such as the Agilent 33220A.

There are three ways in which arbitrary waveforms can be generated using the

Agilent 33220A [Agi09C]. The simples but least effective way to generate arbitrary

waveforms is through the use of the front panel interface of the arbitrary waveform

generator. This involves inputting the waveform point by point specifying the amplitude

and interval between successive points. This waveform can then be saved to the

permanent memory of the arbitrary waveform generator for later use. Of course when a complex waveform made up of many points is needed this method is impractical.

The second method of generating an arbitrary waveform for the Agilent 33220A arbitrary waveform generator is through the use of the Agilent IntuiLink Waveform Editor software [Agi09B]. This software is a GUI which allows waveforms to be generated on a PC and then transferred to the arbitrary waveform generator. The PC to arbitrary waveform generator connection can be made using a USB port, a LAN interface, or GPIB interface.

This software allows the waveform to be generated in three different ways. The first approach is to use a graphical interface in the software. This interface allows you to place preexisting templates of common wave segments such as sin, ramp, sinc, and exponential decay. All the parameters such as phase, offset and frequency of these segments can be configured. In addition the waveform can be drawing using line segments or freehand. Math operations such as addition, multiplication, filtering, taking the absolute value, inverting, mirroring, and clipping can also be performed on these waveforms or segments of the waveforms.

The second approach of creating a waveform is to simply import it from a compatible oscilloscope. This imported waveform can then be directly sent to the arbitrary waveform generator or it can be edited using the graphical interface and then sent to the arbitrary waveform generator. Editing a captured waveform can be useful for things such as adding noise, scaling and performing various other math tests on the waveform. The editing options for the imported waveform are the same as those for the graphically drawn waveform.

The third approach is to create the waveform from XY pairs in a program like Excel or Matlab and then load this file into the Agilent IntuiLink Waveform Editor software. This approach was the one used in this work as it is the most flexible and powerful. The utility of this approach comes from the fact you still have control over every point and at the same time you can easily generate complex waveforms using programs like Matlab. Again once the waveform is loaded into this software from a file it can be edited using all the features previously described.

Another method of transferring an arbitrary waveform to the Agilent 33220A arbitrary waveform generator is through programming [Agi07, Agi09C]. Of course in addition to transferring waveforms to the generator programming also allows users to control the function generator. Like with oscilloscopes programming of the arbitrary waveform generator is the most complex method but also the most powerful and convenient once learned.

Arbitrary waveform generator programming can be divided into direct SCPI programming or driver based programming, and driver based programming can be divided into interchangeable and instrument specific drivers. In both cases the PC to arbitrary waveform generator connection can be made using a USB port, a LAN interface, or GPIB interface allowing both local and remote access to the arbitrary waveform generator. Similarly to the programming of the oscilloscope both methods required the use of a high level programming language as an intermediate interface between the PC and arbitrary waveform generator. It should be noted that while having to use a high level language on top of the SCPI commands or drivers adds some complexity to the interface it also adds convenience. The convenience comes from being able to use

one environment for all needs such as creating waveforms, storing them to files, loading them from files, processing them, transferring them to the arbitrary waveform generator, controlling the arbitrary waveform generator/oscilloscope and collecting waveforms from an oscilloscope.

The advantage, disadvantages, and approaches to programming the arbitrary waveform generator are the same as those for programming an oscilloscope so the details are not repeated here. However in general programming allows waveforms to be created and transferred to the arbitrary waveform generator either point by point, from a file, from saved oscilloscope data, or from a waveform created using high level programming languages such as Matlab. Programming also allows access to all of the arbitrary waveform generator's features, scripted control, scripted waveform transfer, and instrument interchangeability.

Lastly the arbitrary waveform generator can be accessed remotely through the Internet using its built in web server. This is similar to the web server provided for the oscilloscope. The functions of this interface can be divided into three groups. First this interface allows you to view, and in some cases modify, information about the arbitrary waveform generator like its model number, serial number, host name, IP address etc. Second the web server interface allows the users to see and control the arbitrary waveform generator through a GUI of the front panel. This is a Java based GUI which is a virtual equivalent of the physical arbitrary waveform generator, i.e. the virtual GUI has the same layout and look as the physical front panel and screen of the arbitrary waveform generator and all the buttons, and knobs function as they do on the real arbitrary waveform generator. Using this GUI a point by point waveform may be entered as with

the real arbitrary waveform generator. The last function of the web server interface is to

allow SCPI programming of the arbitrary waveform generator. Using the SCPI

commands of this interface also allows waveforms to be entered into the arbitrary

waveform generator.

CHAPTER 5

ACOUSTIC CHAMBER, MEASUREMENT MOUNT AND
SENSOR ARRAY TEST STAND

5.1   Acoustic Chamber

To create a controlled environment for acoustic experimentation an acoustic

chamber was designed and built. The key features of the chamber are its ability to isolate

the experiment inside the chamber from outside noise and to absorb sound inside the

chamber to prevent reverberation and reflections. It should be noted that while the noise

from outside of the chamber could be either reflected back outside or absorbed by the

chamber, sound inside the chamber has to be absorbed by the surfaces of the chamber to

prevent reflections. The material used for sound absorption was foam, however the

chamber was designed in such a way that other materials with different acoustic

absorption properties could be attached to the same chamber structure. For ease of

portability the chamber is also disassemble into small and light pieces. Since the size and

setup of the experiments which are to be performed are not known beforehand the

chamber is designed to be modular allowing its size to be adjusted as necessary for a

wide variety of experiments. Lastly the chamber is designed to be easily opened and

closed allowing the experimental setup to be quickly and effortlessly modified as

necessary.

Figures 5.1 and 5.2 below shows the outside view of the assembled acoustic

chamber from the top and side, respectively. Figures 5.3 and 5.4 below show the inside

view of the assembled acoustic chamber from the top and side, respectively.

Figures 5.1. Outside of View of the Acoustic Chamber from the Top

Figures 5.2. Outside of View of the Acoustic Chamber from the Side

Figures 5.3. Inside of View of the Acoustic Chamber from the Top

Figures 5.4. Inside of View of the Acoustic Chamber from the Side

The acoustic chamber is constructed out of three basic parts and several interconnecting parts. The three basic parts are the floor foam tiles, the ceiling foam tiles, and the side foam tiles. The floor foam tiles are 27.5" x 27.5" x 2" each and are assembled into a 55" x 55" x 2" floor foam cushion. The floor tiles of the floor cushion are not attached together but are simply pushed together by the pressure from the side tiles. Figure 5.5 shows a floor cushion assembled from four floor tiles.

The ceiling foam tiles are also 27.5" x 27.5" x 2" each and are connected into 55" x 27.5" x 2" ceiling tiles through two 1"x 2" x 60" wooden bars. The foam tiles are attached to the wooden bars using Velcro and can be removed from the bars and transported separately. Alternatively the ceiling tiles can be rolled around the wooden bars for a more compact form for transportation. Since the foam tiles are attached to the wooden bars by Velcro other foam types or other materials types with different acoustic absorbing characteristics can be used for the tiles and can be attached to the same wooden bars. The ceiling tiles simply rest on top of the side tile under their own weight. Figure 5.6 shows the two assembled ceiling tiles from the back and front.

The side tiles are made of a plywood panel used as a backbone and a foam cushion. Each plywood backbone is 29.5" x 28.5" x ¼" and each foam cushion is 27.5" x 27.5" x 2". The vertical dimension of the plywood backbone is 29.5" to allow one inch on the bottom and top for a snug overlap with the bottom and top tiles. The horizontal dimension of the plywood backbone is 28.5" to allow for a snug fit along the corner between two side tiles. The foam cushion is attached to the plywood backbone by Velcro. Again using Velcro to attach the foam cushion to the plywood backbone allows the foam

to be removed and other materials to be attached to the same plywood backbone as necessary.

The side tiles can be connected in two ways: a corner connection or a straight connection. A corner connection is used when two tiles form a corner of the acoustic chamber. The corner connection is made of two hinges, one attached to the top and one attached to the bottom of the vertical edge of the plywood backbone, as can be seen in figure 5.1.

A straight connection is used when two tiles form a wall of the acoustic chamber. The straight connection is made of a single hinge with a removable pin attached to the center of the plywood backbone, as can be seen in figure 5.2. A pin with a handle is used so that it could be easily removed allowing the side tiles to be opened and closed like doors for access to the inside of the acoustic chamber. In addition to the single central hinge a straight connection also uses cap molding on the bottom and top of the plywood tiles to align the two tiles with each other, these can be seen as the large plastic pieces above and below the hinge in figure 5.2.

Each side tile has two connections and each of the connections can be either a straight connection or a corner connection. However, the side tiles used in this work all had one corner and one straight connection. This was the case because these connections led to the chamber of the required size for the experiments in this work. Figure 5.7 shows the side tiles from the back and front.
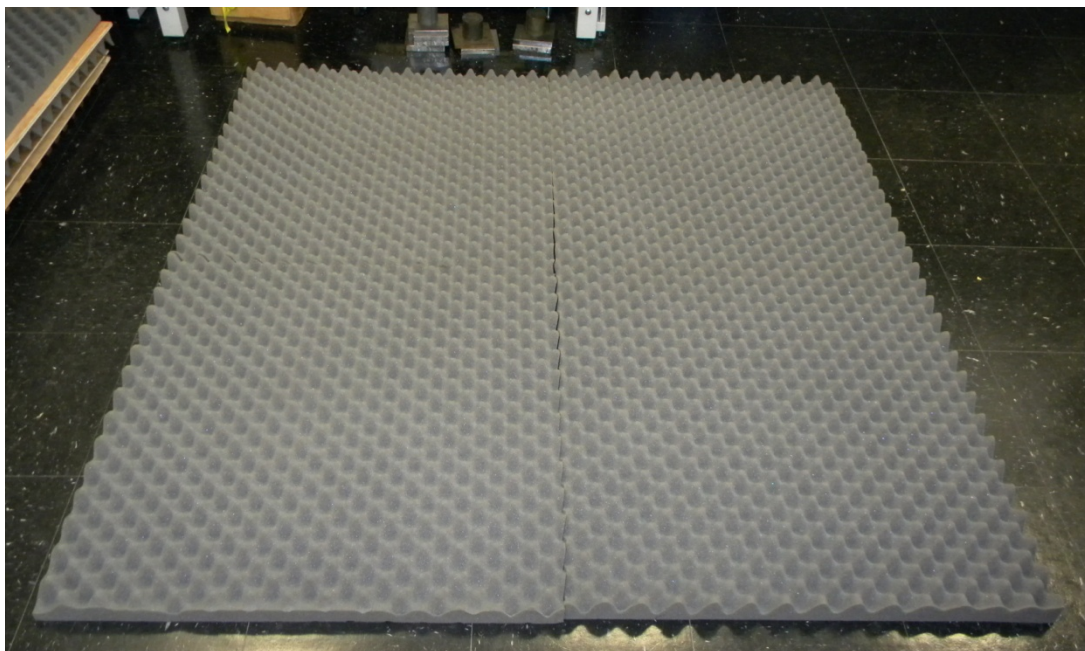
Figures 5.5. Acoustic Chamber Floor Cushion

Figures 5.6. Acoustic Chamber Ceiling Tiles Front and Back
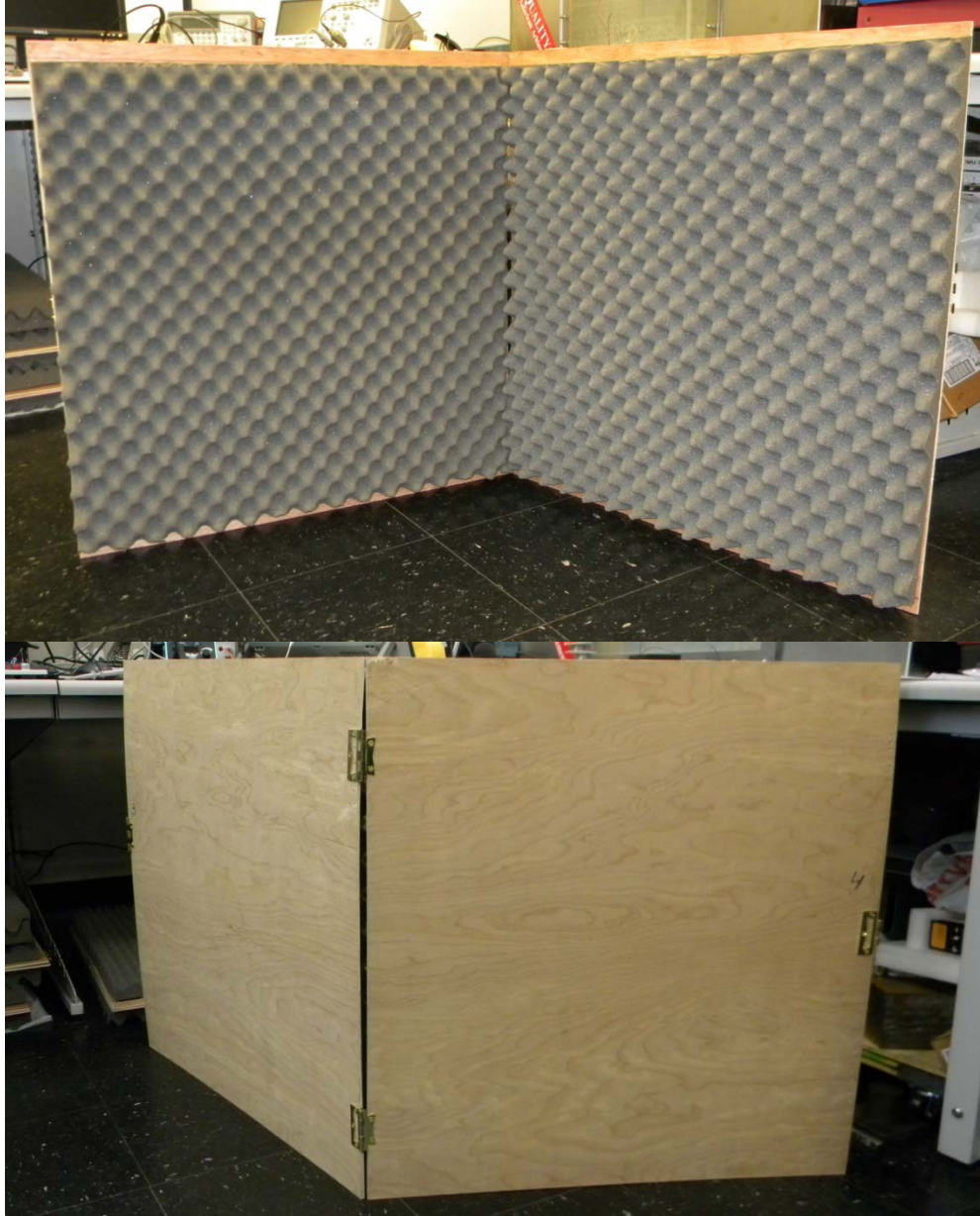
Figures 5.7. Acoustic Chamber Side Tiles Front and Back

The size of the chamber can be easily changed although its shape must remain rectangular. The size of the floor cushion can be simply changed by increasing or decreasing the number of floor tiles used. The size of the ceiling can be changed in both width and length. To increase the length of the ceiling more of the same ceiling tiles can be used and can again rest on the side tiles. To increase the width of the ceiling, wooden

support bars have to be placed along the top of the side tiles and the ceiling tiles will have to rest on them. Additionally the wooden bars to which the ceiling foam tiles are attached will have to be different distances from each other so that they would not run into each other when set on the support bars. The size of the sides of the chamber can be increased by using two straight connection side tiles between corner connection tiles.

The foam used in the acoustic chamber was high density 2" thick polyester-based polyurethane convoluted (egg crate) foam which is specifically designed for sound absorption [AME10]. Besides absorbing sound this foam is also designed to be flame resistant, tear resistant, to not break down due to humidity, and to retain its shape after compression. The absorption versus frequency of this foam is shown in figure 5.8 below. The foam used for this work was the 2" thick foam which is represented by the rhombus dotted line in the figure.
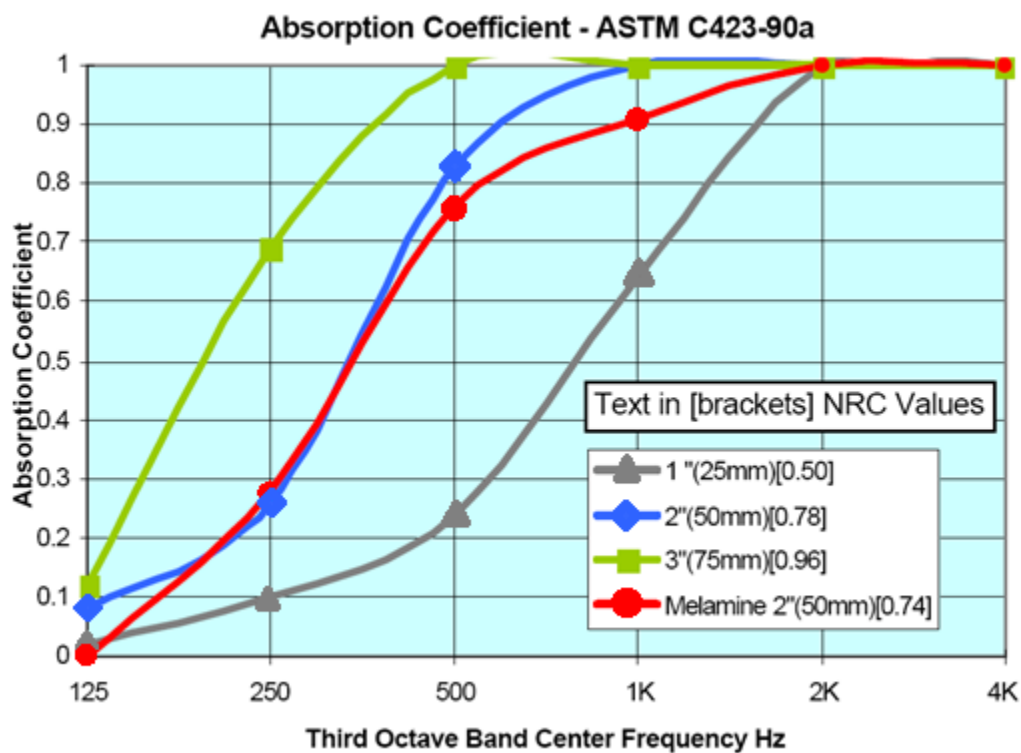
Figure 5.8. Acoustic Foam Absorption VS. Frequency [AME10]

5.2   Measurement Mount

To accurately measure the angle and distance for sound source localization experiments a special microphone mount was designed. The mount was based on the Panavise 333 circuit board vise [PAN10]. This vise was used as it can be rotated around all three axes and the distance and orientation of the vise arms, which hold the microphones, can be easily adjusted. This vise is also based on a heavy yet small steel plate for easy placement.

The main modification to the vise was the addition of a laser based angle indicator. The indicator was constructed out of steel strips, a protractor, a laser pointer and cable ties. The steel strip was bent around the central bar of the vise in such a way as to be perpendicular to it. The strip was then attached to the bar using a screw. A protractor and a second steel strip with a laser pointer attached to it using cable ties, was then screwed on to the first steel strip.

Angle measurements are performed by rotating the second steel strip with the laser pointer along the protractor to the desired angle, any object that is then aligned with the dot created by the laser pointer is at the desired angle. In addition, to accurately measure distances a rope with distance markers was tied around the steel strip. Figures 5.9 and 5.10 below show the front and side views of the measurement mount. It should also be noted that while the figures show two microphones attached to the vise through foam, these pieces could be removed and other systems such as the microphone array data acquisition system could be mounted using the vise clamp arms.
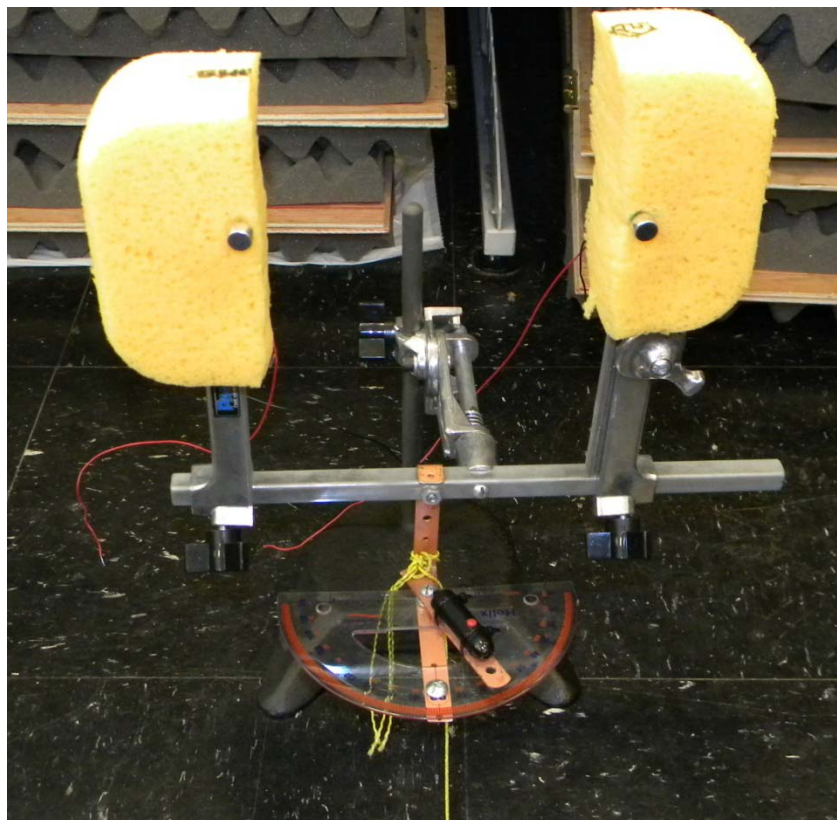
Figure 5.9. Measurement Mount Front View
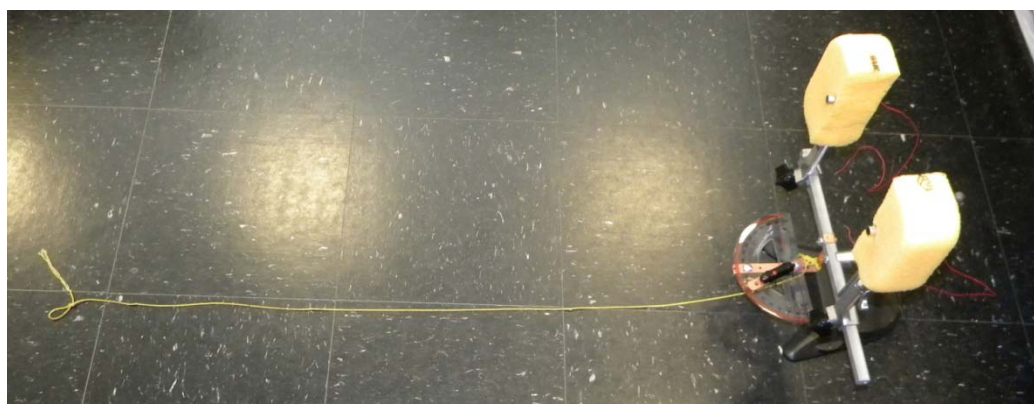
Figure 5.10. Measurement Mount Side View

5.3   Sensor Array Test Stand

In order to conduct a wide variety of acoustic and ultrasound experiments a sensor array test stand was designed and built. The key features of the test stand are its modularity and its configurability. These features allow the user to vary the number, type, and arrangement of sensors while using the same test stand structure. The test stand is also designed to be easily disassembled, reassembled for transportation. Figure 5.11 below shows a picture of the sensor array test stand.
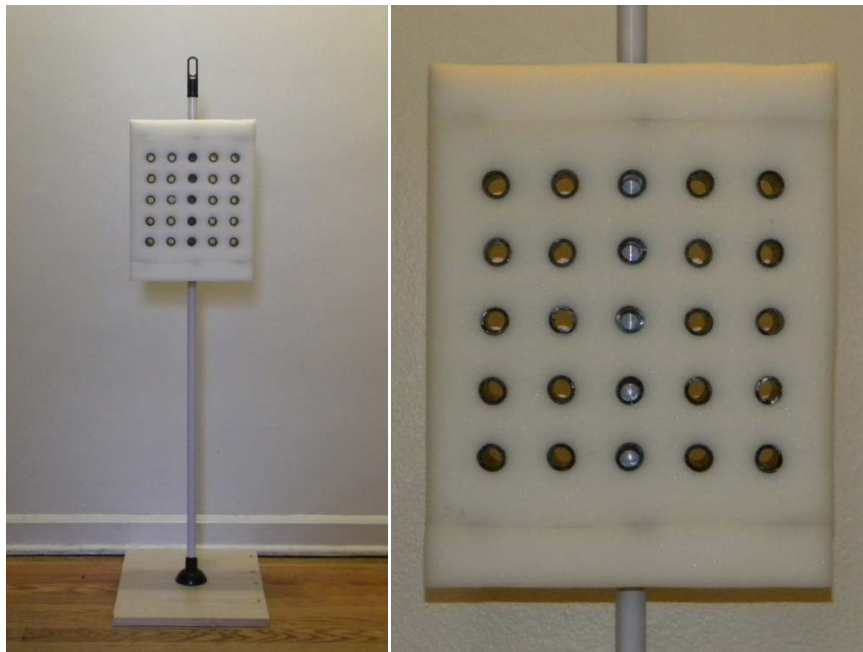
Figure 5.11. Sensor Array Test Stand Front View

Two types of test stand sensor beds were built to accommodate the two types of ultrasound sensors used. The first test bed is designed to hold sensors with a 12mm diameter. This test bed is 240mm x 240mm and contains 25 sensor positions arranged in a 5 x 5 square layout. The inter-sensor distance in both the horizontal and vertical axis is 40mm. The body of this sensor bed is made from a two inch deep medium density foam. The second test bed is designed to hold sensors with a 25mm diameter. It is 420mm x

420mm and also contains 25 sensor positions arranged in a 5 x 5 square layout. The inter-sensor distance in both the horizontal and vertical axis is 76.2mm. The body of this sensor bed is made from a three inch deep high density convoluted foam.

The sensor arrangement used allows various sensor geometries such as square, cross, circle, rhombus, or the full square array to be tested. The inter-sensor distance is used to provide sufficient rigidness to the sensor test beds and also to reduce the reflections in between sensors. Foam is used for the body for two reasons. The first is to reduce reflections from the surface of the body which if created will interfere with sensor readings. The second is to prevent the vibrations of one sensor from being coupled on to others. These microphone vibrations are caused by the pressure changes generated by a sound or ultrasound waves hitting the microphone membrane. Two and three inch foam is also used for two reasons. First this depth is necessary to provide sufficient absorption of sound and ultrasound vibrations. Second this depth allows for the sensors to be moved to the back and front of the test beds thus changing the directionality of the sensors. Three inch convoluted foam is used for the second test bed to provide increased absorption and to provide additional rigidness for the larger sensors.

The sensors are not attached directly to the foam test beds but are instead inserted into a semi-flexible PVC pipe cut to two and three inches. The pipe segments are then inserted into the foam test beds. This was done to create a snug fit for the sensors so that they would not move around unexpectedly. This could not be done with foam as reducing the size of the aperture in the foam would cause it to close around the sensor thus blocking it. Additionally using the flexible PVC pipe to hold the sensors allows different sensor types to be used as the pipe and foam will compares and expand around the shape

and size of different sensors. As stated earlier the sensors can be moved within the PVC pipes to change the directionality of the sensor. The directionality of the sensors in the PVC pipe can be calculated from figure 5.12 below.
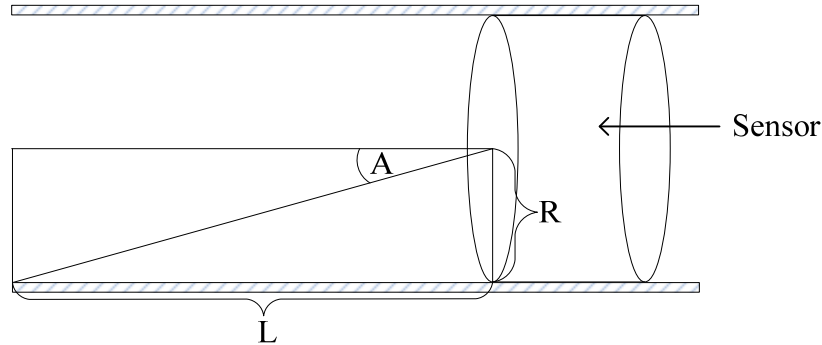
Figure 5.12. Sensor Directionality

Here R is the radius of the sensor, L is the distance between the surface of the sensor and the front of the test bed, and A is the directionality of the sensor. From this figure it can be seen that the directionality is given by equation 5.1 below.

$$A = \tan^{-1}(R/L) \tag{5.1}$$

This directionality calculation is based on the received signal power falling to half of its full value. It should also be noted that when sensor directionality is created using this approach the received signal could be distorted due to the reflection that may be created within the test bed aperture.

Since the foam test beds are not rigid they are attached to a backbone made from a ¼" plywood sheet. To provide access to the back of the sensors 1" and 2" holes were cut in the plywood at the location of each sensor for the first and second test beds respectively, this can be seen in figure 5.13 below. The foam test beds are attached to the plywood using Velcro allowing them to be easily taken off and allowing for different kinds of test beds to be attached to the same backbone.
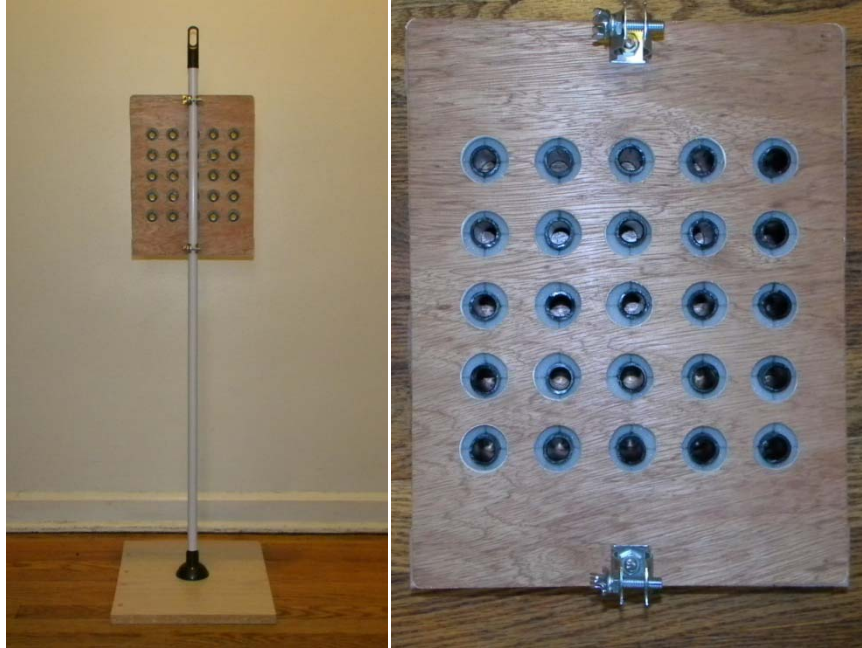
Figure 5.13. Sensor Array Test Stand Rear View

The backbone is attached to a rod stand allowing the height and orientation of the sensors to be easily adjusted. The backbone is attached to the rod through the use of two conduit hangers which are used as pinch clamps, as can be seen in figure 5.13. At the bottom the rod is attached to a ¾" x 18" x 18" plate of wood to provide stability. The rod can be easily screwed into and out of the wooden plate for transportation.

CHAPTER 6

AUXILIARY CIRCUITS AND SENSORS

6.1 Auxiliary Circuits

For both the audio and ultrasound experimentation the voltage levels that the

receiving microphones and sensors produced were on the levels of micro volts. As it is

difficult to analyze voltages at this level directly using an oscilloscope, amplifier circuits

were used. Additionally different frequency ranges were of interest for different

experiments thus the amplifier circuits also contained filters to remove unnecessary

frequencies and noise from the received signals.

For sound experimentation the LM324N quad operational amplifier chip [Nat00]

consisting of four operational amplifiers was used. The circuit for each microphone was a

dual power supply amplifier circuit consisting of two stages of the LM324N operation

amplifier for a total gain of approximately 10000 [Nat02]. Each circuit also contained

three high pass filters and one low pass filter. The corner frequencies for the high pass

filters are 16Hz, 1591Hz, and 1591Hz, and the corner frequency for the low pass filter is

1591Hz. The schematic of the microphone amplification and filtering circuit is shown in

figure 6.1 below. In this figure filter 1 corresponds the 16Hz corner frequency high pass

filter, filters 2 and 3 corresponds to the 1591Hz corner frequency high pass filters and

filter 4 corresponds to the 1591Hz low pass filter. The corner frequencies are arranged to

overlap to allow only a narrow band of relatively high power signals to pass so that noise

would be eliminated. The microphone is powered through a 10kΩ resistor as it is a

condenser type microphone.
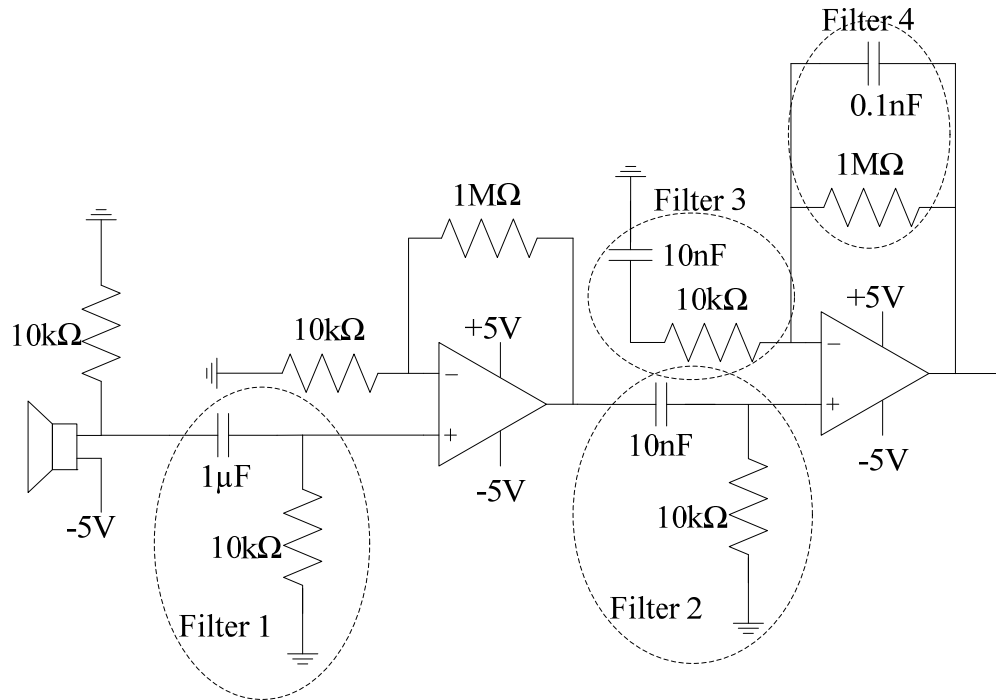
Figure 6.1. Auxiliary Microphone Circuit

For ultrasound experimentation the LM324N quad operational amplifier chip [Nat00] consisting of four operational amplifiers was used. The circuit for each microphone was a single power supply amplifier circuit [Kit02] consisting of two stages of the LM324N operation amplifier for a total gain of approximately 100 [Nat02]. Each circuit also contained two high pass filters with corner frequencies of 1591Hz and 28937Hz. The schematic of the circuit is shown in figure 6.2 below. In this figure filter 1 corresponds the 1591Hz corner frequency high pass filter and filters 2 corresponds to the 28937Hz corner frequency high pass filter.
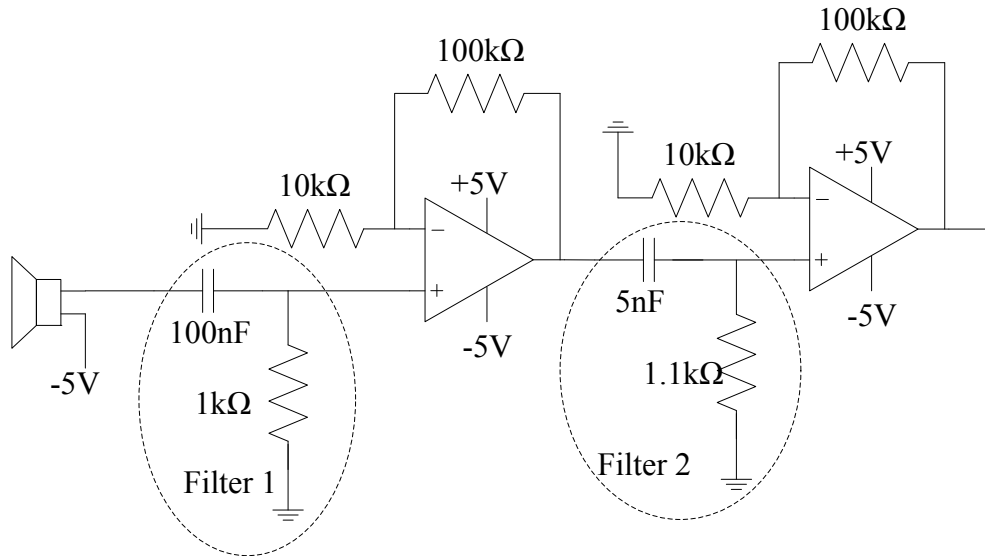
Figure 6.2. Auxiliary Ultrasound Sensor Circuit

6.2   Sensors

In addition to the sensors used in the custom-made microphone array data acquisition system separate microphones and ultrasound sensors were used in conjunction with the oscilloscope based data acquisition experiments. The microphone used was the radio shack model 270-090 PC-Mount condenser microphone. This is a simple omni-directional condenser microphone with a diameter of approximately 0.4 inches and a bandwidth of 20-15,000Hz [Rad10].

Several ultrasound sensors were used. The first was a generic ultrasound resonator sensor with a center frequency of 40 kHz and a total beam angle of 140 degrees for an attenuation of 6dB. This transmitter has a diameter of 12mm. Another ultrasound sensor used was the SensComp K-series 125KHF25 sensor [Sen07]. The 125KHF25 is a 125 kHz transceiver with a highly directional beam pattern. Specifically the total beam angle of the transceiver is 14.5 degrees for an attenuation of 6dB. The sensor is also quite small

with a diameter of 25mm which is also desirable in many applications. The beam angle

and frequency response of the 125KHF25 are shown in figures 6.3 and 6.4 below:
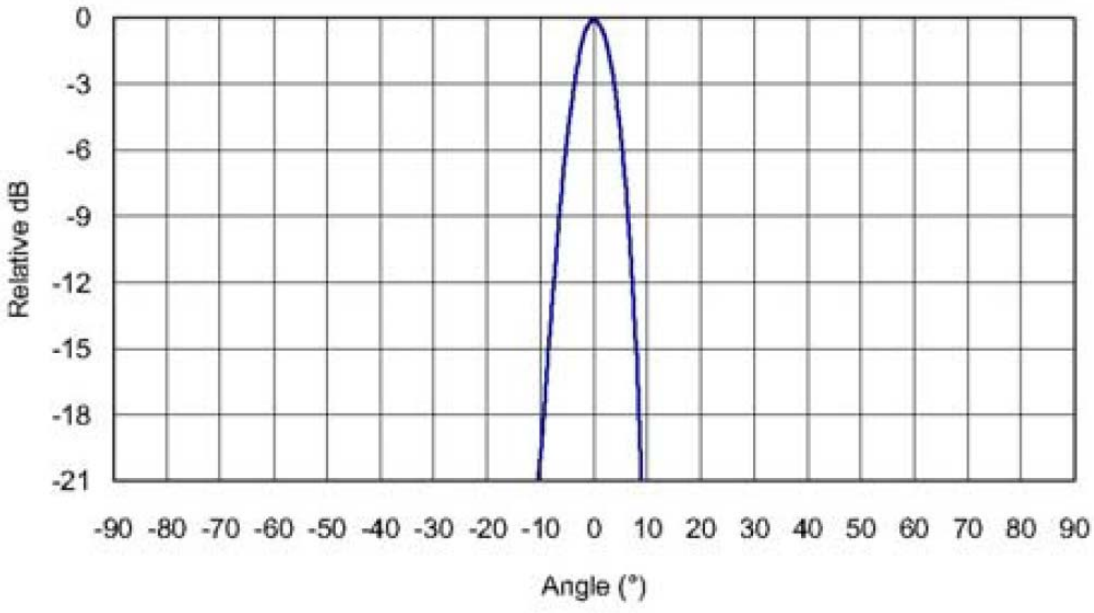
Figure 6.3. 125KHF25 Beam Angle versus Attenuation [Sen07]
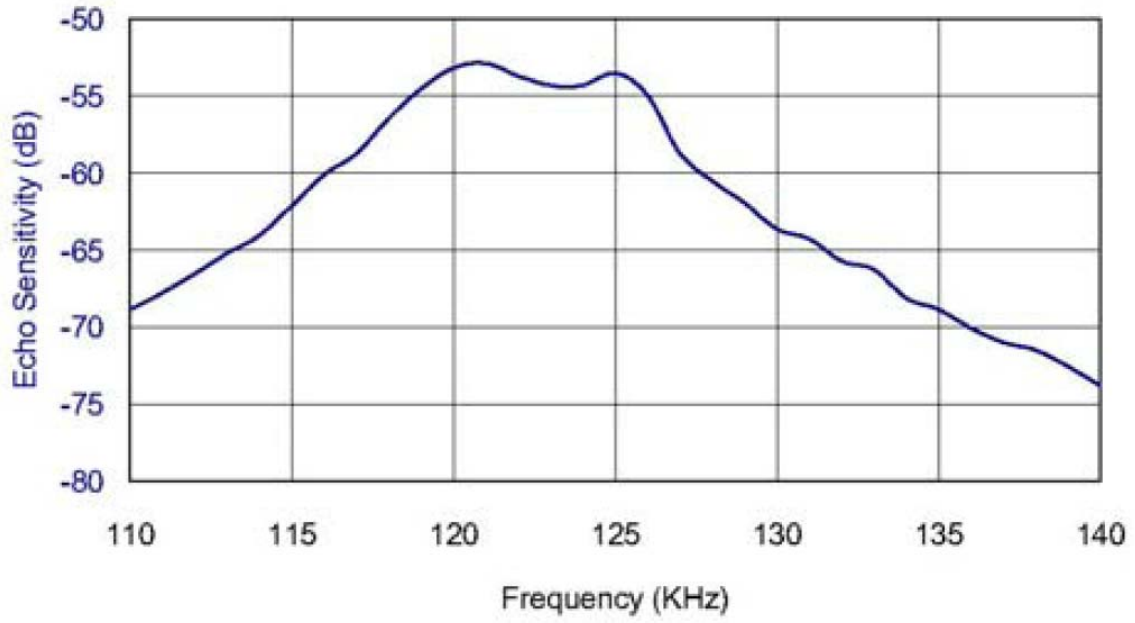
Figure 6.4. 125KHF25 Frequency Response [Sen07]

The last ultrasound sensor used was the Measurement Specialties Piezoelectric film (PVDF) US40KT-01 40 kHz transmitter [Mea01]. This transmitter has the special property of being horizontally omnidirectional and has a vertical total beam angle of 80 degrees to 6dB. This sensor is also of small size with a diameter of 15mm and a height of 26mm. The beam angle and frequency response of the US40KT-01 are shown in figures 6.5 and 6.6 below:

TYPICAL HORIZONTAL BEAM DIRECTIVITY   **TYPICAL VERTICAL BEAM DIRECTIVITY**
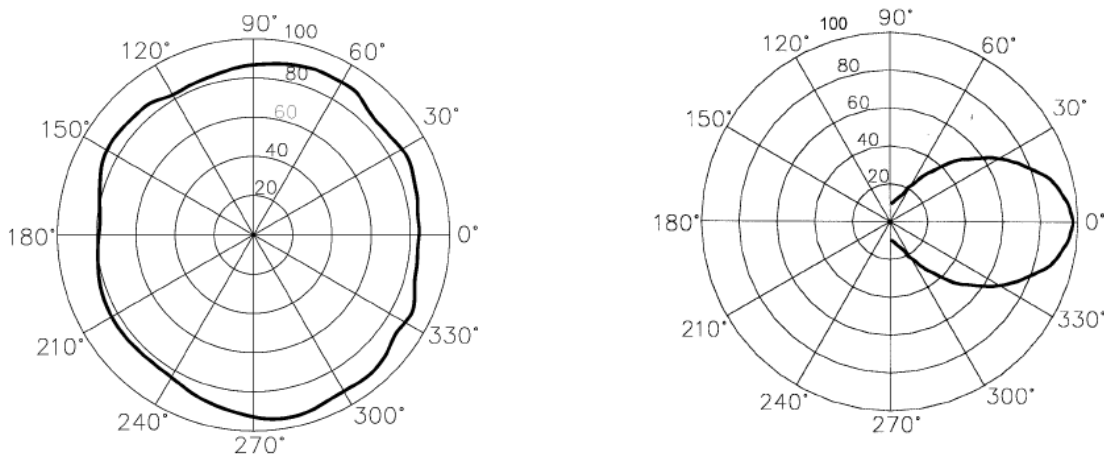
Figure 6.5. US40KT-01 Beam Angle versus Attenuation [Mea01]
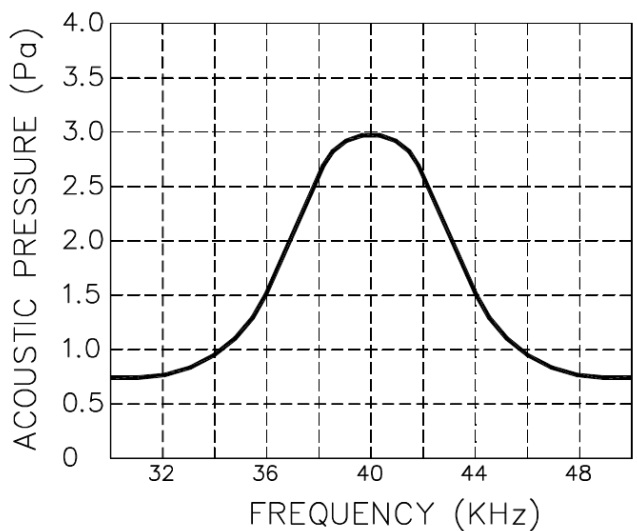
Figure 6.6. US40KT-01 Frequency Response [Mea01]

CHAPTER 7

EXPERIMENTS

7.1   Sound Source Direction of Arrival Estimation (DOAE)

A variety of phase based sound source DOAE experiments were performed. The experiments were varied by the number of microphones used, microphone arrangements, types of microphones used, acquisition systems used, source signals used, and the transmitter to receiver distance. The goal of the experiments was to determine the direction of the sound source with respect to the microphones as described in chapter 2. The direction of the sound source was calculated based on the recorded phase delay and the distance between the receiving microphones.

The first set of experiments involved the CAPTAN based microphone array data acquisition system and a transmitting speaker. The microphone array data acquisition system was mounted on the Panavise base discussed in chapter 5.2, the transmitting speaker was also mounted on a general purpose Panavise base. All 52 microphones of the system collected data at an acquisition rate of 300 Ksps each and two sets of microphones were used. The experiment was carried out in a laboratory room with various non uniform objects around the area of experimentation resulting in a high noise and a highly reflective environment.

The parameters varied in this experiment were the distance to the sound source, frequency of the sound source, the pairs of microphones used, and the angle between the sound source and the microphones. The first test distance was two feet and the second test distance was 5 inches. The sound source signal used was a continuous sine wave of frequencies 1 kHz and 2 kHz, generated by the Agilent 33220A function generator. The

upper frequency was limited to 2 kHz to allow all microphones of the microphone array system to be used without aliasing. As the maximum distance between microphones on the array was 7cm the maximum frequency is limited to 2.4 kHz as was described in chapter 2. The overall geometry of the experiment is shown in figure 7.1 below.

Microphone Receivers

Transmitter (Sound Source)
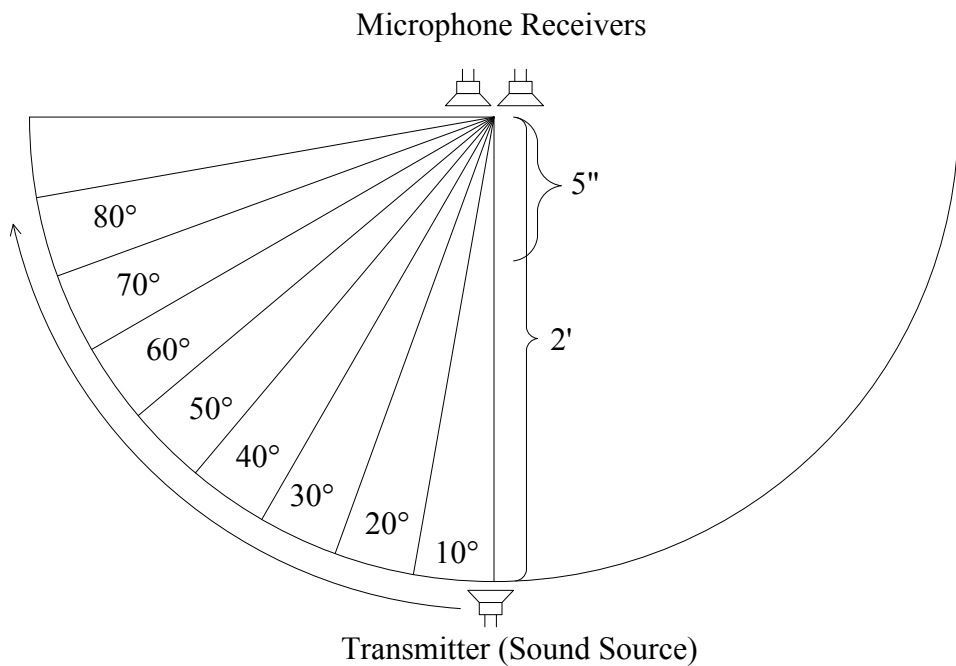
Figure 7.1. Sound Source DOAE Setup

A sample of the overall data collected by the MEMs array is shown in figure 7.2. In this Matlab figure each window represents the data collected by one of the MEM microphones. The sine wave pattern of the source signal cannot be clearly seen because of the large number of cycles present in the graphs. Thus a zoomed in version of the data collected by two of the microphones is shown in figure 7.3. In this graph the phase difference between the data collected by the two MEM microphones can be clearly seen.
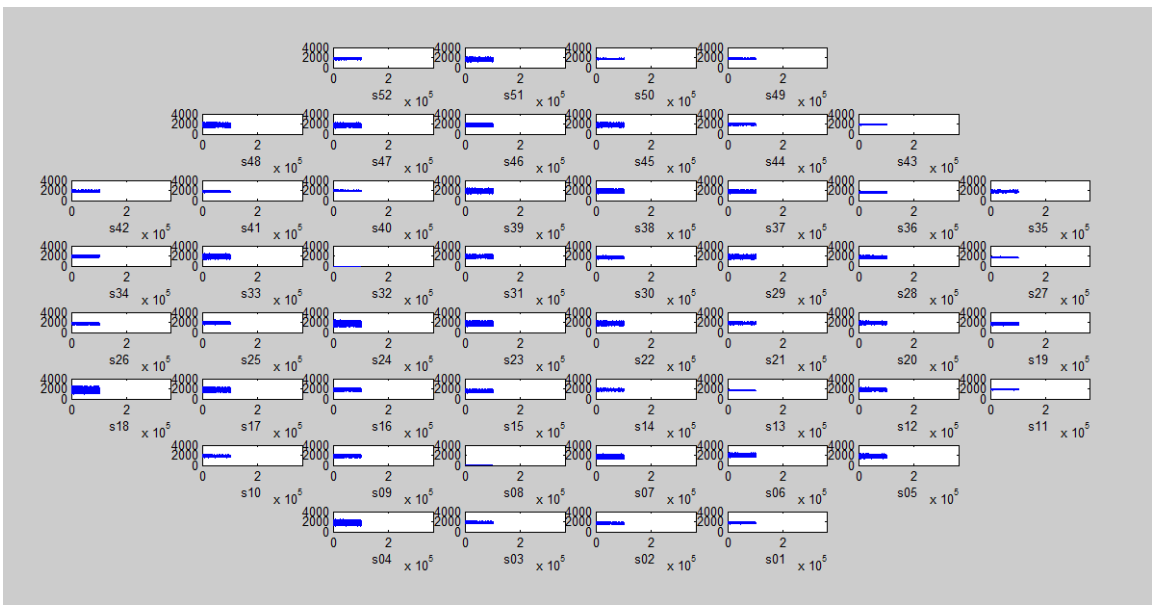
Figure 7.2. Sample Data Collected by MEMS Microphone Array
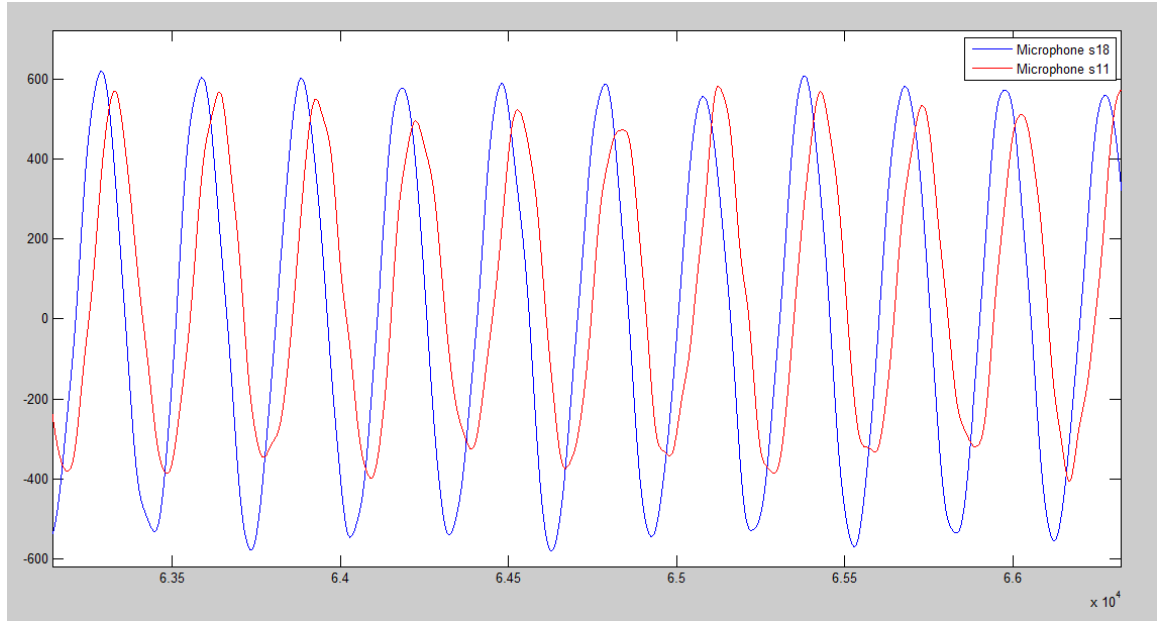
Figure 7.3. Zoomed in Data Collected by Two MEMS Microphones

The sets of microphones used were the outer set and the central inner set as shown in figure 7.4 below. For each set the delay was obtained from each pair of opposing microphones, the results from each pair were then averaged to obtain the delay measurement for the set.
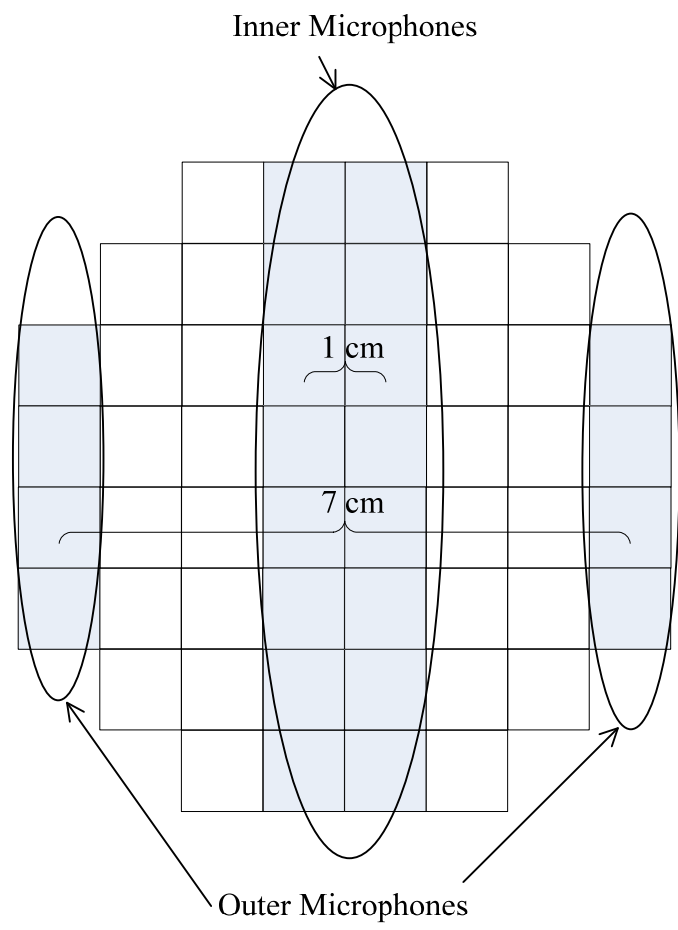
Figure 7.4. Microphones Used

The results of this set of experiments are shown in tables 7.1 and 7.2 below. Here the angle of the sound source to the microphones is shown in the first column, the measurements for the two distances at two frequencies are shown in the second, third and fourth columns and the expected values are shown in the fifth column. The results shown are those averaged for three trials at a frequency of 1 kHz and 3 trials at a frequency of 2 kHz.

Table 7.1. Sound Source DOAE Experiment Set 1, Outer Microphones Results

Angle (°)	Outer Microphones				
	Obtained Delay (ms)				Theoretical (Expected) Delay (ms)
	2' Distance		5" Distance		
	1 kHz	2 kHz	1 kHz	2 kHz	
0	-0.007	0.011	0	0.005	0
10	0.020	0.087	0.036	0.032	0.035
20	0.120	0.062	0.065	0.063	0.070
30	0.065	0.087	0.099	0.109	0.101
40	0.113	0.163	0.124	0.119	0.130
50	0.182	0.054	0.144	0.128	0.156
60	0.146	0.123	0.179	0.145	0.176
70	0.187	0.183	0.185	0.188	0.191
80	0.192	0.188	0.202	0.197	0.200

Table 7.2. Sound Source DOAE Experiment Set 1, Inner Microphones Results

Angle (°)	Inner Microphones				
	Obtained Delay (ms)				Theoretical (Expected) Delay (ms)
	2' Distance		5" Distance		
	1 kHz	2 kHz	1 kHz	2 kHz	
0	0.002	-0.03	0	0	0
10	0.000	0.003	0.004	0.004	0.005
20	0.016	0.018	0.011	0.010	0.010
30	0.018	0.013	0.015	0.012	0.014
40	0.016	00.15	0.019	0.016	0.018
50	0.021	0.018	0.020	0.024	0.022
60	0.021	0.019	0.024	0.026	0.025
70	0.029	0.0.29	0.026	0.028	0.027
80	0.027	0.030	0.027	0.028	0.028

It can be seen from these results that phase based DOAE in a highly noisy and reverberant environment does not produce reliable results at larger distances independent of the frequency of the source signal or the distance between the receiving microphones. This can be seen from the mismatch between the collected data and the expected results,

and also from the fact that the time delays increase and decrease instead of just increasing when the angle between the sound source and receiving microphones increases. It can also be seen that phase based DOAE works better at close distances where the power of the original signal is high compared to the power of the reflection based noise.

In order to reduce the effect of reflection and ambient noise the second set of experiments were carried out inside the acoustic chamber discussed in chapter 5. These experiment also used the CAPTAN based microphone array data acquisition system and a transmitting speaker. The experimental setup and the parameters varied were also the same as in the first set of experiments except for the use of the acoustic chamber.

The results of this set of experiments are shown in tables 7.3 and 7.4 below. Here the angle of the sound source to the microphones is shown in the first column, the measurements for the two distances at two frequencies are shown in the second, third and fourth columns and the expected values are shown in the fifth column. The results shown are those averaged for three trials at a frequency of 1 kHz and 3 trials at a frequency of 2 kHz.

Table 7.3. Sound Source DOAE Experiment Set 2, Outer Microphones Results

	Outer Microphones				
	Obtained Delay (ms)				Theoretical (Expected) Delay (ms)
Angle (°)	2' Distance		5" Distance		
	1 kHz	2 kHz	1 kHz	2 kHz	
0	0.003	-0.005	0	0	0
10	0.015	0.012	0.034	0.035	0.035
20	0.045	0.040	0.068	0.069	0.070
30	0.064	0.077	0.102	0.101	0.101
40	0.060	0.064	0.131	0.132	0.130
50	0.067	0.071	0.153	0.157	0.156
60	0.130	0.121	0.176	0.178	0.176
70	0.180	0.176	0.193	0.189	0.191
80	0.190	0.193	0.199	0.201	0.200

Table 7.4. Sound Source DOAE Experiment Set 2, Inner Microphones Results

	Inner Microphones				
	Obtained Delay (ms)				Theoretical (Expected) Delay (ms)
Angle (°)	2' Distance		5" Distance		
	1 kHz	2 kHz	1 kHz	2 kHz	
0	0.001	0	0	0	0
10	0.003	0.003	0.004	0.005	0.005
20	0.009	0.008	0.010	0.009	0.010
30	0.017	0.016	0.014	0.014	0.014
40	0.016	00.17	0.018	0.017	0.018
50	0.017	0.018	0.021	0.023	0.022
60	0.023	0.021	0.025	0.026	0.025
70	0.026	0.0.24	0.026	0.027	0.027
80	0.028	0.029	0.027	0.027	0.028

From these results it can be seen that performing phased based sound source DOAE inside an acoustic chamber, which absorbs sound and thus reduces reflections, produces some improvement over performing sound source DOAE in a general room environment. This can be seen from the fact that the time delays increase as the angle between the sound source receiving microphones increases. However it can also be seen that the collected data still does not match the expected results thus there are still some reflections present in the environment. Again the frequency of the source signal and the distance between the receiving microphones does seem to affect the accuracy of the results. It can also once again be seen that that phase based DOAE works better at close distances where the power of the original signal is high compared to the power of the reflection based noise.

As stated earlier it can be seen that even within the acoustic chamber some distortions and thus some reflections are still present. Since the surrounding surfaces inside the acoustic chamber absorb most of the sound it was assumed that the reflections

causing the distortions in this set of experiments came from the microphone array itself. This is shown in figure 7.5 below.
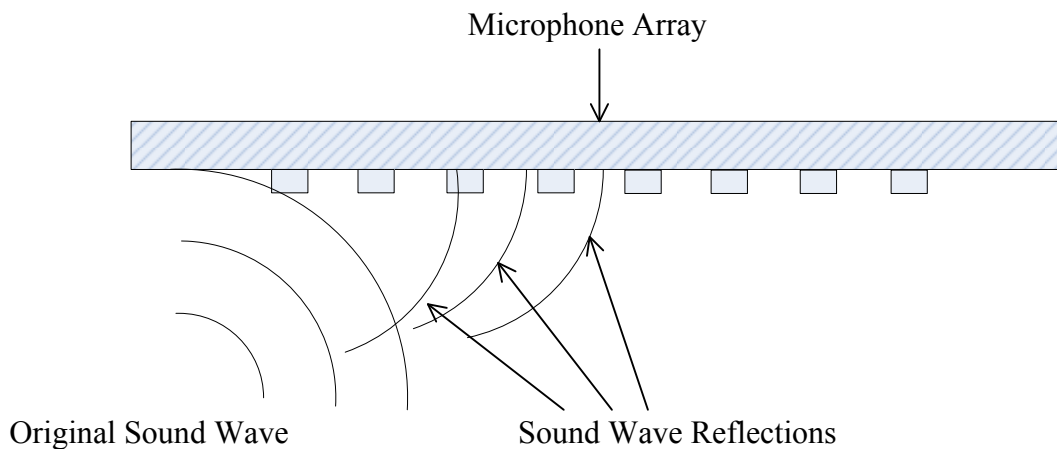
Figure 7.5. Reflections from Microphone Array

In order to reduce the effect of the reflection coming from the microphone array itself an alternate physical setup and acquisition system was used for the third set of experiments. The physical setup consisted of the Panavise vise with a radio shack microphone, described in chapter 6 section 2, attached to each of the two arms of the vise through foam and with nothing in between the vise arms. This setup is shown figures 5.9 and 5.10. Foam was used to hold the microphones to further suppress the reflections from one side of the mount to another and to prevent vibration coupling between the two microphones. In this setup the distance between the microphones was 16 cm. Since there was nothing between the microphones there was nothing to create reflections waves except the foam wrapped arms of the vise itself.

The acquisition system used for this series of experiments was the Agilent MSO6032A oscilloscope. Since a clear signal could not be obtained directly from the microphones an amplification and filtering circuit as discussed in chapter 6 section 1 was used for each microphone. The sound source signal was once again a continuous sine

wave generated by the Agilent 33220A function generator and fed to a speaker on another Panavise vise. Since the distance between the microphones was changed to 16 cm the maximum frequency of the source signal was limited to 1075Hz as discussed in chapter 2. Because of this the two frequencies tested were 700Hz and 900Hz. Since it has been established that correct measurements are obtained at a distance of 5", this set of experiments was only performed for a distance of 2'. This set of experiments was also performed inside the acoustic chamber.

The results of this set of experiments are shown in tables 7.5 below. The results shown are those averaged for three trials at a frequency of 700 Hz and 3 trials at a frequency of 900 Hz.

Table 7.5. Sound Source DOAE Experiment Set 3 Results

Angle (°)	Obtained Delay (ms) Frequency		Theoretical (Expected) Delay (ms)
	700 Hz	900 Hz	
0	0	0	0
10	0.061	0.084	0.081
20	0.112	0.146	0.160
30	0.156	0.215	0.234
40	0.209	0.292	0.301
50	0.244	0.340	0.359
60	0.295	0.391	0.407
70	0.317	0.446	0.442
80	0.344	0.452	0.463

From these results it can be observed that increasing the distance between the microphones and removing any reflective surfaces from in between the microphones significantly improves the accuracy of phase based DOAE even at larger distances. For the 900 Hz sound source signal the measured delays follow the correct pattern and are within a few percent of the expected time delays. For the 700 Hz sound source signal the

measured delays also follow the correct pattern but the delays are a reduced version of the expected values, i.e. each measured delay is approximately 75% of the expected value. Thus the frequency of the sound source signal now has some effects on the measured time delay. This is again attributed to the remaining reflection in the environment.

To further reduce the effects of reflection on the DOAE another set of experiments was performed. Here the physical setup and the parameters varied were the same as for the third set of experiments except for the type of source signal used. This time instead of using a continuous sine wave for the source signal only 20 cycles of a sine wave were transmitted. Then when this sine pulse train wave was received only the first pulse was used for phase comparison. This was expected to further reduce errors due to reflections since the first pulse should arrive before all reflections and thus its phase information should not be distorted. A sample of the data collected for this set of experiments is shown in figure 7.6.
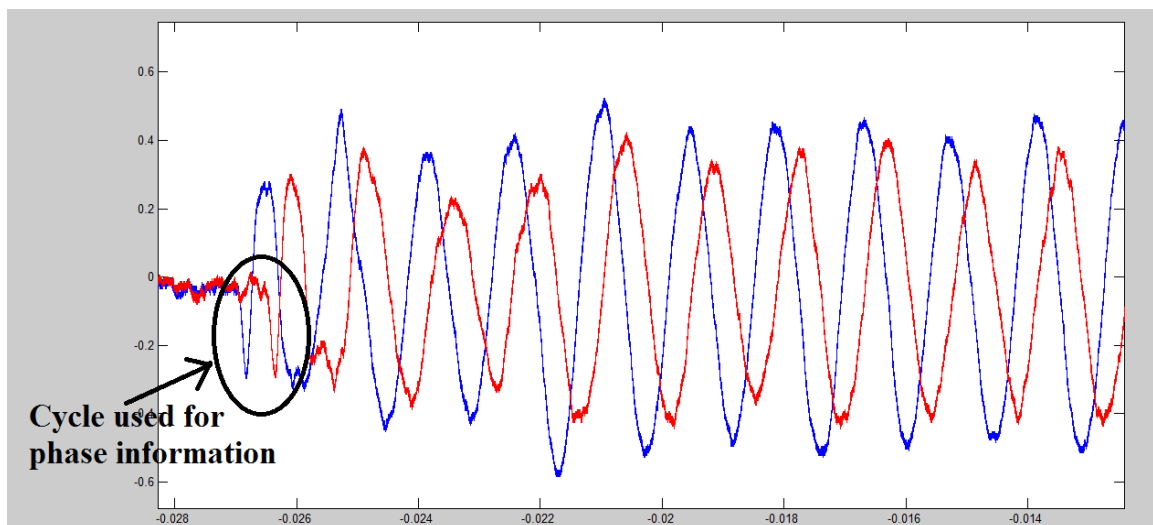

Figure 7.6. Sound Source DOAE Experiment Set 4 Sample Results

Figure 7.6 shows that only the first half of the first cycle was used for phase delay information. In this figure it can also be seen that the first half of the first cycle is relatively clean with a distinct sharp peak and that later cycles are not as sharp and somewhat distorted leading to less accurate phase delay estimation when they are used.

The results of this set of experiments are shown in tables 7.6 below. The results shown are those averaged for three trials at a frequency of 700 Hz and 3 trials at a frequency of 900 Hz.

Table 7.6. Sound Source DOAE Experiment Set 4 Results

Angle (°)	Obtained Delay (ms)		Theoretical (Expected) Delay (ms)
	Frequency		
	700 Hz	900 Hz	
0	0.010	0.015	0
10	0.092	0.092	0.081
20	0.175	0.180	0.160
30	0.250	0.254	0.234
40	0.310	0.320	0.301
50	0.360	0.356	0.359
60	0.405	0.412	0.407
70	0.440	0.442	0.442
80	0.465	0.462	0.463

From these results it can be observed that phased based DOAE which uses the phase information from only the first wave pulse provides accurate results even at larger distances and independent of the frequency of the source signal. For the 900 Hz sound source signal the measured delays follow the correct pattern and are within a few percent of the expected time delays. Similarly for the 700 Hz sound source signal the measured delays also follow the correct pattern, are within a few percent of the expected time delays, and are also within a few percent of the values obtained for the 900 Hz sound source signal. The small error that is still present can be attributed to the inaccuracy of

the positioning of the sound source with respect to the receiving microphones, i.e. the sound source is not placed exactly at 10° but possibly at 9.5° or 12°. This hypothesis agrees with the data as the error gets smaller when then angle between the sound source and microphones gets larger and thus the resultant distance between the sound source and the speakers becomes less sensitive to positioning inaccuracies.

7.2   Ultrasound Matched Filter

Several ultrasound matched filter based experiments were performed. The experiments were aimed at showing how using matched filtering could improve the reliability for ultrasound ranging and how several signals may be localized at the same time. The experiments consisted of creating different types of random signals, transmitting them, capturing them, and then performing cross-correlation between the transmitted and captured signals to determine either the distance to an object or to detect the presence of a specific signal. The ultrasound transducers used were the SensComp 125KHF25 125 kHz transducers. The signals were generated in Matlab and transferred to the Agilent 33220A function generator using the methods described in chapter 4. The acquisition system used consisted of the Agilent MSO6032 oscilloscope and the ultrasound sensor amplification circuit described in chapter 6.

Since most ultrasound transducers are resonators designed to only work in a very narrow band of frequencies and having the optimum performance at their one central frequency not all of the parameter typically used to create a matched filter template can be used for ultrasound matched filtering. The frequency cannot be varied for typical ultrasound transducer matched filtering for the reasons described above. The shape of

individual segments besides their amplitude, to some degree, also cannot be varied as the ultrasound resonator will only generate a sine wave signal of the designated frequency. Another issue that has to be considered when working with ultrasound transducers is that they are inertial elements, i.e. they take several cycles of being powered to get to full amplitude and likewise several cycles of not being powered after being powered to go from full amplitude no signal. For the transducers used for these experiments it took 20 cycles to go from zero to full amplitude at a 10 volt peak to peak input signal and likewise 20 cycles to go back to no amplitude from full amplitude.

Due to the above consideration these experiments only varied the overall segment pattern. Specifically two segment patterns were created through the use of two modulation schemes. The first modulation scheme consisted of a 400 cycle sine wave with each sine wave cycle being multiplied by either a zero or a one thus generating a random pattern template. In this experiment the number of repeated on or off cycles was random leading to the output amplitude of the ultrasound transducer randomly 'charging and discharging'. The second modulation scheme also consisted of a 400 cycle sine wave but this time 20 sine wave cycles at a time were modulated to zero or one, again producing a random pattern template, but also allowing the output amplitude of the ultrasound transducer to fully 'charge and discharge'. For both of these wave templates the 125KHF25 ultrasound transducers were used as a transmitter and receiver, placed in the ultrasound array stand described in chapter 6, at a distance of two feet apart.

Figure 7.7 below shows the original Matlab signal for the first modulation scheme, figure 7.8 shows the measured output of the transmitter for the first modulation scheme, figure 7.9 shows the measured received signal for the first modulation scheme,

figure 7.10 shows the autocorrelation of the transmitted signal for the first modulation scheme, and figure 7.11 shows the cross-correlation between the transmitted and received signal for the first modulation scheme.
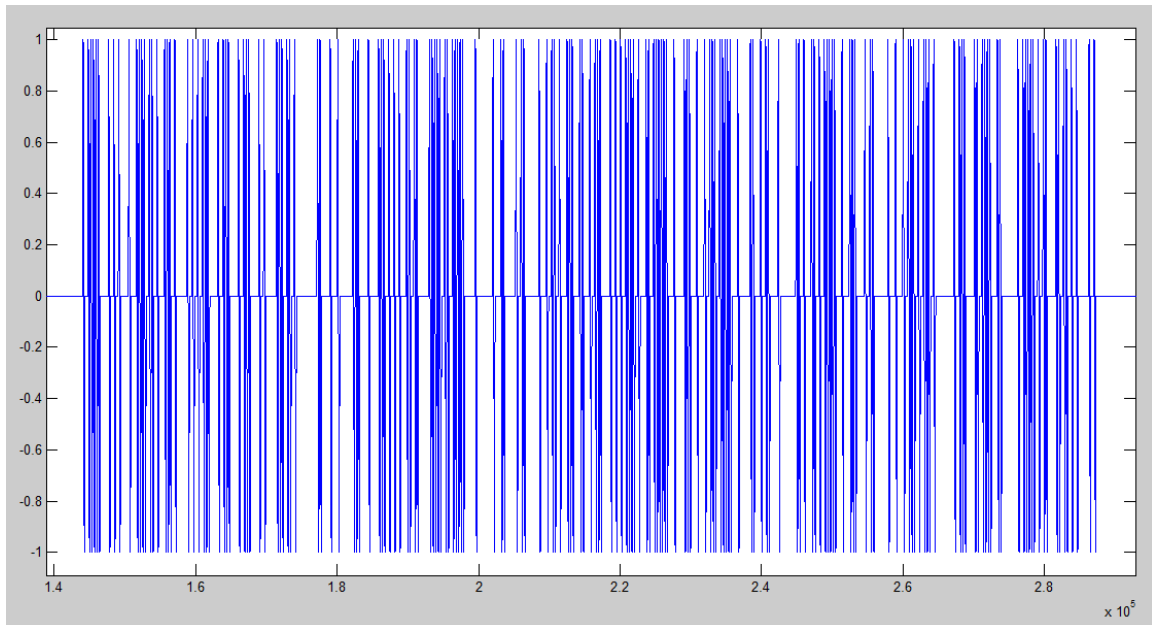

Figure 7.7. Original Matlab Signal for the First Modulation Scheme
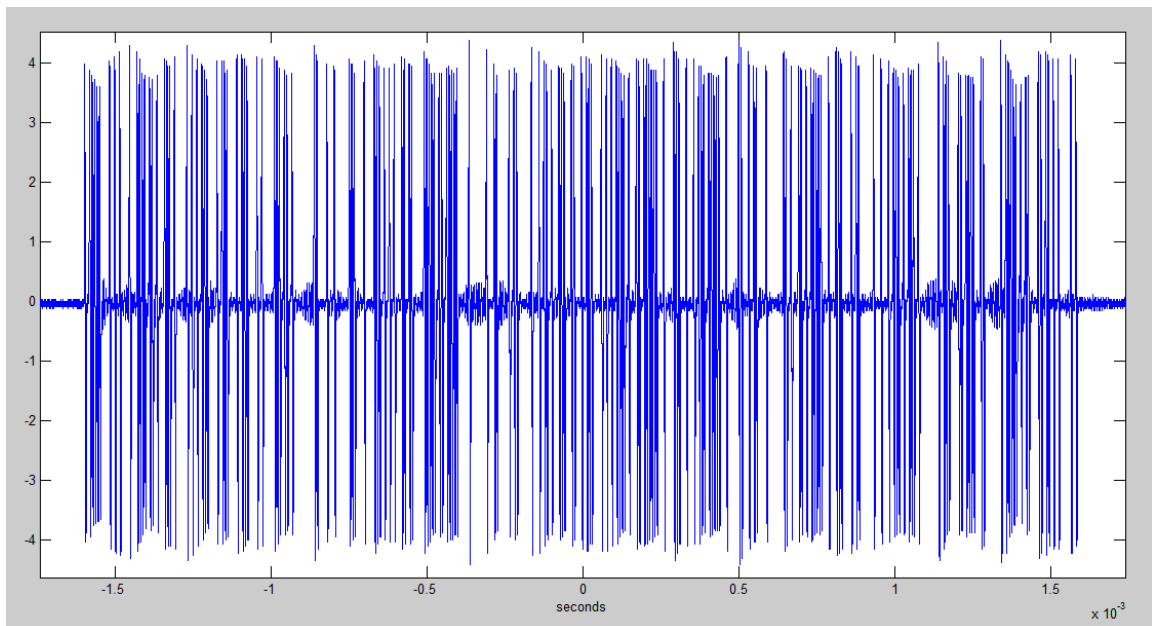
Figure 7.8. Measured Output of the Transmitter for the First Modulation Scheme
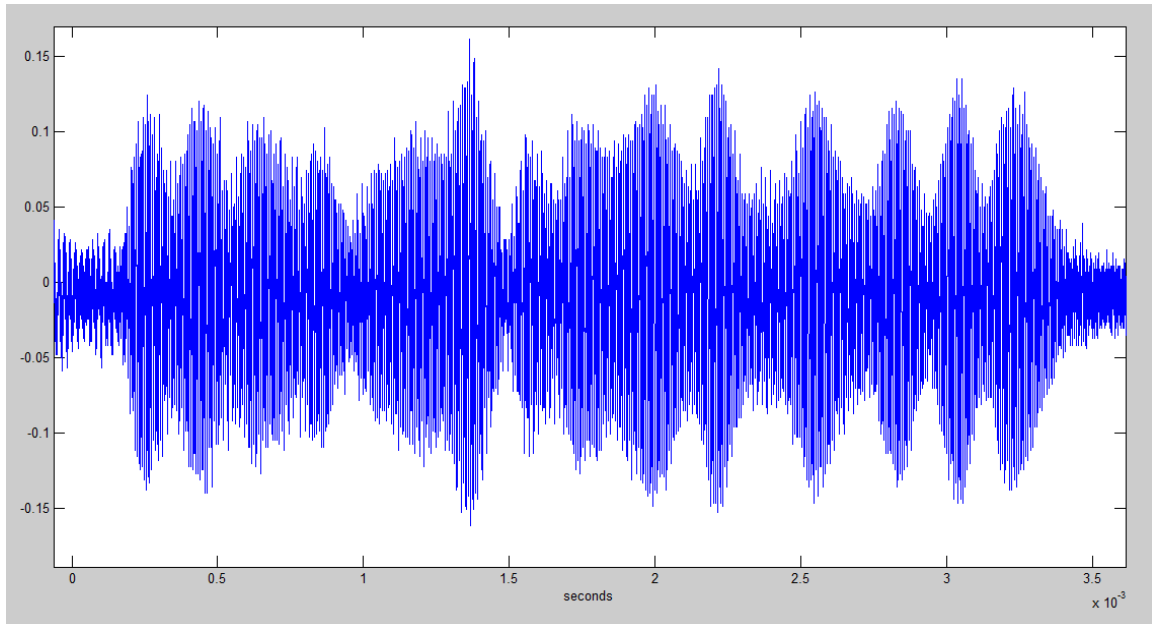
Figure 7.9. Measured Received Signal for the First Modulation Scheme
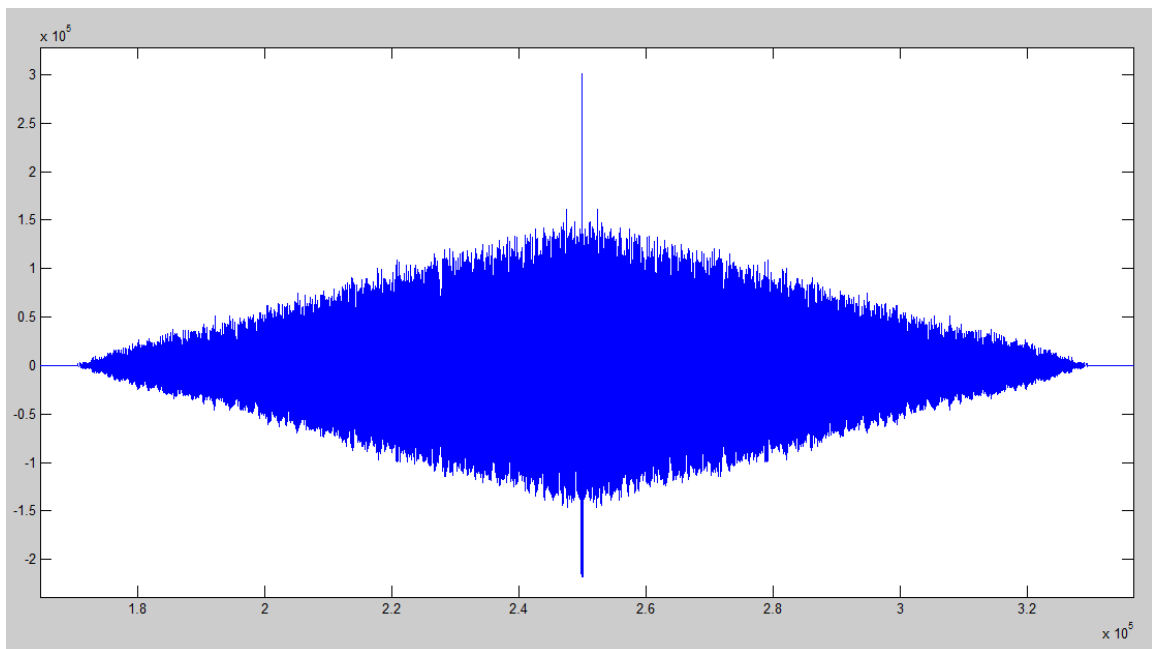
Figure 7.10. Autocorrelation of the Transmitted Signal for the First Modulation Scheme
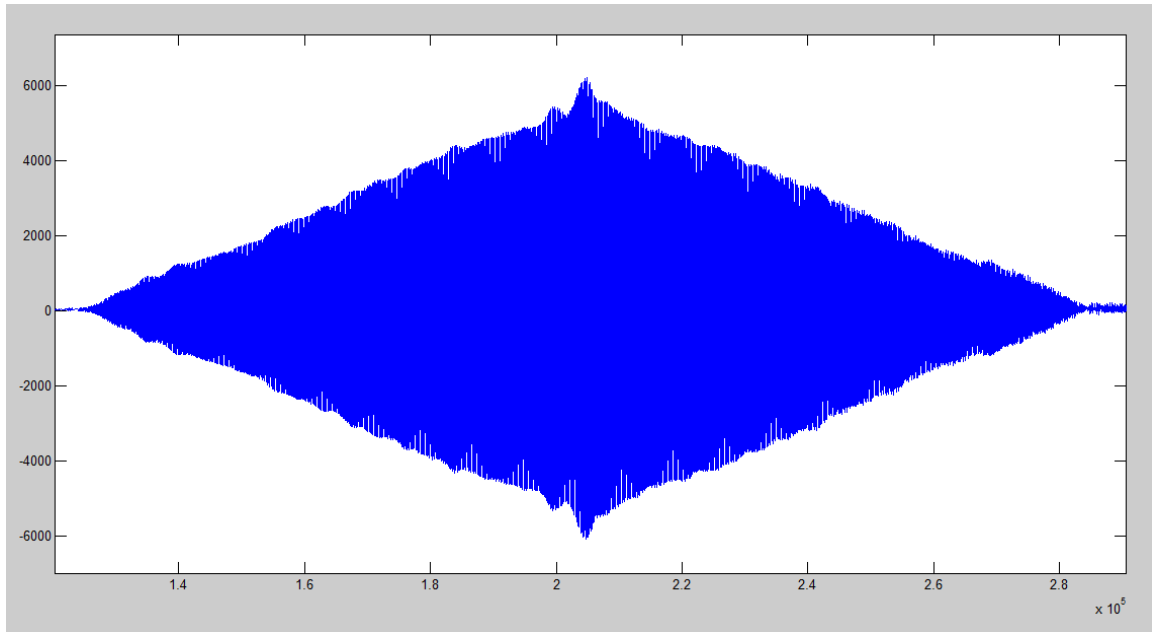
Figure 7.11. Cross-Correlation between the Transmitted and Received Signal for the First Modulation Scheme

When figures 7.7, 7.8, and 7.9 are compared the inertial property of the ultrasound transducers can be seen as a filtering or smoothing affect. As discussed earlier this affect does not allow the ultrasound transceivers to exactly follow the generated wave template as the transducers cannot instantaneously stop or start resonating. Figure 7.10 is the auto-correlation of the transmitted signal with itself and thus is the best possible correlation result which could be achieved. As can be seen from this figure the auto-correlation has a very sharp peak in its center indicating the point at which the signals best overlap. When figure 7.10 is compared with figure 7.11 it can also be seen that the peak for the actual cross-correlation between the transmitted and received signal is not as sharp as that for the auto-correlation. However there is still a significantly sharp peak from which the range measurement can be obtained.

Figure 7.12 shows the original Matlab signal for the second modulation scheme, figure 7.13 shows the measured output of the transmitter for the second modulation

scheme, figure 7.14 shows the measured received signal for the second modulation scheme, figure 7.15 shows the autocorrelation of the transmitted signal for the second modulation scheme, and figure 7.16 shows the cross-correlation between the transmitted and received signal for the second modulation scheme.
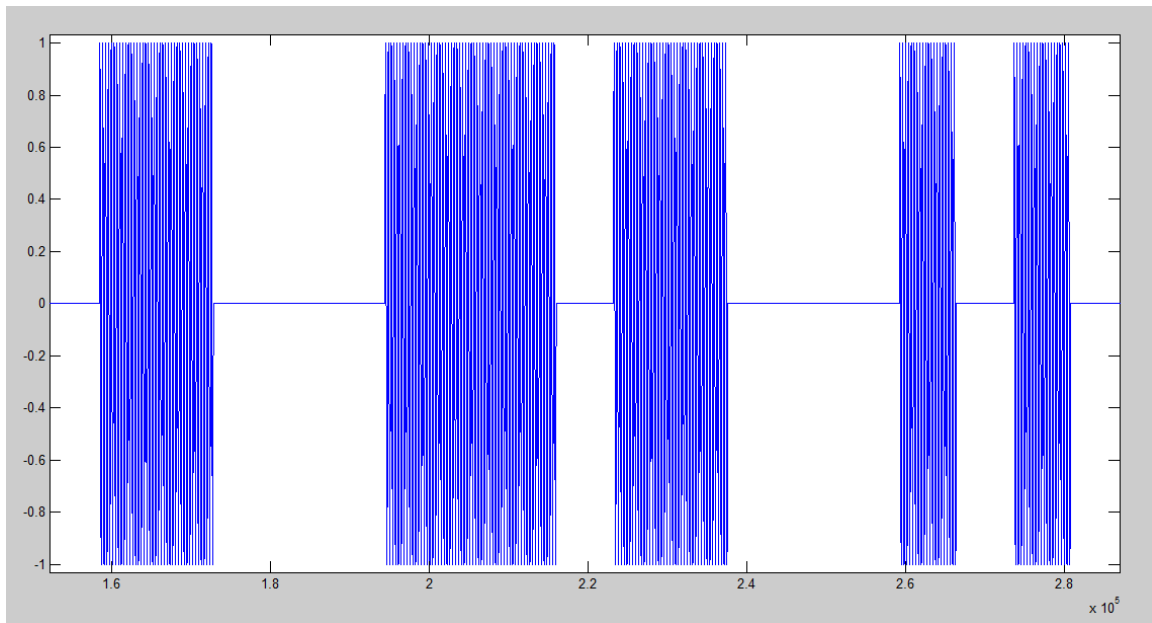
Figure 7.12. Original Matlab Signal for the Second Modulation Scheme
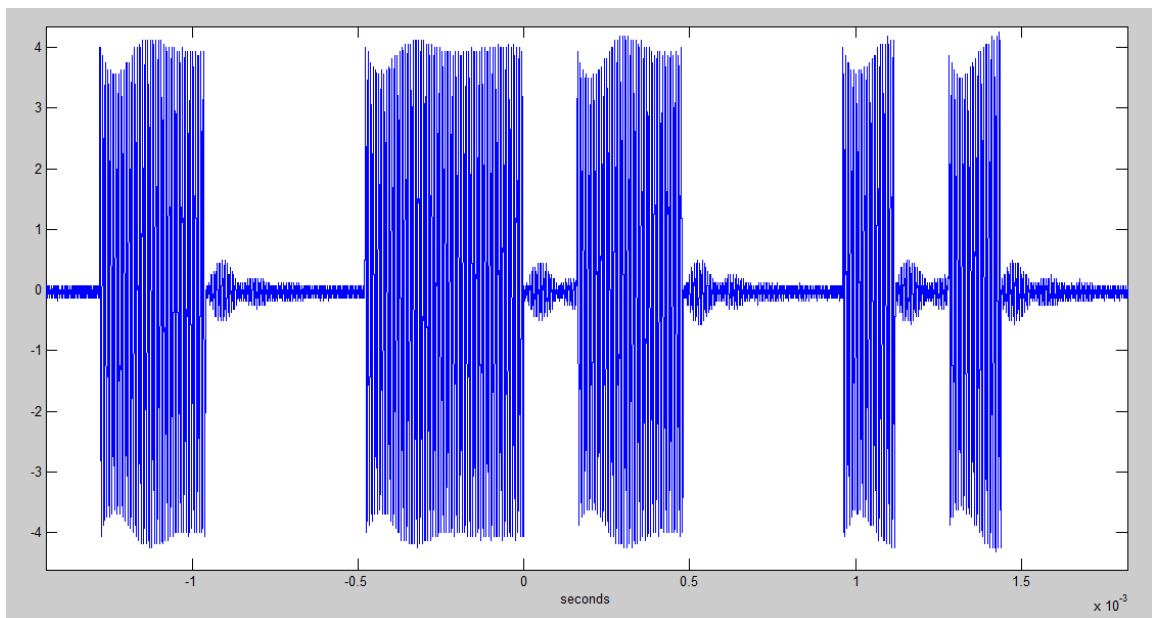
Figure 7.13. Measured Output of the Transmitter for the Second Modulation Scheme
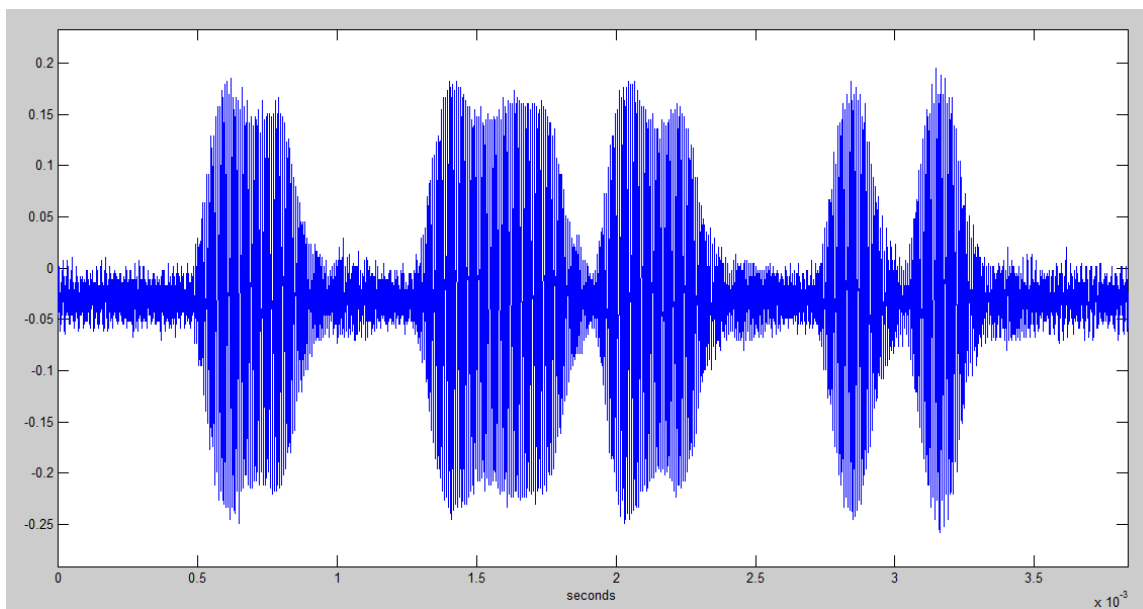
Figure 7.14. Measured Received Signal for the Second Modulation Scheme
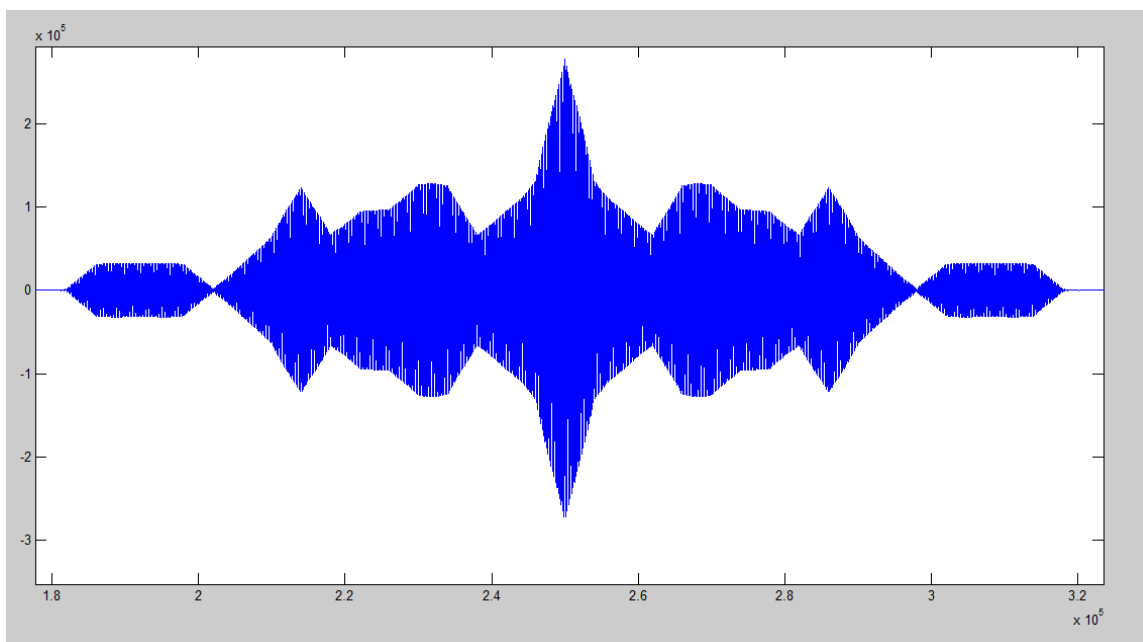
Figure 7.15. Autocorrelation of the Transmitted Signal for the Second Modulation Scheme
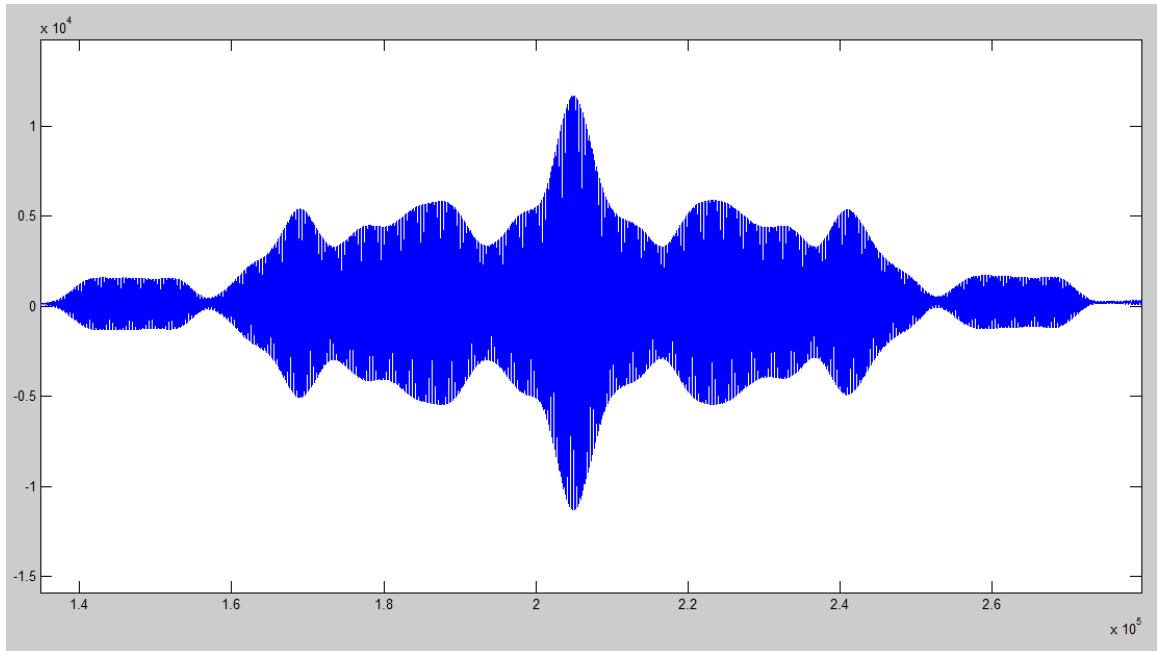
Figure 7.16. Cross-Correlation between the Transmitted and Received Signal for the
Second Modulation Scheme

Figures 7.12, 7.13, and 7.14 show the same smoothing characteristics as for the

corresponding figures for scheme one. However this time since the wave segments were

grouped by 20 pulses the original pattern of the template waveform can be seen much

more clearly in the received signal as seen from comparing figures 7.13 and 7.14. Figure

7.15 again shows the auto-correlation of the transmitted signal with itself and thus is the

best possible correlation result which could be achieved. When comparing figure 7.15

with 7.16 it can be seen that for scheme two the cross-correlation result are much closer

to the auto-correlation results and the cross correlation has a much sharper peak than for

scheme one.

The expected delay for ultrasound ranging can be calculated by equation 7.1

given below:

$$\text{time delay} = \text{distance/speed of sound} \tag{7.1}$$

For the two feet distance used for this experiment the expected delay is given by equation 7.2 below:

$$0.0018\text{sec} = 0.6096/344 \tag{7.2}$$

The collected time delays can be calculated from the cross-correlation results as given by equation 7.3 below:

$$\text{time delay} = (\text{size of signal array} - \text{index of peak point})*$$

$$*\text{captured signal time length/size of signal array} \tag{7.3}$$

For both of the above used modulation schemes the results for this calculation yielded 0.0018 seconds, exactly matching the expected delay. Thus the accuracy of both of the match filters used is quite good. However as the second scheme produced a sharper cross-correlation peak it may be more reliable in the presence of additional noise as the higher and more separated peak will require more noise to make it indistinguishable from surrounding peaks.

Figures 7.17 shows the cross-correlation between the transmitted signals of the two schemes, figure 7.18 shows cross-correlation between the transmitted signal of the first scheme and the received signal of the second scheme, figure 7.19 shows cross-correlation between the transmitted signal of the second scheme and the received signal of the first scheme, figure 7.20 shows cross-correlation between the transmitted second scheme and a received combination of the first and second schemes.
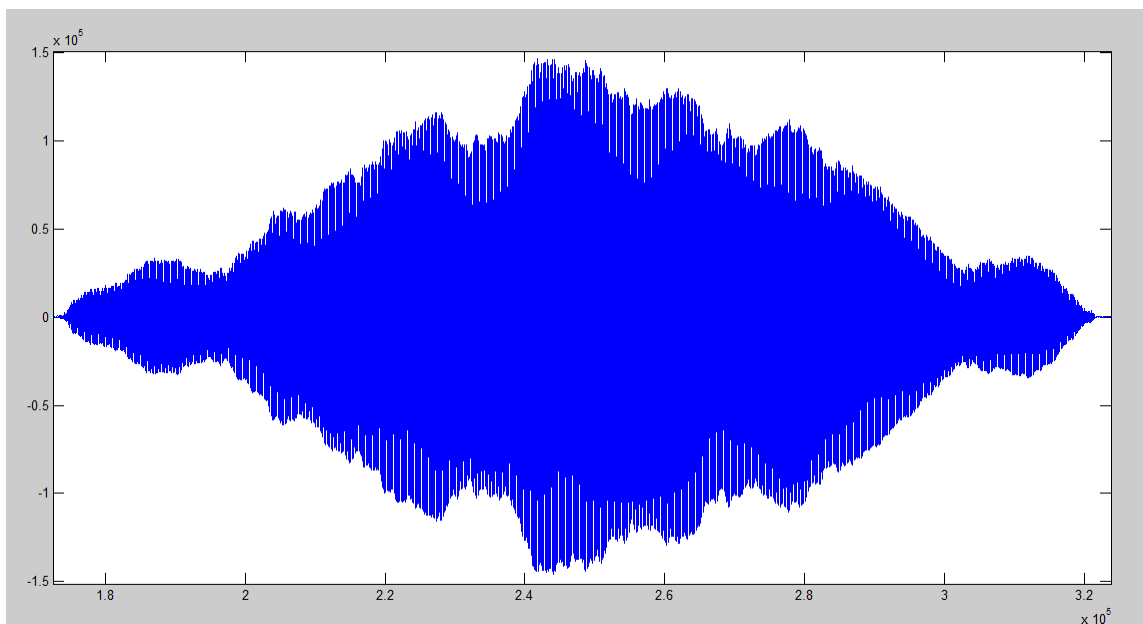
Figure 7.17. Cross-Correlations between the Transmitted Signals of the Two Schemes
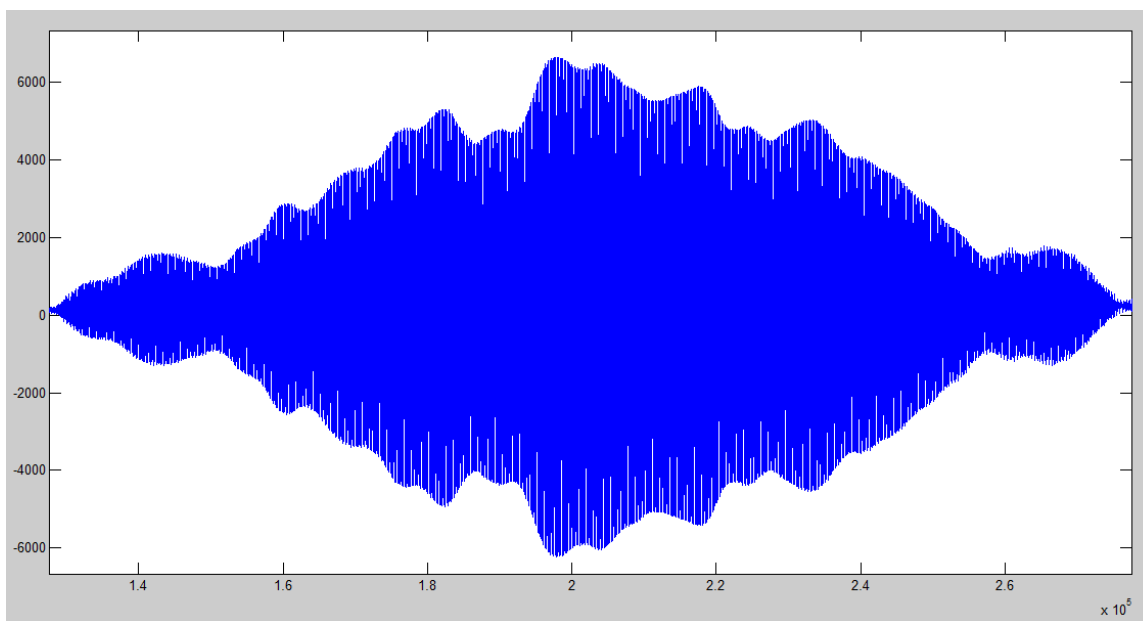
Figure 7.18. Cross-Correlation between the Transmitted Signal of the First Scheme and the Received Signal of the Second Scheme
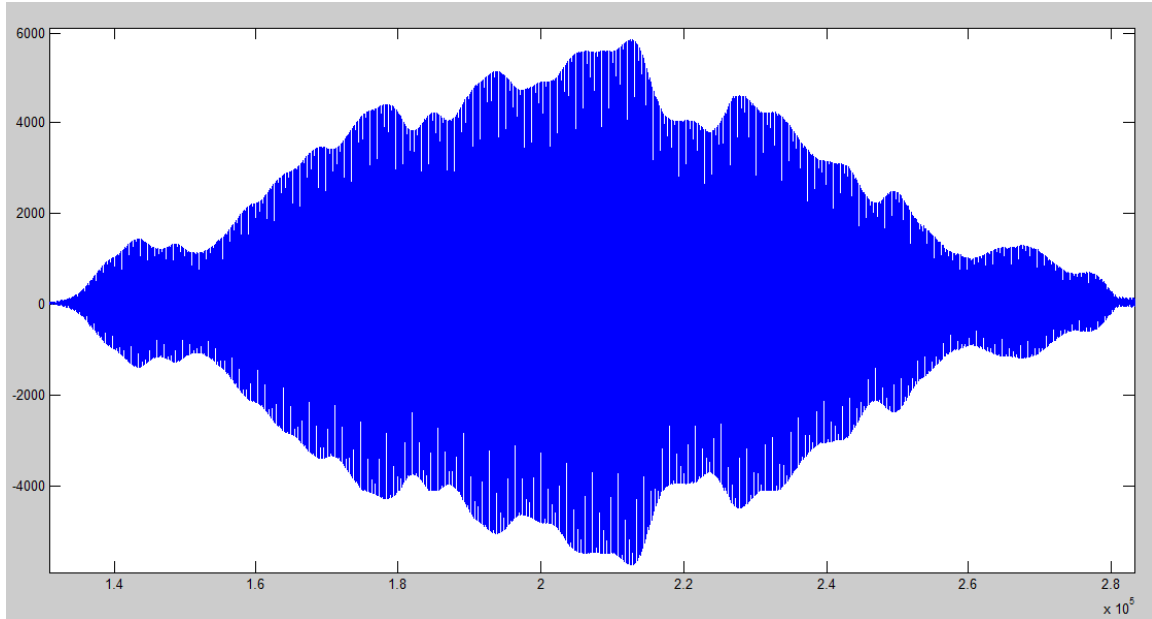
Figure 7.19. Cross-Correlation between the Transmitted Signal of the Second Scheme and the Received Signal of the First Scheme
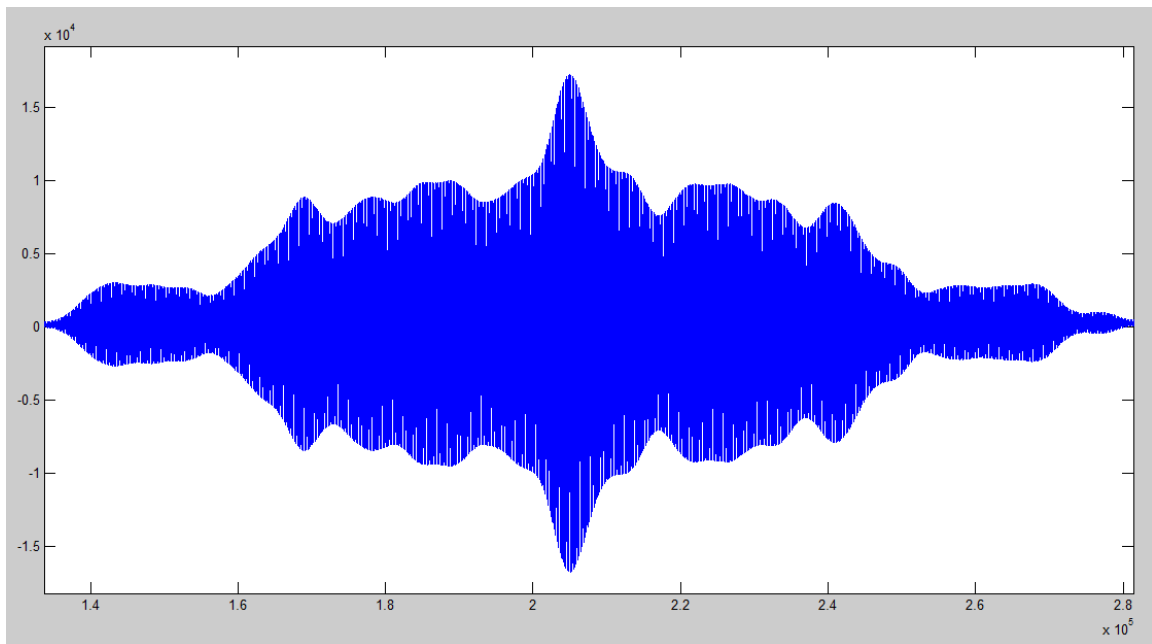
Figure 7.20. Cross-Correlation between the Transmitted Second Scheme and a Received Combination of the First and Second Schemes

From figures 7.17, 7.18, and 7.19 it can be seen that the signals from the two

different modulation schemes do not give a peak when cross-correlation is performed

between them. This is the desired result since this means that cross-correlation does not mistake the two signals for each other and thus only gives a peak when the template signal it is looking for is received. The relatively sharp peak in figure 7.20 shows that when the signals are combined, as when they are transmitted simultaneously, cross-correlation can still find and position the template signal it is looking for in the combination.

7.3   Ultrasound Object Imaging in Air

Another experiment that was performed was a simple object imaging test. Here object imaging does not refer to the imaging of the inside of an object but rather the imaging of the object's external physical shape.

Physically the experiment was carried out inside the acoustic chamber and consisted of a volleyball to be imaged and two ultrasound sensor arrays test stands with the second version of the sensor test beds, as described in chapter 6. Each sensor array consisted of 25 highly directional SensComp 125KHF25 125 kHz ultrasound transducers. The test stands where placed 1.5 feet apart and the volleyball was hung in-between them using a string attached to a metal rod resting on top of the acoustic chamber. The volleyball was positioned midway between the arrays and was at the center with respect to the height and width of each array. An image of this is shown in figure 7.21 below.
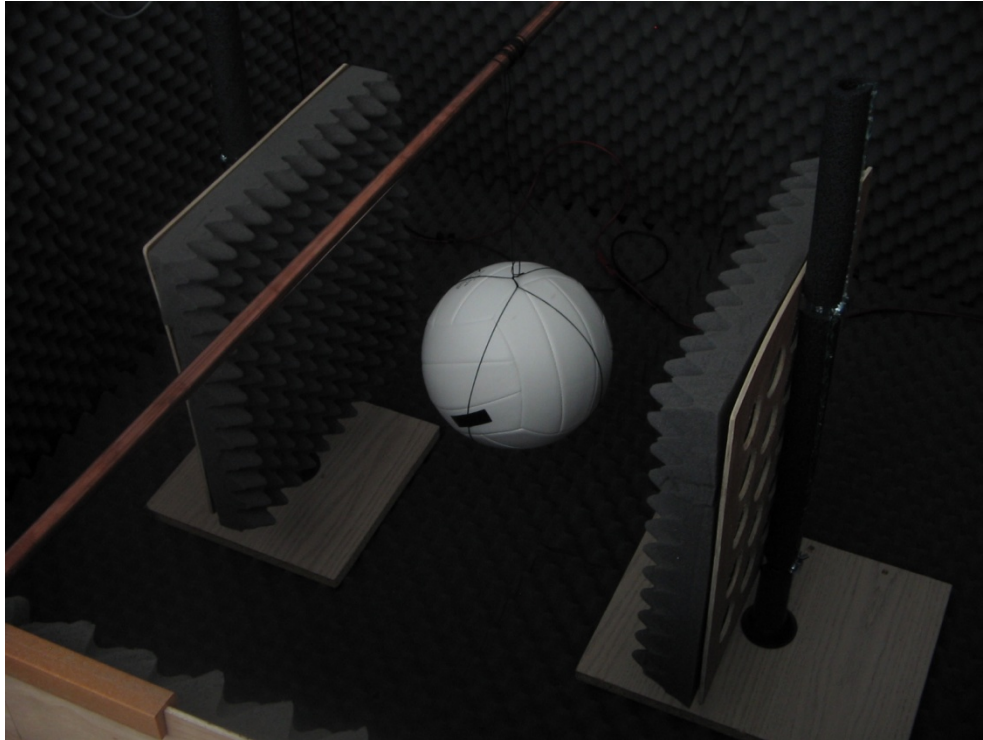
Figure 7.21. Volleyball Imaging Setup

In this setup one of the sensor arrays acted as a receiver array and another acted as a transmitter array. The transmitter array used a 125 kHz, 20 cycle sine wave pulse train which was generated by the built in burst function of the Agilent 33220A function generator. The acquisition system used consisted of the Agilent MSO6032 oscilloscope and the ultrasound sensor amplification circuit described in chapter 6.

The shape of the object was then determined based on the ultrasound 'shadow' the transmitter array produced on the receiver array. The shadow was obtained from the received signal power of each sensor of the receiving array. For the volleyball the received signal power for each microphone is shown in table 7.7, the raw data plot of this data is shown in figure 7.22, and the interpolated plot of the data is shown in figure 7.23.

Table 7.7, Volleyball Image Shadow Power Levels

	Sensor X-axis				
	2437	2184	2478	2205	2162
	2063	878	154	1083	2038
Sensor Y-axis	2627	176	0	243	2532
	2384	910	221	1153	2641
	2376	2758	2105	2145	2387
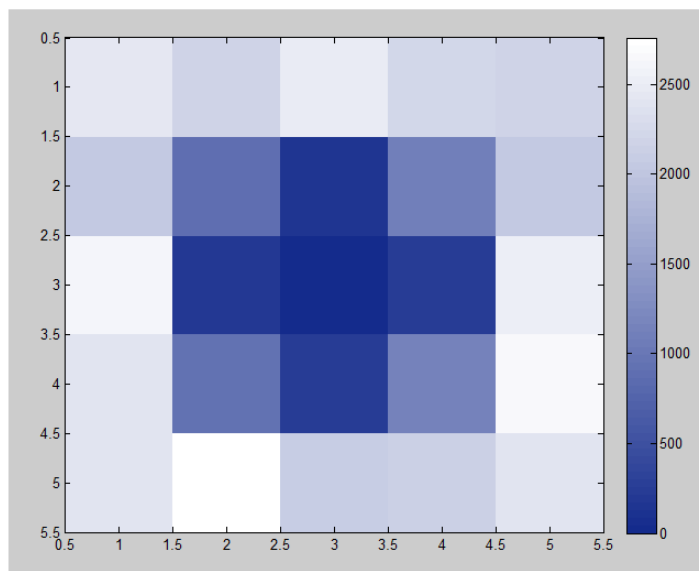
Figure 7.22. Volleyball Imaging Shadow Raw Data
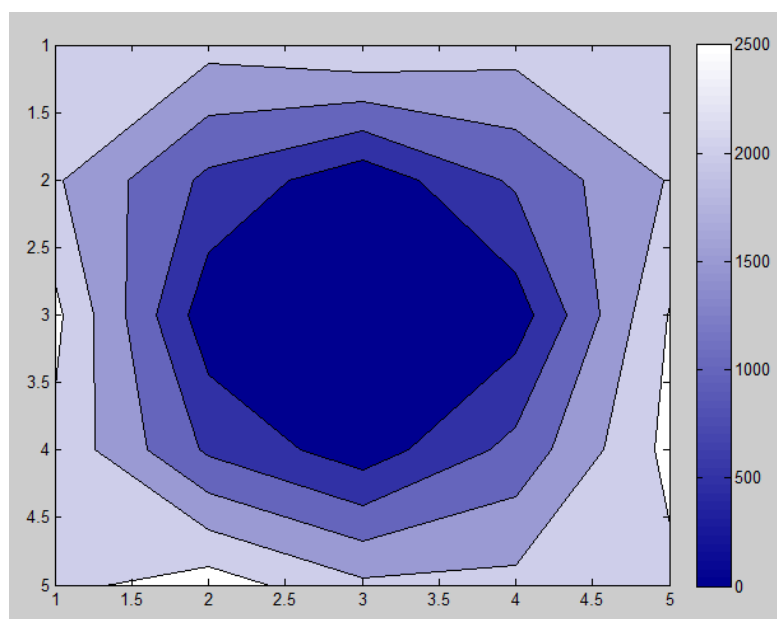
Figure 7.23. Volleyball Imaging Shadow Interpolated Data

From these results it can be seen that the overall shape of the object could be extrapolated to some degree from the obtained power levels. The limitations of this technique are that it only shows the projection of the object in one plane however this could easily be expanded to a three plane projection using two more pairs of sensor arrays. Another limitation is the resolution as can be seen from the poor approximation of the ball in figure 7.23. This however could be improved by using more closely spaced sensors, in which case only the size and directivity of the sensors will be the limiting factor. Since ultrasonic sensors in the MHz range have both high directionality and small sizes this is not an issue. The only other issue is that the projection of an object only shows its outline and not necessarily its overall shape. Ranging with the sensor arrays could be used to obtain the shape of an object to some degree however this could be extremely complex as the surface of an object could be at various angles and could scatter the ultrasound in several directions.

7.4   Ultrasound Localization

Two types of ultrasound source localization experiments were performed, the first was a 2D ultrasound source localization experiment and the second was a 3D ultrasound source localization experiment. For both types of experiments localization was performed based on the delays corresponding to the receiver to transmitter distances and based on the TDOA information between the receivers. As stated in chapter 2 the reason that both the delay between transmission and reception and the TDOA between the receivers is considered is because the delays between the transmission and reception may not always be available since the time of transmission is not always known. However the time at

which the signal is received can typically be obtained thus the TDOA information is more likely to be available. Possible applications of ultrasound localization are ultrasound tagging of objects, robots, and people [Nis06, Nis03], ultrasonic emission detection for issues such as structural or mechanical failure detection [Nel08], and ultrasonic imaging.

Both of the experiments were carried out inside the acoustic chamber described in chapter 5. The first experiment consisted of three generic ultrasound transducers, as described in section 6.2, which acted as receivers and one Measurement Specialties US40KT-01 omnidirectional ultrasound transmitter also as described in section 6.2. The transmitter used a 40 kHz, 20 cycle sine wave pulse train which was generated by the built in burst function of the Agilent 33220A function generator. The acquisition system used consisted of the Agilent MSO6032 oscilloscope and the ultrasound sensor amplification circuit described in chapter 6. The geometry and dimensions of the setup are shown in figure 7.24 below:

Coordinates (x, y, z):
12, √3*12, 0
Rx 3

24"   24"

14.32"

Tx

11.55"   16.66"

9"   7.25"

Rx 1   Rx 2
Coordinates (x, y, z):   24"   Coordinates (x, y, z):
0, 0, 0   24, 0, 0
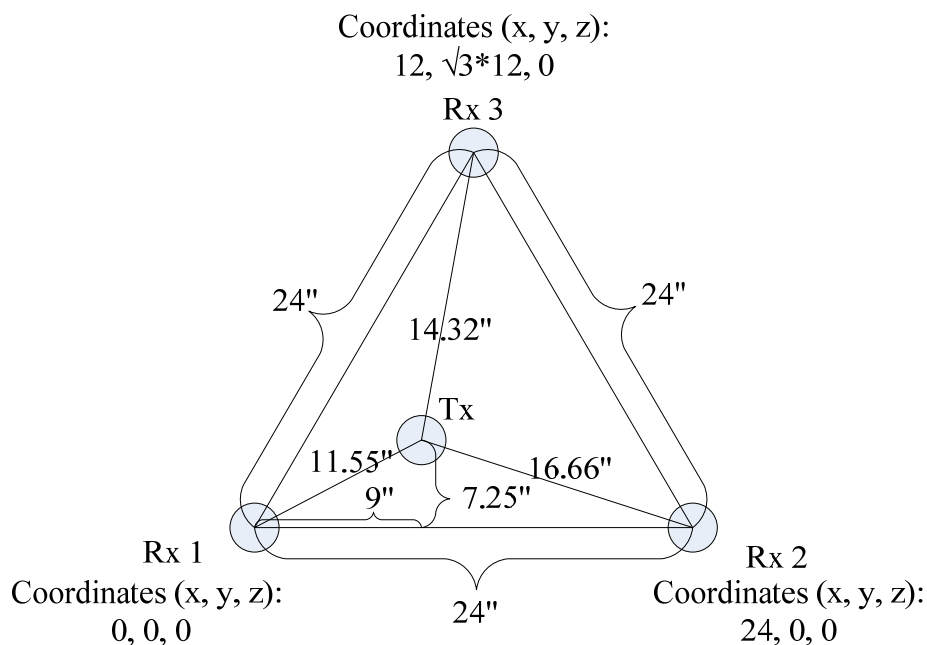
Figure 7.24. 2D Ultrasound Localization Setup

In the above figure the transmitter is labeled Tx, and the receivers are labeled Rx 1 through 3. The receivers were arranged in and equilateral triangle with a side length of 24 inches. The coordinates of each receiver and the transmitter, as well as the distances between each receiver and the transmitter are given by the figure above. Since this was a 2D experiment the transmitter and receivers were all at the same height or equivalently had a z coordinate of 0.

In this experiment the function generator was synchronized with the oscilloscope thus both the time delays (and thus distances) between transmission and reception and the TDOA information between the receivers was available. The collected and expected values for the distances between the receivers and the transmitter and the distances corresponding to the TDOA are given in tables 7.8 and 7.9 respectively.

Table 7.8. Distances between the Receivers and the Transmitter for the 2D Setup

From Receiver	Collected (inches)	Expected (inches)	Error (inches)
1	12.46	11.55	0.91
2	17.41	16.66	0.75
3	14.69	14.32	0.37

Table 7.9. Distances Corresponding to the TDOA Information for the 2D Setup

Between Receivers	Collected (inches)	Expected (inches)	Error (inches)
2-1	4.95	5.11	0.16
2-3	2.72	2.34	0.38
3-1	2.23	2.77	0.54

From these values the coordinates of the transmitter were then obtained using the equations given in chapter 2. Specifically for the case where the distances between the transmitter and receivers are used equations 2.19 through 2.21 are applied. No interpolation algorithm was used but instead the equations were solved two at a time and

then the three pairs of results were averaged. For the case in which only the TDOA

information is used equations 2.19 through 2.23 are directly applied. The collected and

expected values for the coordinates of the transmitter based on the transmitter to receiver

distances and based on the TDOA information are given in tables 7.10 and 7.11

respectively.

Table 7.10. Transmitter Coordinates Based on Distances for the 2D Setup

Coordinate	Collected (inches)	Expected (inches)	Error (inches)
x	9.22	9	0.22
y	7.76	7.25	0.51

Table 7.11. Transmitter Coordinates Based on TDOA for the 2D Setup

Coordinate	Collected (inches)	Expected (inches)	Error (inches)
x	9.09	9	0.09
y	7.24	7.25	0.01

When interpreting the accuracy of these results it should also be considered that

the expected results themselves have an approximate error of +/- ½ inches due to

positioning errors. Thus from these results it can be seen that both methods give

relatively accurate approximations of the ultrasound transmitter's coordinates, with the

TDOA based results being slightly more accurate.

The second experiment consisted of six generic ultrasound transducers as

described in section 6.2, five of which acted as receivers and one of which acted as a

transmitter. The transmitter used a 40 kHz, 20 cycle sine wave pulse train which was

generated by the built in burst function of the Agilent 33220A function generator. The

acquisition system used consisted of the Agilent MSO6032 oscilloscope and the

ultrasound sensor amplification circuit described in chapter 6. The first version of the

sensor array test stand as described in chapter 5 was used to hold the transmitter and receivers. The geometry and dimensions of the setup are shown in figure 7.25 below:
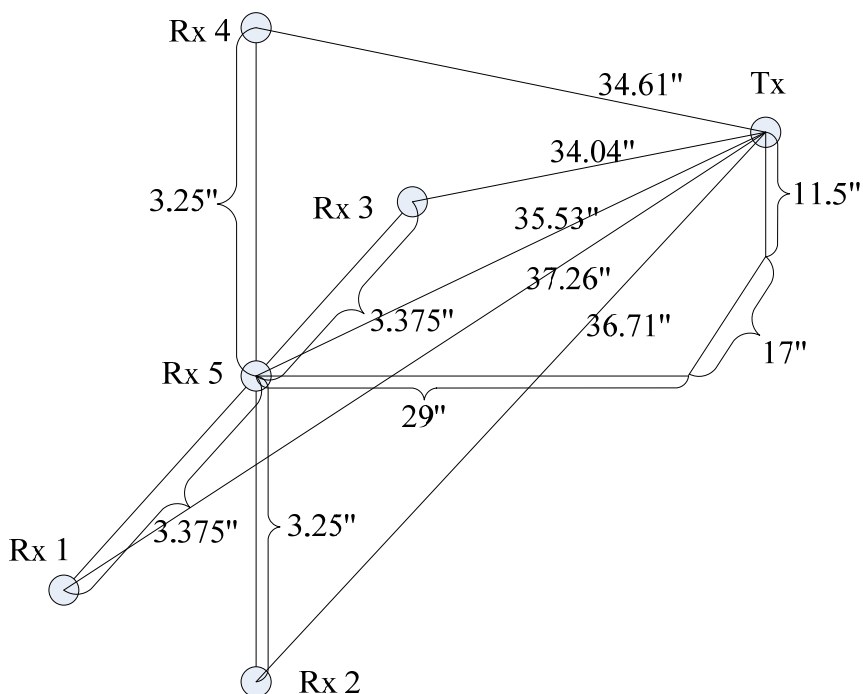

Figure 7.25. 3D Ultrasound Localization Setup

In the above figure the transmitter is labeled Tx, and the receivers are labeled Rx 1 through 5. The receivers were arranged in a plus sign pattern with the distances between each receiver and the transmitter given by the figure above. This specific receiver geometry was used to simplify the calculations as was described in chapter 2.

In this experiment again the function generator was synchronized with the oscilloscope thus both the time delays (and thus distances) between transmission and reception and the TDOA information between the receivers was available. The collected and expected values for the distances between the receivers and the transmitter and the distances corresponding to the TDOA are given in tables 7.12 and 7.13 respectively.

Table 7.12. Distances between the Receivers and the Transmitter for the 3D Setup

From Receiver	Collected (inches)	Expected (inches)	Error (inches)
1	37.921	37.26	0.661
2	37.378	36.71	0.668
3	34.807	34.04	0.767
4	35.213	34.61	0.603
5	36.567	35.53	1.037

Table 7.13. Distances Corresponding to the TDOA Information for the 3D Setup

Between Receivers	Collected (inches)	Expected (inches)	Error (inches)
1-2	0.543	0.55	0.007
1-3	3.114	3.22	0.106
1-4	2.708	2.65	0.058
1-5	1.354	1.73	-0.376

From these values the coordinates of the transmitter were then obtained using the equations given in chapter 2. Specifically for the case where the distances between the transmitter and receivers are used the law of cosines was applied like shown with equations 2.15 through 2.16. No interpolation algorithm was used but instead the two equations were solved for each axis and the pairs of results were averaged. For the case in which only the TDOA information is used equations 2.15 through 2.16 are directly applied. The collected and expected values for the coordinates of the transmitter based on the transmitter to receiver distances and based on the TDOA information are given in tables 7.14 and 7.15 respectively.

Table 7.14. Transmitter Coordinates Based on Distances for the 3D Setup

Coordinate	Collected (inches)	Expected (inches)	Error (inches)
x	16.78	17	0.22
y	12.19	11.5	0.69
z	30.12	29	1.12

Table 7.15. Transmitter Coordinates Based on TDOA for the 3D Setup

Coordinate	Collected (inches)	Expected (inches)	Error (inches)
x	17.17	17	0.17
y	12.51	11.5	1.01
z	29.766	29	0.766

Again when interpreting the accuracy of these results it should also be considered that the expected results themselves have an approximate error of +/- ½ inches due to positioning errors. Thus from these results it can be seen that both methods give relatively accurate approximations of the ultrasound transmitter's coordinates.

CHAPTER 8

CONCLUSION AND FUTURE WORK

8.1   Conclusion

In this work the fundamentals of 2D and 3D sound and ultrasound source localization are presented. The topics of matched filtering, object imaging and how they relate to ultrasound are also explored. A novel FPGA/MEMS based data acquisition and microphone array system is presented and its utilization for the above described topics is compared to standard test equipment and standard sensor based data acquisition systems. In addition to this the capabilities of a generic data generation system (arbitrary waveform generator) are also explored and its applications to signal generation for DOAE, localization, matched filtering, and ranger are presented. The design of an anechoic chamber, precision measurement mount, and several sensor array stands and their utilization for the above described topics are described. Lastly several DOAE, localization, matched filter, and ranging/imaging experiments are conducted using various combinations of these concepts, designs, and equipment.

The fundamentals and variations of the DOAE and localization problem are described to allow for a more complete understanding of the experiments and their results. Specifically the difference between DOAE and localization were explained, the differences between 2D and 3D scenarios were also explained and various parameters such as the geometries, numbers of receivers, signal types, applicable algorithms, types of information used and the minimum amount of information was considered. The types of models used and the mathematics associated with them were derived and explained. The steps used to perform DOAE and localization were presented and the differences between

ultrasound and sound methods were discussed. General considerations and limitations

such as the frequency and spatial sampling theorem, limitations on the types of models

which can be used, and the mathematical limitations were presented. The basics of

matched filtering and the improvements which could be obtained for DOAE, localization,

and ranging based on matched filtering were explained.

The FPGA/MEMS acquisition and microphone array system was described. This

consisted of the presentation of the three main physical boards (NPCB, GEL, and AMA)

and the core architecture (CAPTAN) behind the system. Specifically the three main parts

of the CAPTAN system, namely the node layer, the network layer, and the application

interface layer, were described. The design, features, and limitations of the system and

the architecture were explored. This included discussions of the CAPTAN based system's

acquisition capabilities, networkability, high communication rates, modularity within

nodes and between nodes, modularity in configeware and software, ease of hardware and

software expandability, high processing power and the ability to perform PC based

processing.

In contrast to the custom FPGA/MEMS system, the capabilities and features of a

generic oscilloscope (MSO6032A) based data acquisition system were presented. The

main issues explored were the necessary auxiliary circuits for amplification and filtering,

techniques of interfacing with the oscilloscope, capturing and transferring data from the

oscilloscope to the PC and programming of the scope. The techniques explored included

front panel interface, data capture, and portable storage based transfer, built in

web/network interface, existing software, direct USB link based interface, data capture

and transfer, SCPI programming based interface, data capture and transfer, and driver

programming based interface, data capture and transfer. The advantages, such as speed of use, ease of interface, and interchangeability, and the disadvantages, such as limited number of channels and lack of real-time processing, were also presented. In addition to this the generic data generation system (A33220A) was discussed and the various techniques of interfacing with the waveform generator, creating arbitrary waveforms and transferring arbitrary waveforms from the PC to the waveform generator were explored.

The acoustic chamber, measurement mount, and sensor array test stands were created to allow the various experiments to be conducted in a more controlled manner. The design and features of the acoustic chamber such as its modularity, expandability, and acoustic absorption properties were described. The design and usage of the measurement mount as it relates to the accuracy of source positioning for the localization experiments was discuss. Lastly the design and features of the sensor array test stands such as its adjustability, modularity, and its ability to allow for a large number of sensor geometries to be experimented with were presented.

Four general types of experiments were conducted, specifically the types were sound DOAE, ultrasound matched filtering, ultrasound object imaging, and ultrasound source localization. The sound direction of arrival experiments showed how phased based estimation can be performed, how the CAPTAN based system and generic acquisition and generation systems can be utilized for these types of experiments. The results show how the accuracy of the estimation is affected by various parameters such as the acoustic chamber, the receiver geometries, frequencies used, distances between the transmitter and receiver, and type of interpretation of the received signal.

The matched filter experiments demonstrated how matched filters could be applied to ultrasound and how a generic data generation system could be used to create a variety of useful waveforms. Specifically the matched filter experiment show how different types of filters operate with ultrasound transducers, how these techniques could be used to increase the accuracy of ranging, and how they can be used to simultaneously send multiple transmission on the same medium.

The ultrasound object imaging experiment simply showed how ultrasound ranging could be used for basic object shape/outline detection.

The ultrasound localization set of experiments demonstrate how 2D and 3D localization can be performed based either the TDOA information or the receiver to transmitter distance information. Several applications such as acoustic emission detection and ultrasound tagging are discussed. The results demonstrate that the approaches used give quite accurate positions of the sources for both 2D and 3D cases using either type of information as inputs.

8.2   Future Work

Several steps can be taken in the future to improve this work. The FPGA/CAPTAN based system may be modified to perform general data acquisition across multiple sensors instead of data acquisition for specific types of microphones. This modification would be relatively easy as it would simply involve modifying the AMA board to have general input connectors instead of specific types of attached microphones.

Another direction that could be taken is the development of standardized oscilloscope based data acquisition system through the use of interchangeable instrument

drivers. This would involve the creation of either a command line or GUI style software which would use interchangeable instrument drivers to allow common commands to be used to interface with the various oscilloscopes on the market.

The ultrasound object imaging series of experiments can also be significantly expanded. Specifically ranging/sensor array based techniques could be explored for the possibility of determining the objects shape as oppose to its outline as was done in this work. This would probably involved issues such as determination of surface orientation and a further exploration of matched filtering techniques which allow more accurate ranging measurements to be obtained.

Since this work only considered single frequency sound and ultrasound sources another issued which could be studied is the effect of multiple frequency sources on DOAE and localization. Additionally a variety of DOAE and localization algorithms could also be explored such pulse based TDOA estimation algorithms, phased based TDOA algorithms like GCC-PHAT or interpolation algorithms like NLLS and CIC. All these algorithms could also be tested for their resilience against noise and reflections by using the acoustic chamber. This could be done by gradually increasing the amount of noisy and reflective objects within the chamber and by removing several of the absorbing panels from the chamber. Once these algorithms are tested in an environment like Matlab they could then be implemented in a real-time platform such as the FPGA/CAPTAN system. After this it would be possible to test them for several applications such as person localization, enhanced man machine interface, acoustic emission localization, and object tagging systems.

BIBLIOGRAPHY

[Agi07]   Agilent Technologies, 33220A 20 MHz Function /arbitrary waveform
               generator user's guide. (2007). Retrieved from http://www.
               home.agilent.com/agilent/techSupport.jspx?cc=US&lc=eng&nid=-
               536902257.536883183&pid=127539&pageMode= MN

[Agi09A]   Agilent Intuilink, Data capture. (2009). Retrieved from http://www.home.
               agilent.com/agilent/editorial.jspx?cc=US&lc=en
               g&ckey=1662999&nid=-536902766.536905496&id=1662999

[Agi09B]   Agilent IntuiLink, Waveform editor for function/arbitrary waveform
               generators. (2009). Retrieved from http://www.home.agilent.
               com/agilent/editorial.jspx?cc=US&lc=eng&ckey=1000000918:eps
               g:sud&nid=-536902257.536883183&id=1000000918:epsg:sud

[Agi09C]   Agilent, Transferring arbitrary waveform data to the 33200A family of
               function/arbitrary waveform generators. (2009). Retrieved from
               http://www.home.agilent.com/agilent/techSupport.jspx?pid=12753
               9&pageMode=OV&cc=US&lc=eng

[Agi10A]   Agilent, InfiniiVision 6000 series oscilloscopes programmer's guide.
               (2010). Retrieved from http://www.home.agilent.com/agilent/
               techSupport.jspx?cc=US&lc=eng&nid=-536902766.536905496&
               pid=563883&pageMode= MN

[Agi10B]   Agilent Technologies, InfiniiVision 5000/6000/7000 series oscilloscopes
               user's guide. (2010). Retrieved from http://www.home.agilent.
               com/agilent/techSupport.jspx?cc=US&lc=eng&nid=-536902766.
               536905496&pid=563883&pageMode= MN

[Alg08]   Alghassi, H. (2008). *Eye array sound source localization* (Doctoral
               dissertation). Retrieved from https://circle.ubc.ca/bitstream/
               handle/2429/5114/ubc_2008_spring_alghassi_hedayat.pdf?
               sequence=1

[AME10]   American Acoustical Products, Hushcloth convoluted foams datasheet.
               Retrieved from http://www.aapusa.com/hushcloth_convoluted.
               html

[Ben08]   Benesty, J., Chen, J., & Huang, Y. (2008). *Microphone array signal
               processing*. Berlin Heidelberg: Spring-Verlag.

[Bra01]   Brandstein, M., & Ward, D. (Eds.). (2001). *Microphone arrays Signal processing techniques and applications.* Berlin Heidelberg: Spring-Verlag.

[Gri02]   Griebel, S. M. (2002). *A microphone array system for speech source localization, denoising and dereverberation* (Doctoral dissertation). Retrieved from http://citeseerx.ist.psu.edu/ viewdoc/summary?doi=10.1.1.153.492

[Har08]   Harput, S, & Buzkurt, A. (2008). Ultrasonic Phased Array Device for Acoustic Imaging in Air. *IEEE sensors journal, 8*(11), 1755-1762.

[Hyv00]   Hyvärinen, A., & Oja, E. (2000). Independent Component Analysis: Algorithms and Applications. *Neural Networks*, *13*(4-5), 411-430.

[Hyv01]   Hyvärinen, A., Karhunen, J., & Oja, E. (2001). *Independent component analysis.* New York, NY: John Wiley & Sons.

[IVI09]   IVI Foundation, Getting started guide: Your guide to getting started with IVI drivers. (2009). Retrieved from http://www.ivifoundation .org/ downloads/IVI_GSG v1.01.pdf

[Kit02]   Charles Kitchin (2002), Demystifying single-supply op-amp design. Analog Devices Inc.

[Kn06A]   Knowles Acoustics, SPM0208HE5 Surface mount MEMS microphones datasheet. (2006). Retrieved from http://www.knowles.com/search/product.htm?x_sub_cat_id=3

[Kn06B]   *Knowles Acoustics, SPM0204UD5 Surface mount MEMS microphones datasheet*. (2006). Retrieved from http://www.knowles.com/search/product.htm?x_sub_cat_id=14

[Li06]   Li, Y., Yang, J., Li, X., & Tian, J. (2006). *Ultrasonic intruder detection system for home security*. Berlin Heidelberg: Spring-Verlag.

[Lla01]   Llata, J. R., Sarabia, E. G., & Oria, J. P. (2002). Three-Dimensional Robotic Vision Using Ultrasonic Sensors. *Journal of Intelligent and Robotic Systems, 33,* 267-284. Berlin Heidelberg: Spring-Verlag.

[Mat10]   Mathworks Matlab, Instrument control toolbox – documentation (2010). Retrieved from http://www.mathworks.com/help/toolbox/ instrument/instrument_product_page.html

[Mea01]   Measurement Specialties, US40KT-01 Piezoelectric film transmitter.
           (2001). Retrieved from http://www.meas-
           spec.com/product/t_product.aspx?id=2490

[McC01]   McCowan, I. (2001). *Microphone arrays: a tutorial* (Doctoral
           dissertation). Retrieved from http://idiap.ch/~mccowan/arrays/
           tutorial.pdf

[Mun03]   Mungamuru, B. (2003). *Enhanced sound localization* (Master's. thesis).
           Retrieved fromhttp://hammerhead.stanford.edu/papers/thesis_
           060403.pdf

[Nat00]   National Semiconductor, LM124/LM224/LM324/LM2902 Low power
           quad operational amplifiers. (2000). Retrieved from
           http://www.national.com/ds/LM/LM124.pdf

[Nat02]   National Semiconductor, Application note 31 op amp circuit collection.
           (2002). Retrieved from http://www.national.com/an/AN/AN-
           31.pdf

[Nat10]   National Semiconductor, ADC121S101 Datasheet. (2010). Retrieved from
           http://www.national.com/ds/DC/ADC121S101.pdf

[Nel08]   Nelligan, T. (2008). Ultrasonic Material Analysis. Retrieved from
           http://www.ndtmag.com/Articles/Feature_Article/BNP_GUID_9-
           5-2006_A_10000000000000249031

[Nis03]   Nishitani, A., Nishida, Y., & Mizoguch, H. (2003). Omnidirectional
           Ultrasonic Location Sensor. *In IEEE Conference on Sensors,
           Irvine, CA.*

[Nis06]   Nishida, Y., Aizawa, H. & Hori, T. (2006). 3D Ultrasonic Tagging System
           for Observing Human Activity. *In IEEE/RSJ Intl. Conference on
           Intelligent Robots and Systems, Las Vegas. Nevada*

[Pan10]   Panavise, Model 333 circuit board vise webpage. (2010). Retrieved from
           *http://www.panavise.com/index.html?pageID=1&page=full&--
           eqskudatarq=26*

[Que06]   Queiros, R., Girao, P. S., & Cruz Serra, A. (2006). Cross-Correlation and
           Sine-Fitting Techniques for High Resolution Ultrasonic Ranging.
           *In IMTC Instrumentation and Measurement Technology
           Conference, Sorrento, Italy 24(27).*

[Que06B]   Queiros, R., Martins, R. C., Girao, P. S., & Cruz Serra, A. (2006). A New Method For High Resolution Ultrasonic Ranging In Air. *In XVIII IMEKO World Congress Metrology for a Sustainable Development Conference, 17(22), Rio de Janeiro, Brazil.*

[Pro07]   Proakis, J. G., & Manolakis, D. G. (2007). *Digital signal processing Principles, algorithms, and applications (*4th ed.). Upper Saddle River, New Jersey: Pearson Education.

[Rad10]   Radioshack, Model: 270-090 PC-mount condenser microphone element. (2010). Retrieved from http://www.radioshack.com/product/ index.jsp?productId=2062215#tabsetBasic

[Ran03]   Rangarajan, V. S. (2003). *Interfacing speech recognition and vision guided microphone array technologies* (Master's thesis). Retrieved from http://mit.dspace.org/bitstream/handle/1721.1/29687/ 53867213.pdf ?sequence=1

[Riv08]   Rivera, R., Turqueti, M., & Prosser, A. (2008). A software solution for the control, acquisition, and storage of CAPTAN network topologies. *In 2008 IEEE Nuclear science symposium conference record: October 2008, Dresden, Germany* (pp. 805-808). Piscataway, N.J.: IEEE.

[Sen07]   SensComp, 125KHF25 Piezoelectric transducer. (2007). Retrieved from http://www.senscomp.com/kseries.htm

[STMV06]   STMicroElectronics, TSV99 Operational amplifier datasheet. (2010). Retrieved from http://www.st.com/stonline/products/literature/ds/ 12833/tsv991.htm

[Tel07]   Tellakula, K. A. (2007). *Acoustic source localization using time delay estimation* (Master's thesis). Retrieved from http://brentkirkwood .com/science/documents/BCK_MS_Thesis_Final_20030811.pdf

[Kit02]   Charles K. (2002). Demystifying single-supply op-amp design. Analog Devices Inc. Retrieved from www.ednmag.com.

[Tur08]   Turqueti, M., Rivera, R., Prosser, A., Andresen, J., & Chramowicz, J. (2008). CAPTAN: A hardware architecture for integrated data acquisition, control and analysis for detector development. *2008 IEEE Nuclear science symposium conference record: October 2008, Dresden, Germany* (pp. 3546-3552).

[Tur10]   Turqueti, M., Saniie, J. & Oruklu,E. Scalable Acoustic Imaging Platform
            Using MEMS Array. *In EIT Electro/Information Technology
            conference, May 2010, Normal, IL.*

[Wan96]   Wang, A., Yao, K., Hudson, R. E., Korompis, D., Lorenzelli, F., Soli, S.
            F., & Gao, S. (1996). A High Performance Microphone Array
            System For Hearing Aid Applications. University of Los Angeles,
            Los Angeles, California.

[Wel06]   Wells, P. N. T. (2006). Ultrasound Imaging. UK, Institute of Physical
            Publishing.

[Xil08]   Xilinx Inc. Virtex-4 FPGA User guides, UG070. (2008, December 1).
            FPGA and CPLD Solutions from Xilinx, Inc. Retrieved from
            http://www.xilinx.com/support/documentation/virtex-
            4_user_guides.htm

[Zio00]   Ziomek, J. L. (1995). *Acoustic field theory and space-time signal
            processing*. Boca Raton, Florida: CRC Press Inc.